DEPLETION ANALYSES OF LOW ENRICHED URANIUM FUELS FOR THE NIGERIA RESEARCH REACTOR-1

By

ABDULSAMAD ASUKU

DEPARTMENT OF PHYSICS,

FACULTY OF PHYSICAL SCIENCE,

AHMADU BELLO UNIVERSITY, ZARIA

NIGERIA

MARCH, 2023

DEPLETION ANALYSES OF LOW ENRICHED URANIUM FUELS FOR THE NIGERIA RESEARCH REACTOR-1

By

ABDULSAMAD ASUKU
B.Sc. (Hons) Physics, MSc. Nuclear Physics (A.B.U Zaria)
(P15SCPY9008)

A THESIS SUBMITTED TO THE SCHOOL OF POSTGRADUATE STUDIES, AHMADU BELLO UNIVERSITY, ZARIA

IN PARTIAL FULFILMENT FOR THE AWARD
OF
DOCTOR OF PHILOSOPHY IN NUCLEAR PHYSICS

DEPARTMENT OF PHYSICS,

FACULTY OF PHYSICAL SCIENCE,

AHMADU BELLO UNIVERSITY, ZARIA,

NIGERIA

MARCH, 2023

DECLARATION

I declare that the work in this dissertation entitled **"Depletion Analyses of Low Enriched Uranium Fuels for the Nigeria Research Reactor-1"** has been performed by me in the Department of Physics, Faculty of Physical Sciences. The information derived from the literatures has been duly acknowledged in the text and a list of references provided. No part of this thesis was previously presented for another degree or diploma at this or any other institution.

Abdulsamad ASUKU		
______________________	_____________________	______________
Name of Student	Signature	Date

CERTIFICATION

This thesis entitled “DEPLETION ANALYSES OF LOW ENRICHED URANIUM FUELS FOR THE NIGERIA RESEARCH REACTOR-1” by Abdulsamad ASUKU meets the regulations governing the award of the degree of PhD Radiation Biophysics of the Ahmadu Bello University, Zaria and is approved for its contribution to knowledge and literary presentation.

Prof. S.A. Jonah

______________________	______________________	______________
Chairman, Supervisory Committee	Signature	Date

Prof. Y.V. Ibrahim

______________________	______________________	______________
Member, Supervisory Committee	Signature	Date

Prof. Umar Sadiq.

______________________	______________________	______________
Member, Supervisory Committee	Signature	Date

Dr. A.L. Ahmed

______________________	______________________	______________
Head of Department	Signature	Date

Prof. S. A. Abdullahi

______________________	______________________	______________
Dean, School of Postgraduate Studies	Signature	Date

DEDICATION

To my gorgeous wife and ‘raw gold’ (Hanatu), my beautiful daughters (Yusrah and Ummi), my parents (Ssgt. And Mrs. Asuku Yisa) and my siblings.

ACKNOWLEDGEMENTS

It is often said that no man is an island, I am not an exception. A lot of people contributed one way or the other to the success of this thesis. I may be only able to mention a few here but I most certainly cannot forget the rest.

I am immensely grateful to my supervisory team for the guidance and tutelage they provided me through the course of my PhD programme.

I wish to express a most sincere gratitude to Prof. Y.A. Ahmed (Chairman, Nigeria Atomic Energy Commission) who motivated me throughout this programme.

I am extremely grateful to all academic staff of Physics Department and reactor operators of the Centre for Energy Research and Training, Zaria for their insightful contributions to this work. Worthy of note are Prof. Rabiu Nasiru (former Head, Department of Physics, Ahmadu Bello University, Zaria), and Dr. A.L. Ahmed, (the current Head of Department) who provided an enabling environment for the completion of my programme.

The huge financial and moral support I received from my parents and siblings in my trying times will never be forgotten.

Thanks to my friends and colleagues; Yahaya Muhammed Kabir, Sadiq Umar, Dr. Yusuf Shaidu, Yusuf Bashir Ogrima (OBO), Ahmed Umar, and Dr. Simon John.

Lastly, I am extremely grateful, in the most animated of languages, to the one whose eyes are like leaping fishes a moment seen, the one whom on the petals of her favorite flowers my heart lay contented; my wife, Mrs. Asuku Hanatu Ize. I say *Avor Inya, Jazakillahu Khair* for all your sacrifices.

ABSTRACT

The use of advanced, accident-tolerant, Low Enriched Uranium (LEU) fuel types is one approach to improving the safety, security and fuel cycle performance of nuclear reactors. In spite of the acceptability of UO_2 fuel, uranium-silicide and uranium-molybdenum fuels are being proposed in order to increases the accident tolerance of nuclear reactor cores. Although the as-built fuel of the Nigeria Research Reactor-1 (IRR-1) LEU core is 13% enriched UO_2 clad in Zircalloy, previous research have demonstrated that specific uranium-silicide and uranium-molybdenum such as 19.75% enriched U_3Si_2, U_3Si, and U_9Mo dispersion LEU fuels clad in aluminum also present comparable neutronic characteristics within recommended safety limit for the NIRR-1 Miniature Neutron Source Reactor (MNSR). However, analysis of the depletion characteristics of the as-built UO_2 core as well as the investigated fuel alternates are yet to be conducted as these data are important for optimization of safety, security, fuel management and decommissioning plan a well as conversion of other MNSRs from High Enriched Uranium (HEU) to LEU. Consequently, the SCALE 6.2.3 code system was used to develop new models of the NIRR-1 and perform criticality calculations and depletion analysis for the as-built UO_2, U_3Si_2-Al, U_3Si-Al, and U9Mo-Al LEU cores in the present study, using the HEU core as a benchmark. The results showed that the three Dimensional (3D) KENO-VI estimates of the Clean Cold Core Excess Reactivity (CCCER of the core are in good in good agreement with measured data with a bias of less than 4 %. Consequently, the 3D KENO-VI module of the SCALE 6.2.3 code can be used for criticality safety calculations of MNSRs and similar reactors. The neutron flux distribution data indicated a reduction in the magnitude of the average thermal neutron flux in the alternative LEU cores in the range of 7 – 10 % when compared to that of the HEU core. This implies that the thermal power of the U_3Si_2-Al, U_3Si-Al, and U_9Mo-Al LEU cores would have to be raised by their corresponding magnitude of percentage flux reduction to match the flux of the HEU core. However, the thermal neutron flux in the as-built LEU-UO_2 core is essentially the same with that of the HEU core. Hence, the as-built LEU core will not compromise NIRR-1 utilization for thermal Neutron Activation Analysis. Although the results show that both the HEU and the LEU cores have a burnup of less than 1 % at the End of Cycle of 216 Effective Full Power Days (EFPD), the Uranium-Silicide fuels have a higher burnup when compared to the UO_2 fuel. The depletion rates were estimated to be – 0.00120 mk/h, - 0.00124 mk/h, - 0.00123 mk/h and – 0.00105 mk/h for the as-built UO_2, U_3Si_2, U_3Si and U-9Mo LEU cores respectively. In all cases, the LEU cores depleted at a slower rate than the HEU core implying an improvement in the fuel economy of the cores compared to the HEU core. The core lifetimes after addition of top Beryllium Shim plates when the reactor is operated continuously for 216 EFPD were estimated to be 38.62, 37.34, 37.53, and 43.78 years for the as-built UO_2, U_3Si_2, U_3S i and U-9Mo LEU cores respectively. These estimated core lifetimes are 26% higher than that of the HEU. Consequently, the LEU cores show better fuel cycle performance and demonstrated an advantage of extended core lifetime for utilization in Neutron Activation Analysis. These results are useful in the development of a decommissioning plan for the NIRR-1 and fuel management of accident-tolerant alternative fuels to optimize their performance as promising alternatives to the UO_2 fuel.

TABLE OF CONTENTS

LIST OF FIGURES

LIST OF TABLES

NOMENCLATURE

ATF	Accident Tolerant Fuel
BOC	Beginning of Cycle
CERT	Centre for Energy Research and Training
CCCER	Cold Clean Core Excess Reactivity
EFPD	Effective Full Power Days
ER	Excess Reactivity
EOC	End of Cycle
GTRI	Global Threat Reduction Initiative
HEU	Highly Enriched Uranium
IIC	Inner Irradiation Channels
IAEA	International Atomic Energy Agency
LEU	Low Enriched Uranium
LPRR	Low-Power Research Reactor
MCNP	Monte Carlo N-Particle Code
MNSR	Miniature Neutron Source Reactor
NAA	Neutron Activation Analysis
NIRR-1	Nigeria Research Reactor – 1
OD	Outer Diameter
RERTR	Reduced Enrichment for Research and Test Reactors
RR	Research Reactor
SCALE	Standardized Computer Analysis for Licensing Evaluation
RNSD	Reactor and Nuclear Systems Division
ORNL	Oak Ridge National Laboratory
OIC	Outer Irradiation Channels
U-Al	Uranium-Aluminum
UO_2	Uranium Dioxide

SRF	Safety Reactivity Factor
MPRR	Multipurpose Research Reactor

CHAPTER ONE

1.0 GENERAL INTRODUCTION

1.1 Background of the Study

Research reactors (RRs) are reactors used in the civilian domain for Neutron Activation Analyses (NAA), radioisotope production, material testing and training (Glaser, 2005; Ahmed *et al*, 2006). Low-Power RRs (LPRRs) are small RRs having a nominal power of about 30 kW. Miniature Neutron Source Reactors (MNSRs) are LPRRs (Yang, 1992; CIAE, 1993; Balogun *et al*, 2005; Jonah *et al*, 2006; Amjad *et al*, 2012) designed and manufactured by the China Institute of Atomic Energy (CIAE). Among the operators of MNSRs include China (MNSR-Institute of Atomic Energy, MNSR-IAE and MNER-Shenzhen, MNSR-SZ), Ghana (Ghana Research Reactor-1, GHARR-1), Pakistan (Pakistan Research Reactor-2, PARR-2), Syria (Syrian MNSR), Iran (Esfahan Nuclear Technology Centre MNSR, ENTC MNSR) and Nigeria (Nigeria Research Reactor-1, NIRR-1).

The program to covert reactors in the civilian domain from High Enriched Uranium (HEU) to Low Enriched Uranium (LEU) began in 1978. The program was called the “Reduced Enrichment for Research and Test Reactors” (RERTR). Since 2015, the name of the program has changed from RERTR to Global Threat Reduction Initiative (GTRI) (Glaser, 2005). However, the conversion of MNSR type reactors from the use of HEU fuel to LEU fuel was started under the auspices of the International Atomic Energy Agency (IAEA) Coordinated Research Project entitled “Conversion of MNSRs to LEU” in 2006 (Glaser, 2007; Jordi, 2011; Jordi, 2014, Meyer, 2015). Around the same year, the NIRR-1 MNSR was commissioned with a HEU (90.2 % UAl_4 in Aluminum clad) fueled core, joined the list of reactors under consideration for conversion to LEU.

Between 2009 and 2016, 28 civilian RRs have either undergone successful conversion or have been closed. As at 2016 the stock pile of HEU used in civilian applications total 60 tons (NASEM, 2016). The NIRR-1, which attained first criticality with HEU fuel in February 2004, was eventually converted and attained second criticality with 13 % Uranium-diokide (UO_2) LEU fuel clad in Zircalloy-4 on 2nd November, 2018. However, there are other MNSRs, including MNSR-SZ, PARR-2, Syrian MNSR, and ENTC MNSR, that are still using HEU.

The UO_2 is mostly preferred as fuel for reactors over uranium metal due to greater stability and a high melting point (roughly 2850°C) but has a disadvantage of a poor thermal conductivity, particularly at higher temperatures and irradiation levels (IAEA, 2022). This leads to large temperature gradients and thermal stresses. Consequently, better alternatives or possible replacements such as uranium-silicide and uranium-molybdenum fuels, which fall into the category of fuels called Accident-Tolerant Fuels (ATF), are being proposed in order to increase the accident tolerance of nuclear reactor cores due to their greater thermal conductivity compared to UO_2 fuel which results in lower fuel centreline temperatures and reduces risk of accidents in reactors (Ibikunle, 2018; Alhmoud *et al*, 2011).

Three specific uranium-silicide and uranium-molybdenum fuels have been identified and shown to display neuronic properties that qualify them to be suitable as alternative LEU fuels for MNSR-type LPRR on a generic design basis (Lell and Matos, 2005). They include 19.75% enriched U_3Si_2-Al, U_3Si-Al and U_9Mo-Al LEU fuels. This has attracted the focus of facility-specific-design research of MNSR on these fuels since 2005 (Jonah *et al*; 2009, Albarhoum, 2011; Amjad *et al*, 2012). However, most recently, using the Monte Cralo N-Particle (MCNP) code, Ibikunle (2018) demonstrated that the neutronic parameters of the 19.75% enriched U_3Si_2-Al, U_3Si-Al and U_9Mo-Al LEU cores within recommended safety limit for the NIRR-1 when compared with the standard HEU core. Yet, Ibikunle *et al* (2018) failed to investigate the depletion parameters of the fuels and the as-built UO_2 core of the NIRR-1.

Though there are several studies evaluating the neutronic performance of U_3Si_2-Al, U_3Si-Al and U_9Mo-Al LEU fuels for generic and reactor-specific MNSRs, (there are comparatively few studies which look at the depletion performance of these fuels for reactor-specific MNSRs. Moreover, as there are some differences in number of active fuel pins, dummy pins, fuel impurities, initial core excess reactivity, the depletion performance should be evaluated specifically for NIRR-1 in order to determine their performance compared to the traditional HEU core and the current LEU core.

Simulation of depletion (fuel-cycle-related) parameters of fuels for use in commercial reactors is very important in fuel management and safety-related analyses in reactor design, licensing and spent-fuel transport storage system design among others (IAEA, 1992; IAEA, 2002; IAEA, 2006 Dawahra, 2015). It is the prediction of the long-term changes in reactor fuel composition caused by exposure to neutron flux during reactor operation. How these properties (fuel-cycle-related parameters) change has an important effect on the fuel management of a reactor, as well as on its stability and control and should be known to ensure that the reactor will operate safely throughout its lifetime (James and Louis, 1976; Lamarsh and Baratta, 2001; Dawahra, 2015; Sogbadji, 2011).

The aim of the present study is to investigate the depletion performance of the as-built 13% enriched UO_2 fueled NIRR-1 MNSR and the 19.75% enriched alternative U_3Si_2, U_3Si and U9Mo LEU dispersion fuels.

1.2 Problem Statement

Even though UO_2 fuel is generally acceptable as fuel for nuclear reactors, it has a disadvantage of a poor thermal conductivity, especially at higher temperatures and irradiation levels (Simon and David, 2018). This results in large temperature gradients and thermal stresses. Hence, uranium-silicide and uranium-molybdenum fuels are among the fuels being proposed in order to increases the accident tolerance of nuclear reactor cores because they have been shown to have higher thermal conductivity compared to UO_2. For example, at average fuel temperature, U_3Si_2 has a thermal conductivity of 16.78 W/m.K compared to that of UO_2 which is 3.29 W/m.K (Hartanto *et al*, 2020). Uranium-Silicide fuels also have a higher fissile density, which may enable some new cladding concepts that would otherwise require increased enrichment limits to compensate for their neutronic penalty (YU et al., 2016; Ibikunle, 2018; Alhmoud *et al*, 2011). Although the as-built fuel of the NIRR-1 LEU core is 13% enriched UO_2 clad in Zircalloy, Jonah *et al*, (2009) and Ibikunle, (2018) have demonstrated that specific uranium-silicide and uranium-molybdenum fuels such as 19.75% enriched U_3Si_2, U_3Si, and U_9Mo alternate LEU fuels clad in aluminum are suitable for the NIRR-1 MNSR on neutronic basis. However, the concentrations (atom densities or mass) of various isotopes in an operating reactor core such as the NIRR-1 are continually changing due to nuclear reactions such as fission, neutron capture and radioactive decay. In addition some decay products of fission process in the reactor core have large absorption cross section for thermal neutrons. This affects neutronic parameters of the reactor including effective multiplication factor (or core excess reactivity), neutron flux distribution and power distribution, and this affects the stability, control and longevity of the reactor. Hence, in spite of the of characteristics of being 'accident-tolerant' and showing suitable neutronics performance for the NIRR-1, the U_3Si_2, U_3Si, and U_9Mo LEU fuel should also show comparable or better depletion performance so as to serve as better alternatives or replacement to the UO_2. Furthermore, in order to ensure an effective fuel management, neutron economy and provide data to support decommissioning plan and the conversion of other MNSRs, it is imperative that an analysis of the depletion performance of the as-built 13% enriched UO_2 clad in Zircalloy and 19.75% enriched U_3Si_2, U_3Si, and U_9Mo alternate LEU fuels clad in aluminum be conducted.

1.3 Aim and Objectives of the Research

The aim of this research is to investigate the depletion performance of the as-built UO_2 and alternate U_3Si_2–Al, U_3Si–Al and U9Mo-Al LEU dispersion fuels to support conversion of LPRRs to LEU, using the SCALE 6.2.3 code system.

The objectives of this research are as follows:

1. To generate cross section library NIRR-1 MNSR using the SCALE 6.2.3 code system.

2. To develop a new model of the NIRR-1 MNSR and evaluate the Neutonic parameters such as CCCER, shutdown margin, control rod worth and safety reactivity factor of the NIRR-1 core fueled with the as-built UO_2 clad in Zircalloy, and the U_3Si_2 –Al, U_3Si –Al and U_9Mo-Al dispersion fuels at the beginning of Cycle based on the model developed.

3. To evaluate the moderator-to-fuel ratio and the average neutron flux distribution of the as-built NIRR-1 core and the alternate U_3Si_2 –Al, U_3Si –Al and U_9Mo-Al dispersion fuels.

4. To evaluate ^{235}U and ^{238}U core loading requirement and the concentration of ^{235}U, ^{238}U, and build-up of ^{239}Pu as well as ^{135}Xe and ^{149}Sm at the End of Cycle (EOC) length of 216 Effective Full Power Days (EFPD).

5. To investigate the effect of burnup on the reactivity of the NIRR-1 core fueled with the as-built UO_2 and the alternate U_3Si_2 –Al, U_3Si –Al and U_9Mo-Al and estimate the cores and their depletion rates..

6. To evaluate the top beryllium shim worth and core life time of the NIRR-1 fueled with the as-built UO_2 core and the alternative U_3Si_2 –Al, U_3Si –Al and U_9Mo-Al dispersion fuels.

1.4 Justification

Decommissioning plan is a safety requirement by Nuclear Regulatory Authorities. Information on the burnup of the as-built UO_2 core of the NIRR-1 will contribute to the eventual decommissioning plan of the NIRR-1.

Predicting the core composition changes in a reactor is crucial for effective and efficient control and safe use of a reactor throughout its lifetime (Khattab, 2005; Zafar, 2009; Sogbadi, 2012, Leenaers, 2016). The analyses of the depletion performance of the NIRR-1 fueled with the U_3Si_2–Al, U_3Si–Al and U_9Mo-Al LEU dispersion fuels will provide new data on the core composition changes associated with the LEU dispersion fuels and the effect of these changes on their neutronic parameters. This will assist in fuel management and inform the long-term safety of the fuels for commercial use and support their use in the conversion of LPRRs from HEU to LEU.

The methodology in this work will be adaptable to model similar MNSRs and other LPRRs. This work can also be slightly modified to contribute to the design and possible establishment of a generic LEU core that will serve as a base model for a LEU conversion study of commercial LPRRs.

This research will also highlight the importance of evaluating alternative fuel types for MNSRs to optimize their performance and contribute to the sustainable development of Research Reactors in the nuclear industry.

1.5 Scope/Limitation of the Research

This work attempt to develop a new model for the NIRR-1and estimate some neutronic parameters such as CCCER, CRW, SDM and SRF of the as-built UO_2 and alternate as U_3Si_2–Al, U_3Si–Al and U_9Mo-Al LEU fuels. The depletion analysis and investigation of the effect of burnup on reactivity is also covered. Lastly, the core lifetimes with the as-built core and alternate cores are determined. SCALE 6.2.3 code system which couples 1-D XSDRNPM and 3-D KENO VI transport calculation code with ORIGEN depletion code using TRITON code sequence was used for the calculations. However, effects of lumped fission products on reactivity as well as core thermal-hydraulic parameters that affect neutron flux distribution where not considered in this study.

CHAPTER TWO

2. LITERATURE REVIEW

2.1 Introduction

This chapter present the relevant theoretical frameworks applied in the calculations in this work and a review of some related studies available in literature.

2.2 Criticality and Reactivity

A reactor is said to be “Critical” if the neutron chain reaction is self-sustaining and the neutron population is neither increasing nor decreasing (DOE, 1993). The multiplication factor is the equation which ensures that the neutron life-cycle in a reactor core can be traced. The multiplication factor can either be an infinite multiplication factor k_∞ or an effective multiplication factor k_{eff}. The infinite multiplication factor is defined as:

$$k_\infty = \frac{Neutron\ production\ from\ fission\ in\ one\ generation}{Neutron\ absorption\ \ in\ the\ previous\ generation} \tag{2.1}$$

The infinite multiplication factor takes account of the neutron population in an infinitely large reactor. Since realistically, no reactor is infinitely large, the effective multiplication factor is conceptualized to take care of a reactor of finite size. A finite reactor must have a finite number of neutron leakages and thus another term that takes care of neutron leakage is added to the denominator of Equation (2.1) rewritten as equation (2.2):

$$k_{eff} = \frac{Neutron\ production\ from\ fission\ in\ one\ generation}{\begin{matrix}Neutron\ absorption\\ in\ the\ previous\ generation\end{matrix} + \begin{matrix}Neutron\ leakage\\ in\ the\ previous\ generation\end{matrix}} \tag{2.2}$$

k_{eff} is also defined as the product of six different factors sometimes called the “six factor formula”. It is written as

$$k_{eff} = L_f \rho L_{th} f \eta \varepsilon \tag{2.3}$$

where;

L_{th} = thermal non-leakage factor

L_f = fast non-leakage factor

ρ = resonance escape probability

η = reproduction factor

f = thermal utilization factor

ε = fast fission factor

These factors are mathematically expressed as;

$$L_{th} = \frac{number\ of\ thermal\ neutrons\ that\ do\ not\ leak\ from\ reactor}{number\ of\ neutrons\ that\ reach\ thermal\ energies} \quad (2.3a)$$

$$L_f = \frac{number\ of\ neutrons\ that\ do\ not\ leak\ from\ reactor}{number\ of\ fast\ neutrons\ produced\ by\ all\ fission} \quad (2.3b)$$

$$\rho = \frac{number\ of\ neutrons\ that\ reach\ thermal\ energy}{number\ of\ neutrons\ that\ start\ to\ slow\ down} \quad (2.3c)$$

$$\eta = \frac{number\ of\ fast\ neutrons\ produced\ by\ thermal\ fission}{number\ of\ thermal\ neutrons\ absorbed\ in\ the\ fuel} \quad (2.3d)$$

$$f = \frac{number\ of\ thermal\ neutrons\ absorbed\ in\ the\ fuel}{number\ of\ thermal\ neutron\ absorbed\ in\ any\ reactor\ material} \quad (2.3e)$$

$$\varepsilon = \frac{\text{number of fast neutrons produced by all fissions}}{\text{number of fast neutrons produced by thermal fissions}} \quad (2.3f)$$

For a 'critical' reactor, k_{eff} = 1. When a reactor has a value of $k_{eff} < 1$ it is said to be "subcritical" meaning that each generation of neutron is characterized by a decreasing neutron population (DOE, 1993). On the other hand, when a reactor has a value of $k_{eff} > 1$ it is said to be "supercritical" and it implies that each generation of neutron is characterized by an increasing neutron population.

Assuming N_0 the number of neutrons in the previous generation, and $N_0(k_{eff})$ be number of neutrons in the current generation.Then

$\{N_0(\mathrm{k_{eff}}) - N_0\}$ give the numerical change in neutron population (DOE, 1993). Taking the ratio of this change with $N_0(\mathrm{k_{eff}})$

$$\frac{\{N_0(\mathrm{k_{eff}}) - N_0\}}{N_0(\mathrm{k_{eff}})} \tag{2.4}$$

Cancelling N_0 out of equation (2.4), we obtain

$$\rho_{ex} = \frac{(k_{\mathrm{eff}}) - 1}{(k_{\mathrm{eff}})} \tag{2.5}$$

where;

ρ in Equation (2.5) represents the symbol for reactivity. ρ is measured in mk (pronounced as “millikay”), %k/k, pcm, among other units. A reactor is subcirtical when $\rho < 0$, supercritical when $\rho > 0$, and critical when $\rho = 0$.

2.3 Atom Density

The atom density isotopes or mixtures in the regions of the reactor can be calculated (SCALE, 2018) using equation (2.6).

$$\begin{cases} N_i = \frac{\rho N_A}{M_i} \\ N_{mix} = \frac{\rho N_A}{M_{mix}} \\ N_i = \frac{w_i \rho N_A}{M_i} \end{cases} \tag{2.6}$$

where;

ρ = mass density of the isotope or mixture

N_A= Avogadro’s number

M_i = Molar mass of the isotope

M_{mix} = Molar mass of the mixture

w_i = weight fraction or percentage by weight of the isotope

Alternatively, the atom densities of various isotopes in a mixture can also be calculated using Equation (2.7) if the atom density N_{mix} of the mixture is known.

$$N_i = \gamma_i N_{mix} \tag{2.7}$$

where γ_i is the isotope's natural abundance.

However, the homogenized atom densities of nuclides in the regions of a reactor are calculated by multiplying Equation (2.6) or Equation (2.7), by the effective volume fraction f_i of the nuclide in that region and summing over the nuclide in the region. This is given in equation (2.8) as:

$$N_z = \sum_i N_i \, f_i \tag{2.8}$$

where

N_z is the homogenized atom density of nuclide *i*

N_i is the region atom density of nuclide *i*

f_i is the effective volume fraction of nuclide *i*

2.4. The SCALE 6.2.3 code system

The SCALE Code System is a widely-used modeling and simulation suite for nuclear safety analysis and design that is developed, maintained, tested, and managed by the Reactor and Nuclear Systems Division (RNSD) of Oak Ridge National Laboratory (ORNL). SCALE provides a comprehensive, verified and validated, user-friendly tool set for criticality safety, reactor and lattice physics, radiation shielding, spent fuel and radioactive source term characterization, and sensitivity and uncertainty analysis. SCALE provides an integrated framework with dozens of computational modules including three deterministic and three Monte Carlo radiation transport solvers that are selected based on the desired solution strategy. SCALE includes current nuclear data libraries and problem-dependent processing tools for continuous-energy (CE) and multigroup (MG) neutronics and coupled neutron-gamma calculations, as well as activation, depletion, and decay calculations. SCALE includes unique capabilities for automated variance reduction for shielding calculations, as well as sensitivity and uncertainty analysis. SCALE's graphical user interfaces assist with accurate system modeling, visualization of nuclear data, and convenient access to desired results (Goluoglu *et al*, 2011).

2.4.1 Installation and testing of the SCALE 6.2.3 code system

The minimum computer requirement for installation of the code is a 4GB RAM computer system running on windows 7 or earlier versions (for users of a Windows Operating System). The code is recommended to be installed in drive C of a personal computer by first clicking on the SCALE-6.2.3-setup executable (.exe) file. The prompts are then followed to the end and a 'Fulcrum' graphical user interface shortcut is displayed on the desktop. Secondly, a Java development Environment (JDE) is installed in order to enable installation of the SCALE-6.2-data. Thirdly, the SCALE-6.2-data-setup (.jar) file is clicked and all the SCALE data files including ENDF libraries are selected and installed. In order to test the success of SCALE installation it is recommended to attempt to run several sample input problems using the 'Fulcrum' graphical user interface by clicking on the 'run' tab.

2.4.2. Relevant theoretical framework of SCALE

2.4.2.1 Time independent boltzmann transport equation

The general time independent Boltzman transport equation (SCALE Wieselquist *et al*, 2020) is written as

$$\overrightarrow{\Omega} \cdot \nabla\psi\left(\overrightarrow{r}, E, \overrightarrow{\Omega}\right) + \sum_t(\overrightarrow{r}, E)\,\psi\left(E, \overrightarrow{r}, \overrightarrow{\Omega}\right) = S\left(\overrightarrow{r}, E, \overrightarrow{\Omega}\right) \tag{2.9}$$

Equation (2.9) is a balance condition that states that the losses due to leakage (first term) and collisions (second term) must equal the source of neutrons, at some point in space $\overrightarrow{r}$, Energy E, and direction $\overrightarrow{\Omega}$ per unit volume and energy and solid angle. Other terms in the expression are $\sum_t(\overrightarrow{r}, E)$, the total macroscopic cross section of the medium, which is typically assumed *isotropic, and the flux,* $\psi\left(E, \overrightarrow{r}, \overrightarrow{\Omega}\right)$. Section 2.4.2.2 and 2.4.2.3 discusses the Boltzman transport equation solved by SCALE using deterministic approach (XSDRNPM) and Monte Carlo approach (KENO) respectively.

2.4.2.2 SCALE deterministic transport (XSDRNPM)

In multigroup schemes, the continuous-energy (CE) balance equations are converted to multigroup form by first selecting an energy structure and then writing a multigroup equivalent of the point equation which requires multigroup constants that tend to preserve the reaction rates that would arise from integrating the CE equations by group (Wieselquist *et al*, 2020). First, defining the following multi-group values for g,

$$\psi_g(x, \mu) = \int_g \; dE\psi(x, E, \mu) \tag{2.10}$$

and

$$\psi_g(x) = \int_{-1}^{1} d\mu\psi_g(x, \mu) \tag{2.11}$$

and

$$\sum_{tg}(x) = \frac{\int_g \; dE \sum_{tg}(x,E)\, W(x,E)}{\int_g \; dEW(x,E)}$$

where $W(x,E)$ is the weighting function used to compute the multigroup cross sections at a particular location and $\psi(x,E,\mu)$ is the angular flux as a function of angles expressed in direction cosine units; i.e., $\mu = cos\ \varphi$ and $\eta = cos\ \xi$.

The following multigroup form of 1-D equation (Wieselquist *et al*, 2020) solved by SCALE XSDRNPM code for a reactor with cylindrical geometry is:

$$\frac{\mu}{r}\frac{\partial\left(r\psi_g(r,\mu)\right)}{dr} - \frac{1}{r}\frac{\partial(\eta\mu)}{d\phi} + \sum_{tg}(r)\,\psi_g(r,\mu) = S_g(r,\mu) + F_g(r,\mu) + Q_g(r,\mu) \qquad (2.12)$$

In Equation (2.12), S_g, F_g, and Q_g are the scattering, fission, and fixed sources, respectively. The multigroup form of the fission source is

$$F_g(r,\mu) = \frac{\chi_g}{2\pi \mathrm{k}} \sum \overline{v\sum_{fg'}}(x)\psi_{g'}(x) \qquad (2.13)$$

where χ_g is the fraction of the fission neutrons that are produced in group g, and $v\sum_{fg'}$ is the average of the product of v, the average number of neutrons produced per fission and $\sum_f$, the fission cross section. Equation (2.12) is solved by XSDRNPM using discrete-ordinates difference approach. Details of this approach can be found elsewhere (Wieselquist *et al*, 2020).

2.4.2.2 SCALE monte carlo transport (KENO)

The equation KENO solves may be derived in the following manner, starting with the time dependent Boltzmann neutron transport equation (SCLE manual, 2018) which may be written as

$$\frac{1}{\mathrm{v}}\frac{\partial\Phi}{\partial t}(X,E,\Omega,t) + \Omega\ \cdot\nabla\Phi(X,E,\Omega,t) + \sum_t(X,E,\Omega,t)\Phi(X,E,\Omega,t)$$

$$= S(X,E,\Omega,t) + \int_{E'}\int_{\Omega'}\sum_s(X,E' \to E,\Omega' \to \Omega,t)\Phi(X,E',\Omega',t)d\Omega' dE' \qquad (2.14)$$

where

$\Phi(X,E,\Omega,t)$ = neutron flux (neutrons/cm^2/s) per unit energy at energy E per steradian about direction Ω at position X at time t moving at speed v corresponding to E;

$\sum_t(X,E,\Omega,t)$ = macroscopic total cross section of the media (cm^{-1}) at position X, energy E, direction Ω and time t;

$\sum_s(X,E' \to E,\Omega' \to \Omega,t)$ = macroscopic differential cross section of the media (cm^{-1}) per unit energy at energy E′ per steradian about direction Ω′ at position X, and time t for scattering to Energy E and direction Ω;

$S(X,E,\Omega,t)$ = neutrons/cm^3/s born at position X and time t per unit energy at energy E per steradian about direction Ω (excludes scatter source).

Defining $q(X,E,\Omega,t)$ as the total source resulting from the external source, scattering, fission, and all other contributions, the following relationship can be written (SCLE manual, 2018).

$$q(X,E,\Omega,t) = S(X,E,\Omega,t)$$

$$+ \int_{E'}\int_{\Omega'}\sum_s(X,E' \to E,\Omega' \to \Omega,t)\Phi(X,E',\Omega',t)d\Omega' dE' \qquad (2.15)$$

Combining Equations (2.14) and (2.15), assuming media to be stationary and ignoring time-dependence, yields

$$\Omega \cdot \nabla\Phi(X,E,\Omega) + \sum_t(X,E,\Omega)\Phi(X,E,\Omega) = q(X,E,\Omega) \qquad (2.16)$$

The continuous energy mode solution procedure of SCAALE applied in this work is as follows:

Using the relationship $X' = X - R\Omega$, using an integrating factor on both sides of Equation (2.16), and defining

$$T(R) = \int_0^R \Sigma_t(X - R'\Omega, E)dR',$$

the following equation can be written

$$\Phi(X, E, \Omega) = \int_0^\infty q(X - R\Omega, E, \Omega)e^{-T(R)}dR \quad (2.17)$$

At this point, the problem becomes an eigenvalue problem (SCLE manual, 2018). If there is no external source, the source may be defined as

$$q(X, E, \Omega) = \int\int d\Omega' dE' \Phi(X, E', \Omega')\Sigma_s(X, E' \to E, \Omega' \cdot \Omega) + \frac{1}{k}Q'(X, E, \Omega) \quad (2.18)$$

where

k is the largest eigen value of the integral equation,

$\mathbf{Q}'(\mathbf{X}, \mathbf{E}, \Omega)$ is the is the fission source at position X for energy E and direction Ω (all fission contributions to point E from all energy points in the previous **generation),**

$\Sigma_s(X, E' \to E, \Omega' \cdot \Omega)$ is the scattering cross section for scattering at position X from energy point E and direction Ω' to energy point E and direction Ω.

Assuming the fission neutrons to be isotropic, the fission source $Q'(X,E,\Omega)$ can be written as

$$Q'(X, E, \Omega) = \frac{1}{4\pi}\int_{E'}\int_{\Omega'} d\Omega' dE' \Phi(X, E', \Omega')\chi(X, E' \to E)v(X, E')\Sigma_f(X, E') \quad (2.19)$$

Where

$\chi(X, E' \rightarrow E)$ is the fraction of neutrons born at energy point E from fission at energy point E′ in the media at position X,

$v(X, E')$ is the number of neutrons resulting from a fission at energy point E′ at position X,

$\sum_f(X, E')$ is the macroscopic fission cross section of the material at position X for a neutron at energy point E′.

Substituting Equation (2.18) into Eq. (2.17) yields the following equation:

$$\Phi(X, E, \Omega) = \int_0^{\infty} \mathrm{dR}\ \mathrm{e}^{-\mathrm{T(R)}} \left\{\frac{1}{\mathrm{k}}(X - \mathrm{R}\Omega, E, \Omega)\right\}$$

$$+ \int_{E'} \int_{\Omega'} d\Omega' dE' \Phi(X, E', \Omega') \sum\nolimits_s (X, E' \rightarrow E, \Omega' \cdot \Omega) \tag{2.20}$$

The definition of k may be given as the ratio of the number of neutrons produced in the (n + 1)*th* generation to the number of neutrons produced in the n*th* generation or the largest eigenvalue of the integral equation (SCALE manual, 2018). Using Equation (2.19), Equation (2.17) can be written as

$$\Phi(X, E, \Omega) = \int_0^{\infty} \mathrm{dR}\ \mathrm{e}^{-\mathrm{T(R)}} \left\{\frac{1}{\mathrm{k}} \int_{E'} \int_{\Omega'} v(X - \mathrm{R}\Omega, E') \sum\nolimits_f (X - \mathrm{R}\Omega, E') \chi(X - \mathrm{R}\Omega, E' \rightarrow E)\ \Phi(X - \mathrm{R}\Omega, E', \Omega') dE' \frac{\mathrm{d}\Omega'}{4\pi} + \int_{E'} \int_{\Omega'} d\Omega' dE' \Phi(X - \mathrm{R}\Omega, E', \Omega') \sum\nolimits_s (X - \mathrm{R}\Omega, E' \rightarrow E, \Omega' \cdot \Omega)\right\} \tag{2.21}$$

Writing Equation (2.21) in generation notation, multiplying and dividing certain terms by St(X,E) and multiplying both sides of the equation by ν(X,E) $\sum_f$ (X,E), yields the following equation, which is solved by KENO in the continuous energy mode:

$$\frac{\nu(X,E)\,\Sigma_f(X,E)}{\Sigma_t(X,E)}\Sigma_f(X,E)\;\Phi_n(X,E,\Omega) = \frac{\nu(X,E)\,\Sigma_f(X,E)}{\Sigma_t(X,E)}\Sigma_t(X,E)\;\int_0^\infty \mathrm{dR}\;\mathrm{e}^{-\mathrm{T(R)}}$$

$$\left\{\frac{1}{\mathrm{k}}\int_{E'}\int_{\Omega'}\frac{\nu(X-\mathrm{R}\Omega,E')\Sigma_f(X-\mathrm{R}\Omega,E')}{\Sigma_t(X-\mathrm{R}\Omega,E')}\chi(X-\mathrm{R}\Omega,E'\to E)\;\Phi_{n-1}(X-\mathrm{R}\Omega,E',\Omega')dE'\frac{\mathrm{d}\Omega'}{4\pi}+\right.$$

$$\left.\int_{E'}\int_{\Omega'}\frac{\Sigma_s(X-\mathrm{R}\Omega,E',\Omega\cdot\Omega')}{\Sigma_t(X-\mathrm{R}\Omega,E')}\Sigma_t(X-\mathrm{R}\Omega,E')\;\Phi_n(X-\mathrm{R}\Omega,E',\Omega')dE'\mathrm{d}\Omega'\right\} \tag{2.22}$$

where n indicates the n*th* generation and n-1 is the (n − 1)*th* generation. The left-hand side of Equation (2.22), $\nu(X,E)\,\Sigma_f(X,E)\,)\;\Phi_n(X,E,\Omega)$ is the fission production for the n*th* generation.

The solution strategy used by KENO solves Equation (2.22) by using an iterative procedure. The fission production at point X at energy point E due to neutrons in the (n − 1)*th* generation, normalized to the system multiplication, is

$$\frac{1}{\mathrm{k}}\int_{E'}\int_{\Omega'}\frac{\nu(X-\mathrm{R}\Omega,E')\Sigma_f(X-\mathrm{R}\Omega,E')}{\Sigma_t(X-\mathrm{R}\Omega,E')}\chi(X-\mathrm{R}\Omega,E'\to E)\;\Phi_{n-1}(X-\mathrm{R}\Omega,E',\Omega')dE'\frac{\mathrm{d}\Omega'}{4\pi}$$

The collision points used in KENO are chosen by selecting path lengths from the distribution

$$\mathrm{e}^{-\mathrm{T(R)}}$$

which is the probability of transport from any position X − RΩ to position X.

The first collision density of neutrons at energy E per unit solid angle about Ω resulting from the fission source produced by the (n − 1) generation (SCLE manual, 2018), normalized to the system multiplication, is

$$\Sigma_t(X,E)\;\int_0^\infty \mathrm{dR}\;\mathrm{e}^{-\mathrm{T(R)}}\int_{E'}\int_{\Omega'}\frac{\Sigma_s(X-\mathrm{R}\Omega,E')(X-\mathrm{R}\Omega,E')}{\Sigma_t(X-\mathrm{R}\Omega,E')}$$

$$\chi(X - \mathrm{R}\Omega, E' \to E)\, \Phi_{n-1}(X - \mathrm{R}\Omega, E', \Omega') dE' \frac{\mathrm{d}\Omega'}{4\pi}$$

The scattering source at position X emerging at energy E and direction Ω resulting from previous collisions in the same generation, is

$$\int_{E'} \int_{\Omega'} \frac{\sum_{\mathrm{s}}\left(X - \mathrm{R}\Omega, E', \Omega \cdot \Omega'\right)}{\sum_{\mathrm{t}}(X - \mathrm{R}\Omega, E')} \textstyle\sum_{\mathrm{t}}(X, E')\, \Phi_n(X, E', \Omega') dE' \mathrm{d}\Omega'$$

The collision density at energy E, per solid angle about Ω is

$$\textstyle\sum_{\mathrm{t}}(X, E) \displaystyle\int_0^{\infty} \mathrm{dR}\, \mathrm{e}^{-\mathrm{T(R)}} \int_{E'} \int_{\Omega'} \frac{\sum_{\mathrm{s}}\left(X - \mathrm{R}\Omega, E', \Omega \cdot \Omega'\right)}{\sum_{\mathrm{t}}(X - \mathrm{R}\Omega, E')} \textstyle\sum_{\mathrm{t}}(X - \mathrm{R}\Omega, E')\, \Phi_n(X - \mathrm{R}\Omega, E', \Omega') dE' \mathrm{d}\Omega'$$

The total collision density times $\frac{\nu_{\mathrm{g}}(X,E) \sum_{\mathrm{fg}}(X,E)}{\sum_{\mathrm{tg}}(X,E)}$ is the relationship from which KENO picks the source points for the next generation.

2.5 Neutronic Parameters

Determination of neutronic parameters is essential whenever any form of modification is made to a reactor. Parameters like the control rod worth, core excess reactivity, shutdown margin are to be known with accuracy because they are related to the fuel element and are thus essential for conversion. A brief discussion of these parameters is given in sub-section 2.5.1 – 2.5.3.

2.5.1 Control rod worth (CRW)

The CRW of a reactor is the measure of the total reactivity change associated with complete withdrawal of a Control Rod. It can be calculated using neutron transport codes Ibikunle *et al* (2018). This is done by calculating the k_{eff} with CR ‘in’ (completely inserted into the core) and the k_{eff} with CR ‘out’ (completely withdrawn from the core) and then substituting their respective values into equation (2.23).

$$CRW = \frac{k_{eff_{out}} - k_{eff_{in}}}{k_{eff_{out}} \times k_{eff_{in}}} \quad (2.23)$$

2.5.2 Clean cold core excess reactivity (CCCER)

The CCCER of a nuclear reactor is a measure of the deviation of a freshly loaded core from criticality (CNSC, 2003). It is calculated computationally by obtaining the k_{eff} of the fresh reactor core with CR "out" using transport codes. The value of the k_{eff} is then substituted in Equation (2.5) to obtain the core excess reactivity.

2.5.3 Shutdown margin

The shutdown margin of a nuclear reactor is defined as the negative reactivity by which the reactor is critical if all CRs were fully inserted in the core except the most reactive one (being the one with the highest worth and usually called the safety rod which is assumed to be fully withdrawn). In other words, shutdown margin (SDM) is the difference between the core excess reactivity and the CRW (Ibikunle *et al*, 2018) given by Equation (2.24)

$$SDM = CRW - \rho_{ex} \quad (2.24)$$

2.6. Fuel Burnup/Depletion

Fission products or fission fragments produced during a fission reaction in the reactor core possess large absorption cross section. As the reactor continues to operate, these fission fragments build up in the reactor core and reduce the core reactivity there by contributing to the depletion of the reactor fuel. Fission fragments, also known as poisons, are put into serious consideration in thermal reactor design. There are important fission products/poisons of concern in reactor core design and analysis. The concentrations and activities of individual fission fragment in nuclear fuel have application in radiation hazard assessments, spent fuel analysis and so on (Omar, 2013).

The term "Burnup" measures how much thermal energy is obtained from an operation of nuclear reactor. It can be calculated in two ways:

i. As a fraction of atoms that underwent fission in percentage (% FIMA, fission per initial metal atom).

ii. As the actual energy released per mass of initial fuel in megawatts-days per metric ton of heavy metal (MWd/tHM) or other related units (Duderstadt and Hamilton, 1976).

The following sub-section discusses the theory of fuel burnup.

2.6.1 Fuel depletion equation

A coupled set of production-destruction equation is useful in describing the concentration of different fuel isotopes in the reactor. The general production-destruction equation (Duderstadt and Hamilton, 1976) satisfied by a fission product specie j is:

$$\frac{\partial n}{\partial t} = \gamma_j \Sigma_f \phi + \sum_i \left(\lambda^{i\to j} + \sigma^{i\to j}\phi\right) n_i - \left(\lambda^j + \sigma_a^j \phi\right) n_j \qquad (2.25)$$

where;

γ_j is the fraction of fission events that produces a fission product species j,

$\lambda^{i\to j}$ is the decay rate of isotope i to produce isotope j (beta, alpha, neutron, etc. decay)

$\sigma^{i\to j}$ is the transmutation cross section for the production of isotope j by neutron capture in isotope j

It has been shown that regardless of whether the fission products undergo transmutation and decay, the total inventory of direct fission products plus their progeny increases in time as

$$\frac{\partial n_{fp}}{\partial t} = \sum_j \frac{\partial n_j}{\partial t} = \sum_j \gamma_j \Sigma_f \phi \qquad (2.26)$$

2.6.2 Solution to the fuel depletion equation

The typical approach to solving the depletion equation from a known time t_i of fuel composition to an unknown time to time t_i +1 is: (i) determination of the appropriate multigroup constants for the composition at t_i, (ii) determination of the critical CR positions or soluble poison concentration by solving the multigroup diffusion equations for the flux at t_i (adjusting the control rod positions or boron concentration until the reactor is critical), and (iii) integrating the various fuel and fission product production–destruction equations from t_i to t_i +1. Note that the neutron flux solution could be made with a multigroup transport calculation or with multigroup or continuous energy Monte Carlo calculation, and the preparation of cross sections could involve infinite media spectra and unit cell homogenization calculations (Weston, 2007) or could be based on fitted, precomputed constants. The integration of the production–destruction equations can be for a large number of points, using the neutron flux at each point; for each fuel pin, using the average flux in the fuel pin; for each fuel assembly, using the average flux over the fuel assembly; and so on (Weston, 2007).

Assuming that the flux is constant in the interval $t_i < t < t_{i+1}$, the production–destruction equations can be written in matrix notation as:

$$\frac{d\boldsymbol{N}(t)}{dt} = \boldsymbol{A}\big(\phi(t_i)\big)\boldsymbol{N}(t) + \boldsymbol{F}\big(\phi(t_i)\big), t_i \leq t \leq t_{i+1} \tag{2.27}$$

The general solution to this equation is of the form

$$\boldsymbol{N}(t_{i+1}) = exp[\boldsymbol{A}(t_i)\Delta t]\boldsymbol{N}(t_i) + A^{-1}(c)\{exp[A(t_i)\Delta t] - 1\}\boldsymbol{F}(t_i) \tag{2.28}$$

2.7 Design Basis of the MNSR Fuel Lattice and Fuel Element

At the “heart” of the NIRR-1 is a birdcage-shaped device known as the fuel cage and made of aluminum alloy, consisting of the following: an upper grid plate, a lower grid plate, a control rod guide tube and 4 tie rods. Ten concentric circles of lattices are arranged in the upper and lower grid plates. In total there are 355 lattice positions in the grid, amongst which the central one is reserved for the control rod guide tube while the 4 tie rods are evenly arranged on the eighth circle. The 350 lattice positions are preserved for fuel rods. The lattice pitch between circles and rods are listed in Table 2.1. The MNSR fuel loading by design is 347 fuel rods; and 3 dummy rods which are aluminum alloy, identical in shape and dimensions to the fuel rods.

Table 2.1 The MNSR Fuel Cage Lattice

Circle No.	0	1	2	3	4	5	6	7	8	9	10
Lattice No.	1	6	12	19	26	32	39	45	52	58	65
Diameter of circle (mm)	0	21.9	43.8	65.7	87.6	109.5	131.4	153.3	175.2	197.1	219
Radial pitch (mm)	0	11.47	11.47	10.86	10.98	10.78	10.58	10.70	10.58	10.68	10.58

2.8 Safety Features of the NIRR-1 MNSR

A very important feature of NIRR-1 MNSR and similar facilities is the inherent safety due to limited core excess reactivity designed to be less than ½ β_{eff} and large negative total temperature coefficient of reactivity. How this inherent safety feature works is explained as follows: At low power, when fission rate is too low to generate much heat, addition of positive reactivity via control rod withdrawal has been shown to produces an exponential rise (i.e a constant log rate increase). Whenever an increase in power level result in a significant heating, leading to temperature changes in the fuel, moderator and coolant, there will be a change in reactivity--an effect that occur very rapidly (CNSC, 2003). At low thermal neutron flux, an exponential increase in power will occur. However, as the temperature of the fuel increases due to increase in power, the reactivity will decrease and cause the rate of power increase to slow. Later, the reactivity will decrease even more as the light water (moderator) becomes warmer. The total decrease in reactivity will eventually be enough to cause the reactor to become subcritical and as such the power will reach a maximum and begin dropping. This behavior of the reactor is self-regulating since temperature changes induced by a power increase reduces reactivity and so prevents power from increasing indefinitely (CNSC, 2003). This phenomenon is called negative feedback of reactivity and it characterizes the inherent safety of the NIRR-1 MNSR.

In order to prevent accident or power excursion that will eventually become a nuclear disaster, the NIRR-1 MNSR was designed to incorporate the aforementioned inherent safety measures and other inherent safety measures to prevent radiation leakage. These two major provisions made in the design to increase the safety margin and to enhance the inherent safety of the reactors are summarized below (Ahmed *et. al*., 2006).

I. The ratio of hydrogen to ^{235}U is 197: This increases the degree of under-moderation process of the core and thereby increases the negative temperature reactivity feedback.

II. The ratio of the core height to diameter was optimized to 1.0: this is to take care of axial neutron leakage fraction, to increase the coupling of outlet and inlet flow, mixing of the water coolant and to enable part of the warm coolant to directly enter the core, to shorten the time of temperature feedback and to increase the worth of the top beryllium reflectors-used for the extension of the lifetime of the core.

2.9 Review of Related Previous Works

Conversion study by Lell and Matos (2005) using Monte Carlo Neutron Particle (MCNP) model, found that the excess reactivity of the generic MNSR fueled with UO_2, U_3Si_2-Al, U_3Si-Al and U_9Mo-Al dispersion fuels enriched to 19.75% and the HEU core were comparable and suitable for the generic MNSR. Although the results of the excess reactivity of the HEU and LEU cores match each other, the value of 8.7 mk reported was more than 100 % greater than the maximum allowed value of 4.0 mk for MNSRs. The implication of this is that the safety limits of real operating MNSRs such as CRW, SDM and SRF are exceeded because the model considered a generic design. Hence, the model cannot be used for detailed reactor analysis of actual operating MNSRs. Consequently, there is a need to develop a model for specific MNRSs such as the NIRR-1 as well as use the model developed for detailed analysis of the reactor. This is the focus of the present study.

In examining the core performance with 12.5% enriched UO_2, the generic MNSR core lifetime was predicted using the REBUS-3 code which applies a deterministic model (Liaw and Matos, 2007). It was found that an MNSR core with LEU UO_2 12.5% fuel and a power level of 33 kW can be operated ~25% longer than the HEU core operated at 30 kW. Both cores, as predicted, had the same thermal neutron flux in the experiment positions. Although core lifetime analyses were performed by Liaw and Matos, (2007), the study was entirely dedicated to the UO_2 fuel without making recourse to the alternate U_3Si_2-Al, U_3Si-Al and U_9Mo-Al dispersion fuels. Also, the uranium enrichment, number of active fuel pins and dummy pins in the core lattice used is not the same with the 13% enrichment, 335 active fuel pins and 15 dummy pins of the ‘as-built’ NIRR-1 UO_2 core studied in the present analysis.

Jonah *et al*. (2009) conducted a feasibility study of NIRR-1 MNSR conversion to LEU fuel using the MCNP computer code. They reported 12.45% as optimum enrichment of ^{235}U for UO_2 LEU fuel and initial excess reactivity maintained. They also reported the suitability of the U_3Si_2-Al, U_3Si-Al and U_9Mo-Al dispersion fuels enriched to 19.75% for the NIRR-1. The study was dedicated to the UO_2 fuel and only neutronic parameters of the U_3Si_2-Al, U_3Si-Al and U_9Mo-Al dispersion fuels were considered. Similar to the work of Lell and Matos (2007) the uranium enrichment, number of active fuel pins and dummy pins in the core lattice used is not the same with the 13% enrichment, 335 active fuel pins and 15 dummy pins of the 'as-built' NIRR-1 UO_2 core analyzed in the present study.

Estimation of fuel burnup Rate for core conversion for the NIRR-1 fueled with 19.75% enriched UO_2 using VENTURE PC Code was carried out by Rabba *et al* (2017). The model developed by the authors was a 2D model which did not explicitly represent the fuel pins or other regions of the reactor there by resulting in the overestimation of neutronic and fuel cycle parameters.. Consequently, a new model of the NIRR-1 is required. In the present study an attempt is made to develop a new model of the NIRR-1 using SCALE 6.2.3 code system.

Ibikunle (2018) investigated the same neutronic parameters as Lell and matos (2005) and the excess reactivity calculations by Jonah *et al* (2009), using the same MCNP model implemented through parallel computing and found that the U_3Si_2-Al, U_3Si-Al and U_9Mo-Al dispersion fuels were suitable for the NIRR-1 MNSR with an excess reactivity of about 4.8 mk. The study failed to perform depletion analyses of any of the fuels and this could affect the analysis and acceptability of the general performance of the fuels for commercial use in MNSRs because depletion analysis provide information on the fuel burnup rate, core composition changes with time and their effects on reactivity, ^{239}Pu buildup and core lifetime.

Rabba *et al*, (2020) performed depletion analysis of the NIRR-1 fuel with 19.75% Enriched UO_2 material. Their work demonstrated that the ratio of hydrogen to Uranium affects the reactivity of the reactor. The model approach and fuel characteristics used in the study are different from that of the present study. The present work is a study on the depletion performance of the as-built UO_2 and alternate U_3Si_2-Al, U_3Si-Al and U_9Mo-Al fuels, for the NIRR-1 using the SCALE 6.2.3 code package.

SCALE 6.2.3 was used to estimate the core lifetimes of the NIRR-1 HEU and as-built LEU core (Simon et al, 2021). The core lifetime of the LEU core was found to be higher than that of the HEU core. However, the estimate of the reactor core lifetime was made without consideration of the xenon reactivity worth which has negative reactivity effect on the core excess reactivity of the NIRR-1 and consequently affects the accuracy of core lifetime estimates.. In addition, detailed neutronic analysis of the core was not performed as the aim of the study was to compare the core lifetimes of the HEU and LEU core. Hence, the safety limits of the core such as CRW, SDM and SRF where not estimated. The estimates of these safety parameters are important for critical assessment of the capability of SCALE 6.2.3 for criticality safety analysis of the NIRR-1. In addition Simon *et al* (2021) did not consider alternate fuels such as the U_3Si_2-Al, U_3Si-Al and U_9Mo-Al fuels which are also important in analyzing the core lifetime performance of LEU cores as compared to HEU for the NIRR-1. Furthermore, the model developed did not take into account support structure. These structures are made of aluminum which has negative reactivity effect and affects the accuracy of the CCCER estimate. Consequently, the present study attempts to develop a new model of the NIRR-1 and estimate criticality safety parameters such as CCCER, CRW, SDM and SRF of the NIRR-1. Additionally, fuel depletion analysis for the as-built core and alternate cores is carried out to estimate the fuel burnup and analyze the effect of core composition changes on reactivity. Furthermore core lifetime estimates are made taking into account ^{135}Xe reactivity worth.

Simon *et al* (2022) performed radiological consequence analysis of the NIRR-1 as-built LEU UO2 core. In doing so, SCALE 6.2.3 code was used to estimate the total core inventory of the reactor for use as source term for the radiological consequence analysis. The main focus of the study was an analysis of a hypothetical accident scenario. Hence, detailed neutronic analysis of the as-built core was not presented and this is important for criticality safety assessment of the reactor. The present study is a detailed analysis of the neutronic parameters of the as-built LEU core of the NIRR-1 as well as alternate U_3Si_2-Al, U_3Si-Al and U_9Mo-Al fuels using SCALE 6.2.3 code.

CHAPTER THREE

3. MATERIALS AND METHOD

3.1 Introduction

This chapter presents a list of the materials used in this work and the procedures for the input parameters and input file preparation used for the all the models developed for the NIRR-1 MNSR using SCALE 6.2.3.

3.2 Materials

The materials used in this work are the SCALE 6.2.3 code system and a personal computer having 16GB RAM, 250GB SSD Memory and operating on a windows 10 operating system.

3.3 Methodology

In order to produce an accurate model of the NIRR-1 MNSR using the SCALE 6.2.3 code package, our approach was to first divide the NIRR-1 into its major components, which included the fuel region (represented by a unit fuel cell model), the control region (represented by a control cell model) and regions outside the fuel region. The individual components (regions) were then homogenized to produce a 1-D XSDRN full core multiregion model. Secondly, the individual components were further divided into smaller units for the development of a detailed 3-D KENO-VI model. This information was then supplied to the TRITON code and KENO-VI code to implement an authomated sequence of cross section library/transport calculation for the 1-D TRITON-XSDRN and 3-D KENO-VI NIRR-1 model respectively. All transport calculations were first done for the NIRR-1 HEU core and benchmarked with measured data and MCNP result to demonstrate the fidelity of the SCALE code package. The calculations for the LEU cores were then performed to obtain the neutronic and initial core loading requirements of the cores for further depletion studies. The results of the calculations for the alternative LEU cores were benchmarked with HEU calculated data whereas the result of the as-built UO_2 was benchmarked with only measured data. The two models, a simplified 1-D TRITON-XSDRNPM deterministic model and a detailed 3-D KENO-VI Monte Carlo model developed in the present work was necessary to examine the model that results in the best comparable neutronic parameters between measurement and calculation at the Beginning of Cycle (BOC) for the NIRR-1.

3.3.1 Geometry, Material Layout and Material Composition Data for Regions in the 1-D TRITON-XSDRN and 3-D KENO-VI NIRR-1 MNSR Models.

The major components of the NIRR-1 in our 1-D model included the control, fuel, reflector, water (inside the vessel), vessel, and water (outside the vessel) regions. This partitioning of the NIRR-1 into 6 zones (regions) represented a slice through the center of the NIRR-1 core excluding all the irradiation tubes, cadmium regulators and shim tray. The control region represented a homogenized mixture of cadmium poison material with SS clad, water plus the guide tube which is made up of aluminum for the HEU core. The fuel region is a homogenized mixture of the fuel with aluminium clad and water zone surrounding each fuel pin. However, for the as-built LEU core, the material for the guide tube and dummy pins was replaced with Zircalloy-4 which is consistent with the as-built UO_2 LEU core. The NIRR-1 MNSR fuel cell model for the NIRR-1 fuel pin consisted of three regions, namely: the active fuel region, the clad, and the moderator (water) region. This fuel cell model for the fuel pins is illustrated in Figure 3.1.

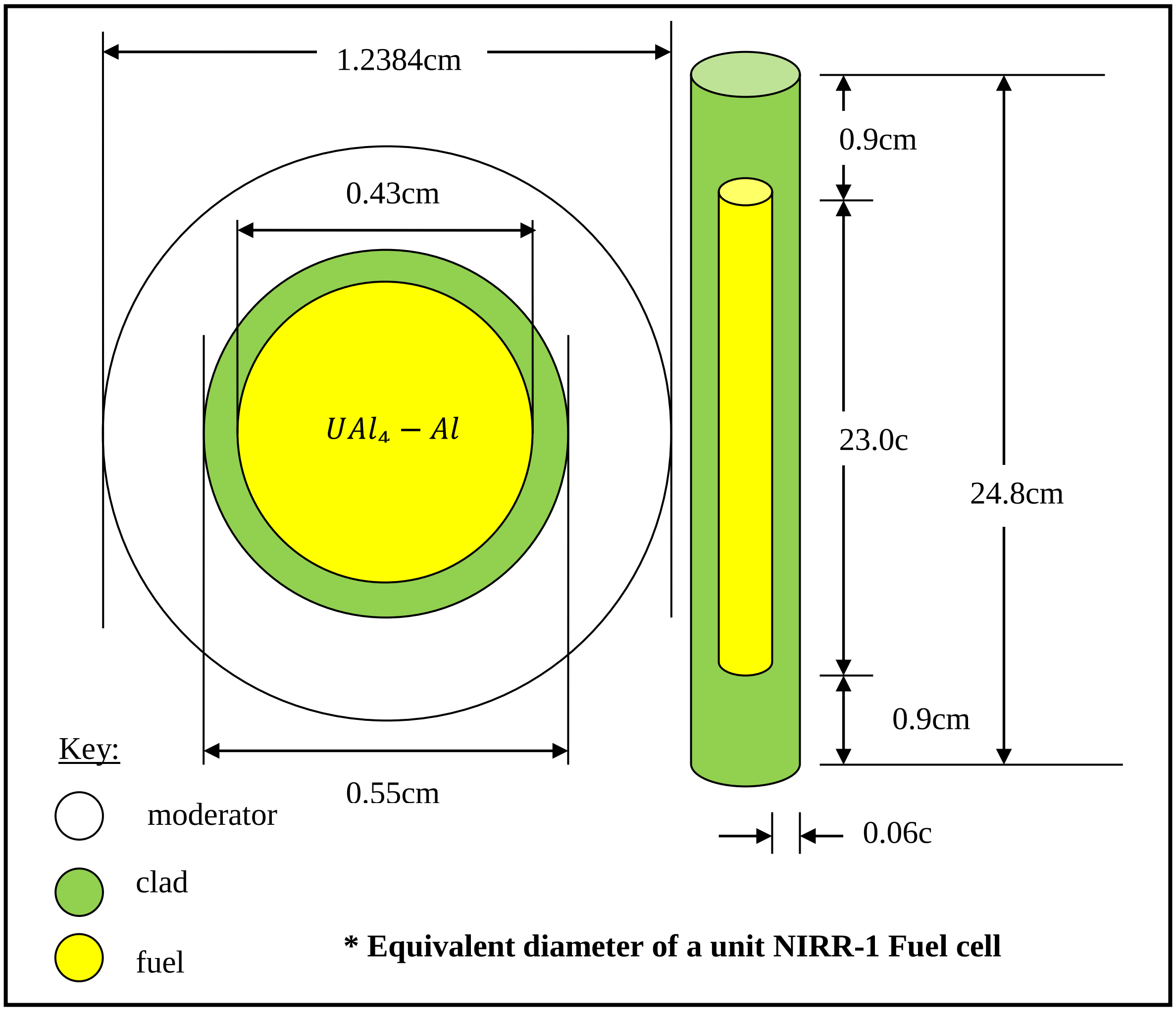

Figure 3.1: The Fuel Cell and the Fuel Rod Model for NIRR-1

The characteristics of the active fuel material used for the fuel cell model of the standard UAl_4-Al HEU core, the as-built NIRR-1 MNSR UO_2 fueled core, U_3Si_2-Al, U_3Si-Al and U_9Mo-Al LEU are presented in Appendix I and II. Although the standard (reference) HEU is made up of 347 active fuel pins, and 3 dummy pins, the as-built UO_2 core is made up of 335 active fuel pins and 15 dummy pins. However, both cores have 4 tie rods. The fuel characteristics used in our model for the U_3Si_2-Al, U_3Si-Al and U_9Mo-Al alternative LEU cores was chosen in order to maintain the core configuration of 347 pins and the fuel pin outer diameter of 5.5 mm of the reference HEU core. However, the volume fraction of the dispersed phase of the U_3Si_2-Al, U_3Si-Al and U_9Mo-Al LEU cores was varied for each of the fuels such that the core excess reactivity is kept approximately the same as the HEU benchmark core. The final volume fractions equivalent of the alternative LEU density in fuel meat used for our simulation were 39.0 vol-%, 37.7 vol-% and 38.2 vol-% for the U_3Si_2-Al, U_3Si-Al and U_9Mo-Al LEU fuels.

For the 1-D model, the reflector region represented a 100% beryllium region. This was because the homogenized atom density of the inner irradiation tubes in the reflector region is negligible compared to that of the beryllium in the same region. It was also difficult to physically introduce the irradiation channels in the reactor into the model. Similarly, the outer irradiation region was also treated as 100% water zones for the above reasons. The water region outside the reactor vessel is infinite as compared to the neutron mean free path and only about 40% of this region (Salawu, 2013) was included in our 1-D TRITON-XSDRNPM model. The geometry of the six zones for the NIRR-1 MNSR 1-D TRITON-XSDRNPM model is presented in Table 3.1.

Table 3.1 Geometry/Zones in the Full Core 1-D TRITON-XSDRNPM Model

Zone number	zone width (cm)	total distance (cm)	Zone Number	Material ID	Number of mesh
control	0.6	0.60	1	1	5
fuel	10.95	11.58	2	2	22
reflector	10.2	21.75	3	3	21
Water (inside)	8.25	30.00	4	4	15
vessel	1	31.00	5	5	2
Water (outside)	40	71.00	6	6	60

Figure 3.2a shows the geometry and material layout of the NIRR-1 while Figure 3.2b shows the 1D model of the NIRR-1 in the x-direction with control rod fully inserted into the core for the purpose of clarity. The case with control rod fully withdrawn from the core is similar to this figure except that the poison material in the control region is replaced with water.

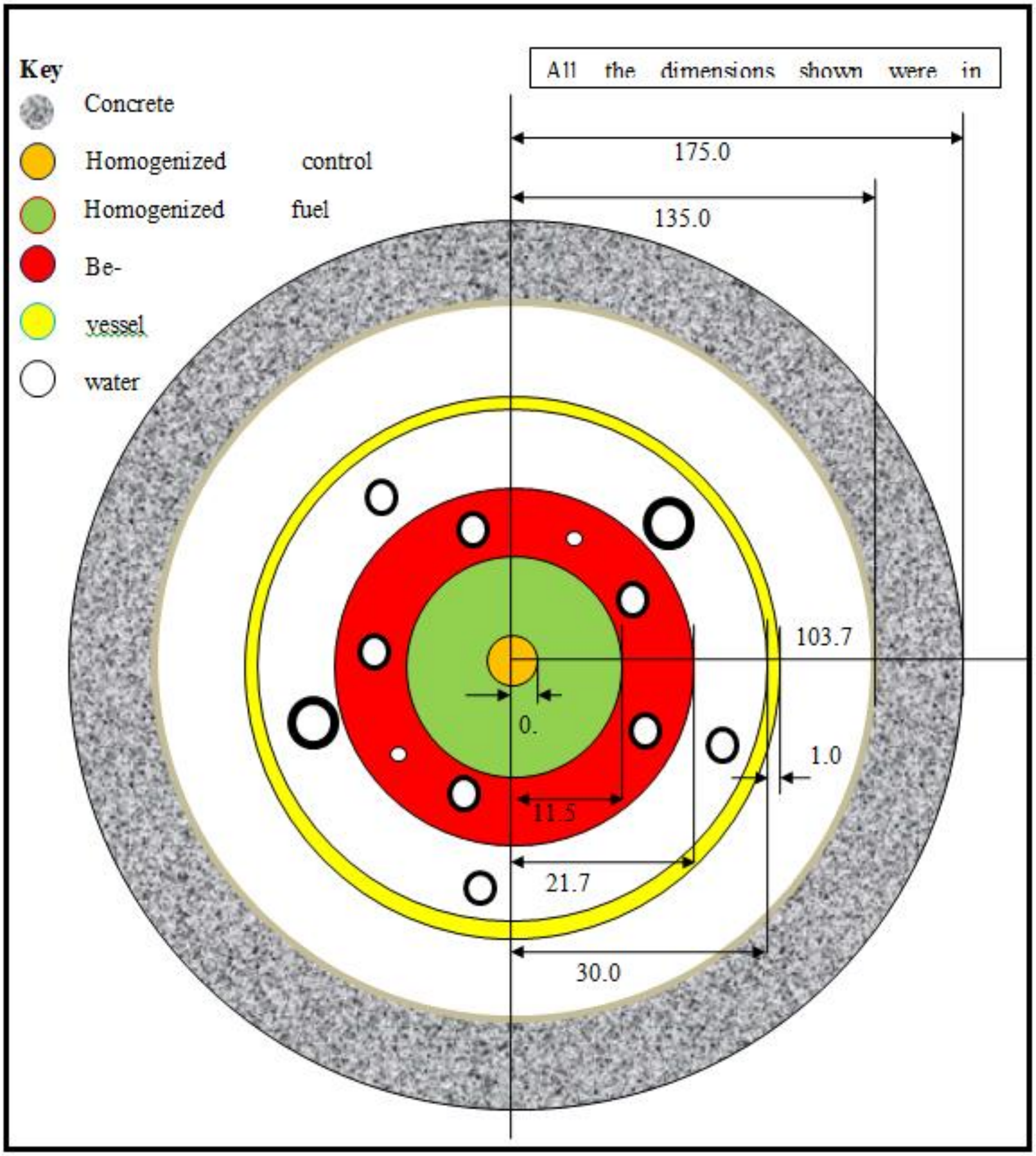

Figure 3.2a: The Geometry and Dimensions of Various Components in the NIRR-1 MNSR (Top View)

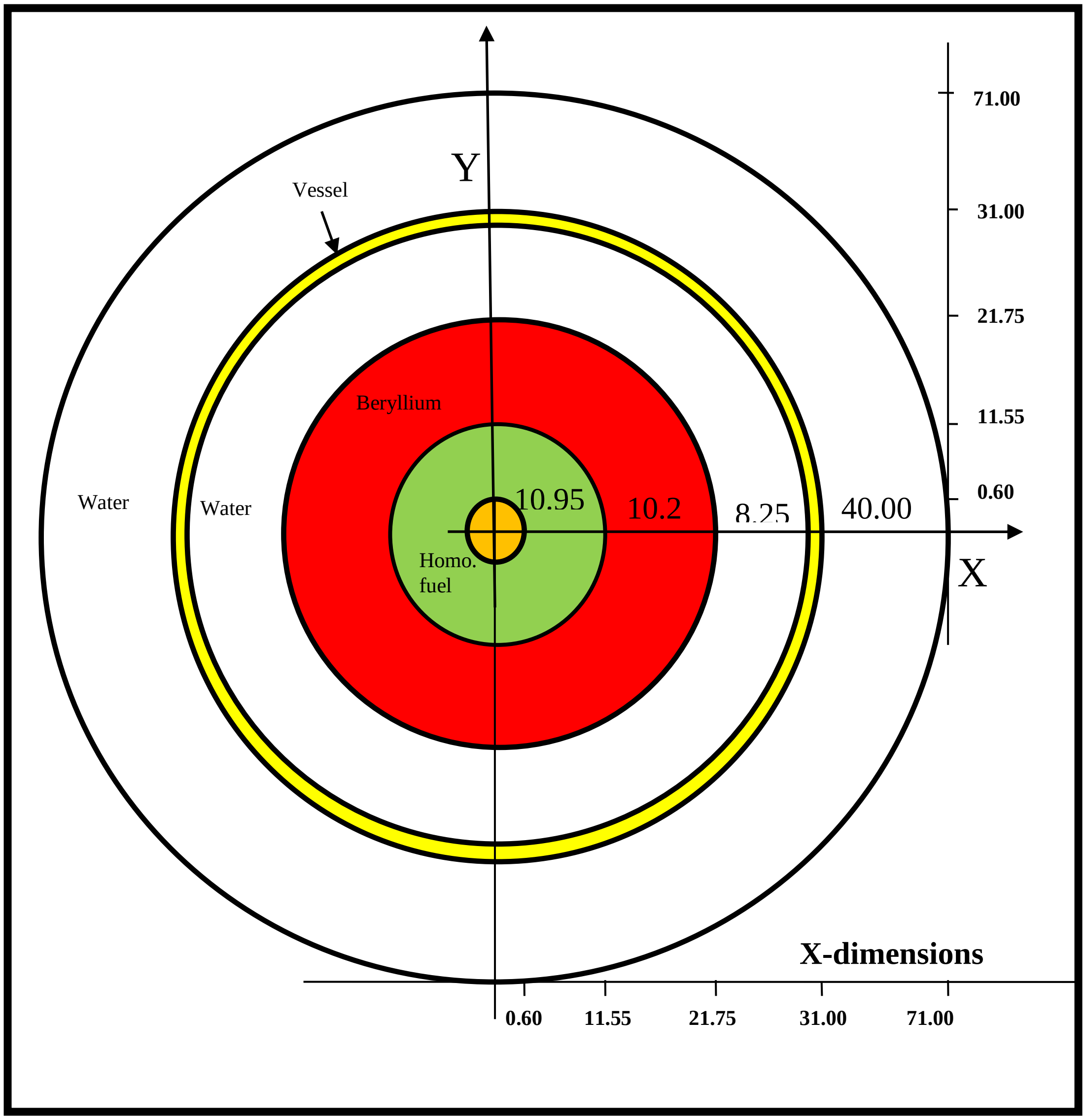

Figure 3.2b The 1-D TRITON-XSDRNPM full core model for NIRR-1 MNSR (with "control in)

In the 3-D KENO-VI model, the lattice specifications of the NIRR-1 core (Table 2.1) were used to explicitly define the core region. The core was modelled as a single unit of ten (10) concentric circles with fuel pins in their lattice positions surrounded by water and with the control region at the center of the assembly. The concentric circles were separated by varying radial pitch as shown in III.3 (Appendix III). All other regions including the control, irradiation sites, cadmium regulators, shim tray, annular and bottom reflector, fission chambers, vessel and slant tube, where modeled explicitly in the 3-D KENO-VI model using different units.

In Figure 3.3(a), the water in the pool makes it difficult to see the reactor vessel and slant tube but this is immediately visible when the pool water is hidden as shown in Figure 3.3(b). In Figure 3.3(c) and 3.3(d), however, the water in the vessel and the vessel respectively were hidden for 3-D visual verification of other reactor components. The shim tray was hidden in

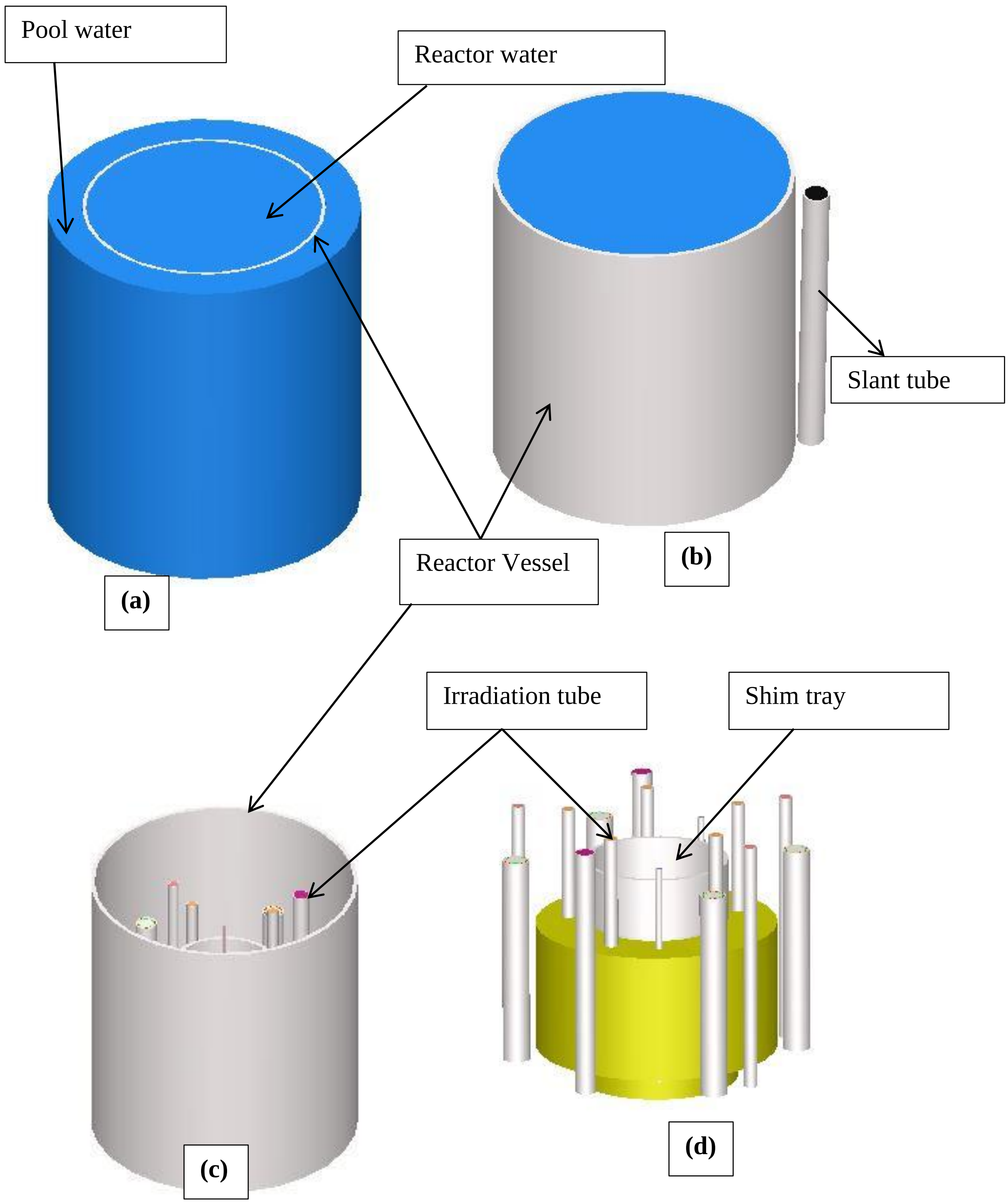

Figure 3.3: 3D KENO-VI Model of the NIRR-1 showing (a) the reactor with poolwater (b) without pool water (c) without pool and reactor water (d) without vessel

Figure 3.4(a) to have a closer look at the annular reflector and the top of the reactor core. In addition, a 3D KENO-VI model of the reactor core with CR fully withdrawn is shown in Figure 3.4(b).

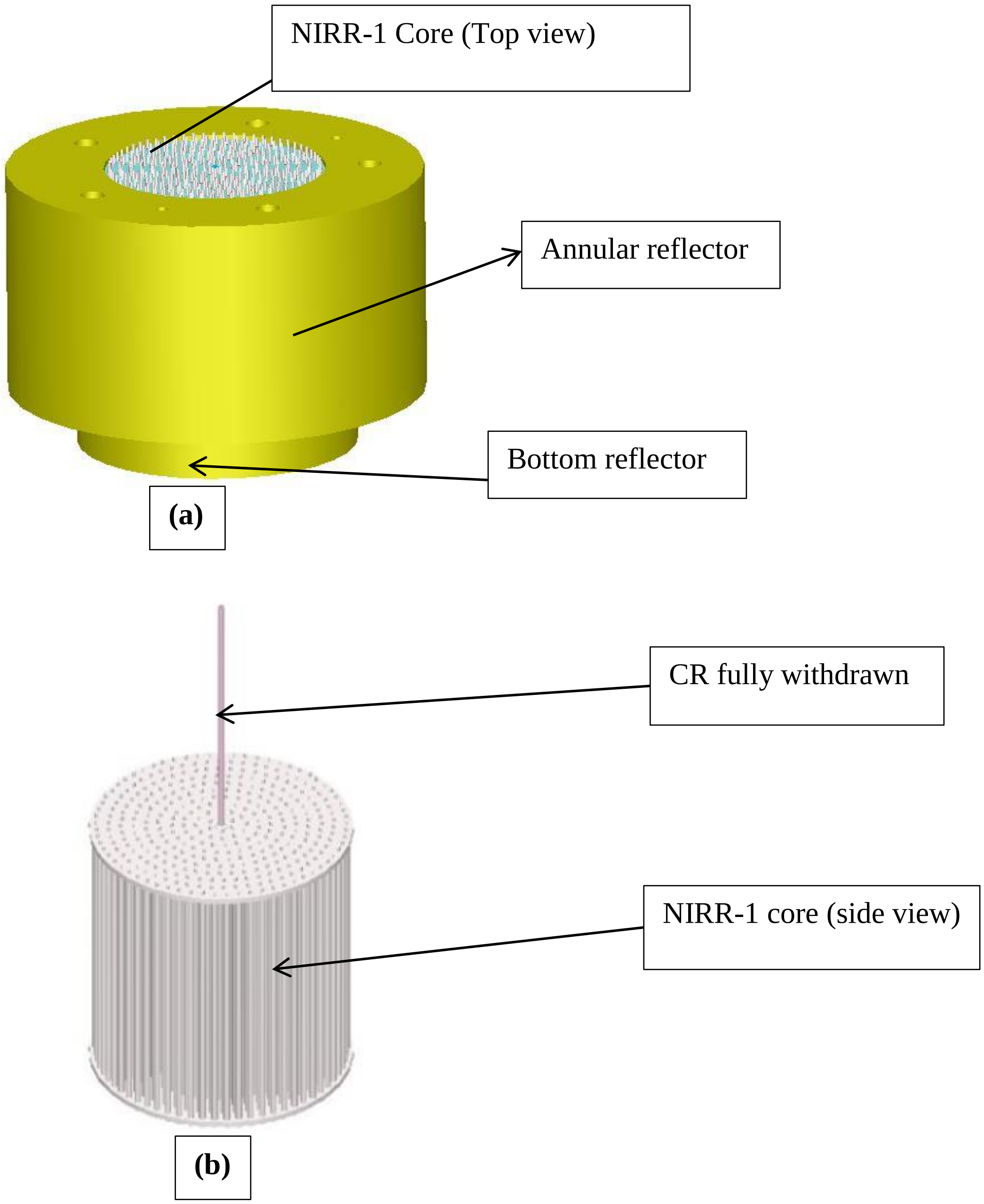

Figure 3.4: 3D KENO-VI Model of the NIRR-1 showing (a) the Bottom and Annular Reflector and containing the Core (b) the core and CR 'fully withdrawn'

Figure 3.5 represent a slice through the top half of the reactor. The calculations of the material composition for the HEU and LEU cores modeled in this work are presented iAppendix I and Appendix II respectively.

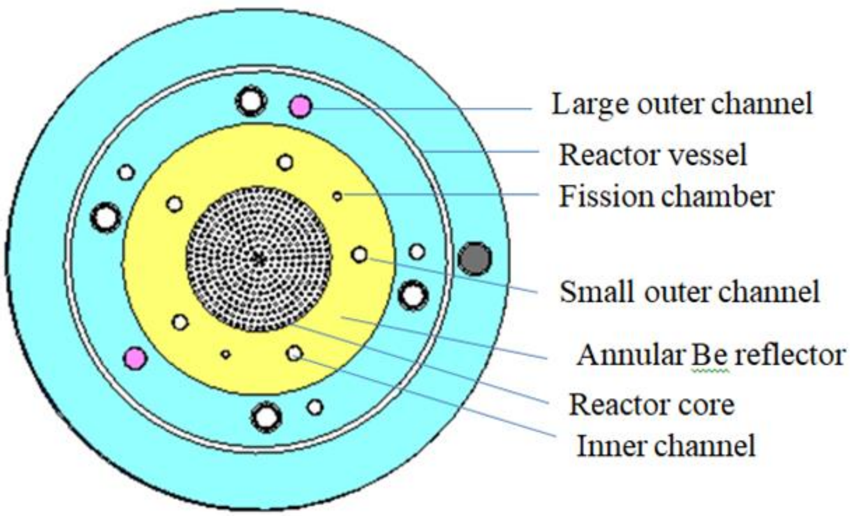

Figure 3.5: 3D KENO-VI Model Showing a 2D Top half Slice of the NIRR-1

3.4 Input Preparation for Cross Section Library Generation

All TRITON inputs are organized into data blocks depending on the chosen sequence of modules. Each data block begins with read block-name and terminates with end. For the cross-section library generation in our work, a blank ".inp" SCALE 6.2.3 input file was created in a specified directory using the "Fulcrum" Graphical User Interphase (GUI). The input structure was specified in four data blocks namely; TITLE, READ COMPOSITION, CELL DATA and MORE DATA blocks respectively. In the tittle block, the "t-xsec" sequence, which is a sub module of the XSProc (Xross Section Processing) SCALE cross section module, was 'called' in order to create a problem-dependent cross section library. This produced 2 sets of cross section library including: the "sysin.microlib library and "sysin.macrolib", required for transport calculations using the TRITON transport sequence and were stored temporarily in logic unit ft04f001 and ft44f001 respectively. The current version of the ENDF library containing 252 energy groups was also specified in the title block and used for cross section collapse. The standalone format for material specification consistent with the zone partitions presented in table 3.5 was used in the "READ COMPOSITION" block in order to specify the atom densities, temperature and isotope identifiers of various regions in the NIRR-1. Three neutron groups structure, that is, 20 MeV, 0.825 MeV and 0.625 eV were specified in the CELL DATA block. The energy values represent the upper boundary of the group beginning with the fast group at 20 MeV and ending with the thermal group at 0.625 eV. All material temperature was defined as 298 K. A shell command, "cp", was used to copy all libraries from their temporary directory to a permanent directory to enable plotting of cross sections of interest against energy which is necessary to analyze the characteristic behavior of the resonance region of a NIRR-1 MNSR core. The cross sections were automatically supplied to TRITON for transport calculations. A "Fulcrum" GUI of the XSProc module showing a typical title and composition block is seen in Figure III.1 in Appendix III.

3.5 Input Preparation for 1-D TRITON-XDRNPM Full Core Transport Model

The TRTITON input is free form and keyword based, starting with a title card record and the remaining data are supplied in data blocks. The order of the data blocks is arbitrary, and many blocks are either optional or their default values suffice for the NIRR-1. Consequently, in preparing the input file for TRITON-XSDRNPM execution, a blank ".inp" file was first created using "fulcrum" in drive C where SCALE was installed. The TRITON-XDRN sequence was then called in the TITLE block using the “=t-XSDRN” command followed by the cross section library name in the PARAMETER block. The material composition data in “READ COMPOSITION” block was divided into six zones consistent with the zone division for the NIRR-1 MNSR in our model using unique zone identifiers. These zones included the fuel, control, reflector, water, Al vessel and water having 1, 2, 3, 4, 5 and 6 respectively as identifiers as shown in Table 3.5. A cylindrical geometry, having a “white” right boundary condition and a “reflected” left boundary condition, divided into 6 zones with unique zone Identifiers (IDs) as mentioned above was also specified in the “MODEL” block. The mesh size for each zone was arbitrarily chosen and optimized. The “END” command was used to terminate the entire sequence. A “Fulcrum” GUI of the T-XSDRN sequence showing a typical “MODEL” block can be seen in Figure III.2 in Appendix 111.

3.6 Input Preparation for the 3-D KENO-VI Transport Model

The input preparation for 3-D KENO-VI model was "similar to the TRITON-XSDRNPM input preparation except in the “PARAMETER” and “MODEL” block. In order to make sure that there is enough neutron distribution in the core, decrease statistical error and allow for source convergence, the KENO-VI simulations were run for 750 active generations and 50 in-active with the number of neutrons per generation defined as 100,000 in the “PARAMETER” block. In the “MODEL” block a 3-D geometry of the NIRR-1 was developed based on KENO-VI approach. The 3-D KENO-VI geometry block consists of specifications for a set of basic building blocks known as units. The unit specification was defined in three distinct components: bodies, media and boundary. In bodies, the shape and array of the units was specified; and in media, the material content of each shape defined was specified; and the unit boundary conditions were also specified. Taking the center of the core as the origin (x,y,z) =

(0,0,0), the NIRR-1 control region was modeled as unit 1 using cylinders. The CR guide tube was set as the outermost cylinder and boundary of control region. Similarly, the fuel pin was modeled as unit 2. Since the NIRR-1 MNSR fuel assembly lattice consists of ten concentric circles, the units of the NIRR-1 MNSR lattice was carefully specified taking advantage of the data for the radial pitch of each fuel pin in each concentric circle of the core (CERT, 2011; Salawu, 2013; IAEATECDOC1844, 2012) as shown in Table 2.1. The exact x and y coordinates were calculated by writing a simple excel code. This was to ensure that all pins were placed in their exact lattice positions. All the x and y coordinates of the pins were then copied from excel to the 3-D KENO-VI geometry block. The top and bottom fuel plugs, tie rods, dummy pins, inner and outer irradiation channel, shim tray, regulators, bottom reflector, and slant tube were modeled as units 3, 4, 5, 6, 7, 8, 9, 10, 11, 12 and 120 respectively. The reactor vessel, pool water, annular reflector and reactor water were defined together as the global unit 13. The “HOLE” command used to place each fuel pin and all other units in their exact lattice positions. KENO-VI default simple grid structure was used for mesh flux tally in the reactor dormain. A “Fulcrum” GUI of the 3-D KENO-VI geometry block showing a typical “MODEL” block can be seen in Figure III.3 in Appendix III.

3.7. Input Preparation for TRITON Depletion Calculation

The depletion sequence employed in the present work is a TRITON sequence that couples both 1-D XSDRNPM and 3-D KENO-VI Monte Carlo transport with ORIGEN depletion. The depletion input preparation procedure and structure included all the processes and data blocks already mentioned in Section 3.6 in addition to the BURNDATA, DEPLETION block, and OPUS blocks. In the BURNDATA block, depletion steps were specified from the BOC up to a maximum of 216 EFPD which corresponds to an average of 3 hours a day, 3 days a week, and

48 weeks a year for 12 years of NIR-1 MNSR operational history (Yahya *et al., 2017*) at the EOC. In the DEPLETION block only the fissionable materials of the fuel was specified. The OPUS block was specified to extract and process nuclides of interest from ORIGEN output, which is a binary (.bin) file.

3.8 SCALE Data Acquisition and Analysis

SCALE output files are stored in the same directory as the input file. The output files consist of a summary file ('filename'.msg), and detailed output file ('filename'.out). SCALE data acquisition was performed by extracting (copying) relevant information such as plots, tables, concentrations etc. from the output files via the 'Fulcrum' GUI. Depending on the required output, the input file was first opened by double-clicking directly on the file or alternatively by double-clicking on the 'Fulcrum' (an executable file which was automatically created on the desktop when SCALE was installed) and then selecting 'open new' and then selecting the input file. The input pane was then rightclicked on and a drop down menu appeared from which the associated output was selected for viewing, copying and analysis. The k_{eff} from the output files was used to calculate neutronic parameters such as CCCER, CRW, SDM and SRF. The neutron flux was calculated by normalizing the scalar flux from the output files using the reactor thermal power and k_{eff} data.

3.9 SCALE Validation Study

In nuclear criticality safety applications, SCALE 6.2.4 was validated against 600 critical experiments with a variety of fissile material types and enrichments, energy spectra, and accompanying materials. The apparent bias of KENO-VI code has been reduced in recent years as nuclear data and processing have improved. When considering all categories of systems examined, the bias is less than 2.2% Δk (SCALE Manual, 2018).

In reactor physics applications, SCALE 6.2.4 was validated against more than 160 Light Water Reactor (LWR) fuel isotopic measurements, 230 decay heat measurements, short cooling time decay heat measurements in six types of fissile nuclides, and initial critical full-core eigenvalue measurements for one LWR and two non-LWRs. SCALE calculations compare well with the 40 measured nuclides of importance to burnup credit, decay heat, and radiation shielding applications. The bias in assembly decay heat is on average less than 1% for Pressurized Water Reactors (PWRs) and less than 2% for Boiling Water Reactors (BWRs). for the analyzed assembly experiments. The results for the fissile material experiments at cooling times up to ~100 s, as relevant to loss-of-coolant accident scenarios, show generally good agreement between calculated and measured values of energy release following fission (SCALE Manual, 2018).

CHAPTER FOUR

4. 0 RESULTS AND DISCUSSION

4.0. Introduction

This chapter presents and discusses the results of depletion and related calculations for the NIRR-1 MNSR fueled with the as-built UO_2 core, U_3Si_2-Al, U_3Si-Al and U_9Mo-Al LEU cores.

4.1 NIRR-1 Cross section Library

4.1.1 Resonance Self-Shielded Cross Section

The cross-section library generation for the NIRR-1 was carried out with the T-XSEC submodule of the XSProc module. This produced a library containing numerous nuclear reaction types of all the isotopes in the NIRR-1 core. The Resonance Shielded ^{238}U Cross Section for capture reaction is one of the most important cross sections in reactor analysis due to resonance effects at temperatures above 0K and is useful in analyzing and understanding the characteristic spectrum in a reactor (Salawu *et al*, 2013; Wiarda, 2016). The energy dependent resonance self-shielded cross section is shown in Figures 4.1, for the as-built UO_2, and alternative U_3Si_2-Al, U_3Si-Al and U_9Mo-Al LEU cores compared with the HEU core. From the figure, it is observed that the NIRR-1 MNSR core has three different regions in the energy spectrum which vary with resonance shilded cross section. These regions included the low energy (thermal energy region; 0 – 0.625eV), the intermediate energy or resonance energy (epithermal energy region; 0.625 eV – 0.825 MeV) and the high energy (fast energy region; 0.825 MeV – 20 MeV) which vary with ^{238}U resonance shielded cross section. The thermal and fast energy regions for both HEU and LEU were observed to display similar behaviour. The exception was in the resonance region where the difference is caused by the difference between the Doppler broadening in the LEU and HEU cores. The low energy region depicted an approximate inverse velocity behavior (1/v) with respect to the ^{238}U resonance shielded cross section. Careful observation of the spectrum revealed that the boundary between the low energy region and the high energy region is greater than 1 eV. This implies that the NIRR-1 MNSR cannot be regarded as a purely thermal system. The first resonance, as seen in the figures corresponds to excitation energy of about 7 eV. This implies that neutrons near this energy are more likely to undergo parasitic absorption in ^{238}U.

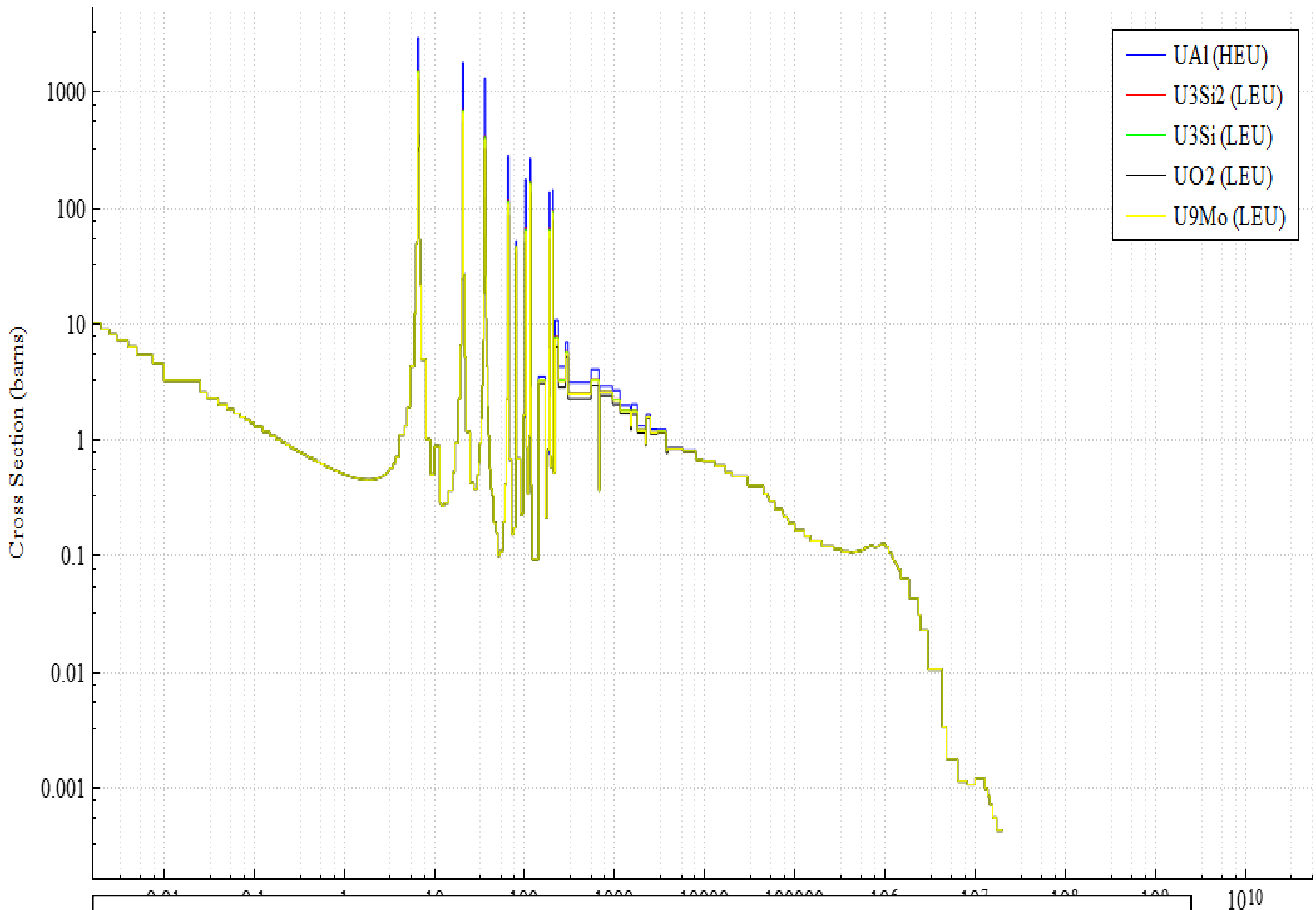

Figure 4.1: Resonance Shielded ^{238}U Cross Section for Capture Reaction in the Core of the NIRR-1 MNSR (HEU and LEU)

4.2 Models of the NIRR-1 and Neutronic Parameters for the HEU and LEU Cores

To test the validity of our model, the cold clean core excess reactivity (CCCER) of the HEU core was first calculated, it was then benchmarked with measured data from the Safety Analysis Report (SAR) of NIRR-1 and MCNP calculated data. The calculated CCCER for the HEU core was then used as a benchmark for the alternative LEU cores design. Two models were developed to calculate reactor parameters. The first model, a 1-D TRITON-XSDRNPM deterministic model, was an attempt to significantly simplify the MNSR design and analyze its results for use in MNSR reactor physics calculation while the second model is a very detailed 3D KENO-VI Monte Carlo model. The neutronics parameters for the two models are discussed in Section 4.2.1 – 4.2.2.

4.2.1. 1-D XSDRNPM full core model

Table 4.1 presents the result of the clean cold core excess reactivity for the NIRR-1 MNSR using the 1-D TRITON-XSDRNPM model. The calculated CCCER was found to be 9.48 mk for the HEU core whereas the clean NIRR-1 HEU core measured excess reactivity (measurement reported during the on-site start-up and power rising experiment of the HEU core) was 4.97 mk (CERT, 2011). The bias between calculated and measured data was found to be (9.48 – 4.97) = 4.51 mk which is equivalent to a deviation of 90.7%. This was majorly due to the non-inclusion of top aluminum shim tray, 4 stainless steel-clad adjuster rods with Cd sleeves in water filled guide tubes. In order to further test the validity of our 1-D calculations, the MCNP calculated data for the generic MNSR was adapted for the NIRR-1.

Table 4.1 1-D TRITON-XSDRN NIRR-1 MNSR HEU (UAl_4) Calculated CCCER

Parameter	HEU Calculated (reference)	HEU Measured (reference)	MCNP calculated (reference)
k_{eff} with CR out	1.009574	–	–
Excess reactivity (mk)	9.48 (this work)	4.97 (CERT, 2011)	9.11 (IAEATECDOC1844, 2012)

It should be noted that the MCNP calculated CCCER for the generic MNSR (having 345 fuel pins) based on a water temperature of 20^{o}C was found to be 7.74 mk (IAEA TECDOC-1844, 2012). When this was adapted for the NIRR-1 to include 2 additional fuels pins (worth = +1.73 mk) making a total of 347 fuel pins as in the NIRR-1, water temperature of 25^{o}C (worth = – 0.36 mk) as presented in Table 4.1, the CCCER became (7.74 + 1.73 – 0.36) = 9.11 mk for the NIRR-1. Using this MCNP result for the NIRR-1, to validate our 1-D XSDRNPM calculation, the bias between both calculations was found to be (9.48 – 9.11) = 0.37 mk, Consequently, our 1-D XSDRN calculation compare well with MCNP result adapted for the NIRR-1, with a deviation of (0.37/9.11 × 100) = 4.06 %. Hence, on this basis, the CCCERs of the U_3Si_2-Al, U_3Si-Al and U_9Mo-Al alternative LEU cores were found to be approximately 9.5 mk as observed in Table 4.2. Therefore, the magnitude of the CCCER of the alternative LEU cores match calculated data for the HEU core. However, the magnitude is almost 100% above the measured value of 4.97 mk for the NIRR-1 MNSR.

For the as-built UO_2 core, only measured data from the commissioning report of the core was used as a benchmark. The magnitude of the CCCER was found to be 5.63 mk whereas the measured CCCER is 3.94 mk as presented in Table 4.3. Hence, the bias between measurement and calculation was 1.69 mk which translate to 43 % higher than measured CCCER.. Since the as-built UO_2 core has no cadmium rabbit introduced into the core and the reactivity regulators were withdrawn from the core, the bias between calculated and measured data was largely attributed to the non-inclusion of top shim tray in the model.

Table 4.2: 1-D TRITON-XSDRN NIRR-1 MNSR Alternative LEU Calculated CCCER

Parameter	U_3Si_2-Al	U_3Si-Al	U_9Mo-Al	HEU
k_{eff} with CR out	1.009582	1.009555	1.009597	1.009574
Excess reactivity (mk)	9.49	9.46	9.51	9.48

Table 4.3 1-D TRITON-XSDRN NIRR-1 MNSR As-Built UO_2 Calculated CCCER

Parameter	LEU Calculated (reference)	LEU Measured (reference)
k_{eff} with CR out	1.005663	–
Excess reactivity (mk)	5.63 (this work)	3.94

4.2.2. 3-D KENO-VI model

The 1D XSDRNPM model is a relatively simplified model of the NIRR-1 and provides an estimate of the excess reactivity of the system that is comparable with MCNP data. However, it is limited to a 1-D approximation of the system such that the reactor is assumed to have a multizone (multiregion) 1-D cylindrical geometry with homogenized material composition in the R-direction (radius of the core). Consequently, the concentric fuel pins occupying different lattice position in the core, the Irradiation channels and Al tubes for fission chambers could not be explicitly modeled. Also, the top aluminium shim tray, 4 stainless steel-clad adjuster rods with Cd sleeves in water filled guide tubes could not be physically created in the model. This resulted in an overestimation of the CCCER with a bias between calculated and measured data of 4.51 mk (90.74%) for the benchmark HEU core earlier presented in Table 4.1. In order to reduce the bias between calculation and measurement, a 3-D KENO-VI simulation of the NIRR-1 MNSR fueled with the HEU core was developed and used as a benchmark for the alternative U_3Si_2-Al, U_3Si-Al, U_9Mo-Al LEU cores and the result is presented in Table 4.4. The CCCER for the HEU core was found to be 4.83 mk (Table 4.4). This compared well with measured value of 4.97 mk. The bias between the calculated and measured value was (4.97 – 4.83) = 0.14 mk which translated to a 3% decrease in calculated value compared to measured value. Although, the maximum allowed CCCER for all MNSRs including the NIRR-1 is 4.0 mk (Ibikunle *et al*, 2018) the NIRR-1 HEU core had its CCCER set to 3.77 mk during its commissioning after insertion of cadmium rabbit having a worth of -1.2 mk (CERT, 2011). Accordingly, -1.2 mk value was subtracted from the calculated value of 4.83 mk to account for the cadmium rabbit insertion into the rector, the result was 3.63 mk, which compared well with the set CCCER for the NIRR-1 HEU core during commissioning. As also seen in Table 4.4, the CCCER, CRW, and SDM of the alternate LEU cores compared well with data for the HEU benchmark core. However, the CCCER was also observed to be slightly greater than the maximum 4.0 mk recommended safety limit for MNSRs while the SDM and SRF was observed to be less than the 2.5 mk and 1.5 mk safety margins respectively (IAEATECDOC1844, 2012). Similarly, insertion of cadmium rabbits having a worth of – 0.86, – 0.81, and – 0.90 mk respectively into one of the unconnected inner irradiation channels was necessary in order to reduce the magnitude of the CCCER of the alternate U_3Si_2-Al, U_3Si-Al, U_9Mo-Al LEU cores obtained in this work to the maximum allowed excess reactivity of 4.0 mk at the BOC This resulted in a SDM and SRF of $\geq$ 2.5 mk and $>$ 1.5 respectively for all the alternative LEU cores which are within safety limits.

Table 4.4: 3-D KENO-VI calculated Neutronic Parameters for the NIRR-1 MNSR (HEU and Alternative LEU).

Parameter	**U_3Si_2-Al**	**U_3Si-Al**	**U_9Mo-Al**	**UAl_4-Al (HEU) Calculated**	**UAl_4-Al(HEU) measured**
k_{eff} CR out	1.00488±0.00005	1.00483±0.00005	1.00492±0.00005	1.00485±0.00005	-
k_{eff} CR in	0.99811±0.00005	0.99797±0.00005	0.99825±0.00005	0.99769±0.00005	-
Excess reactivity (mk)	4.86	4.81	4.90	4.83	4.97
CRW (mk)	6.75	6.80	6.65	7.14	7.00
SDM (mk)	1.89	1.99	1.75	2.32	2.03
SRF=CRW/ER	1.39	1.42	1.36	1.48	1.41

The result of the KENO-VI model for the benchmark HEU core also compared well with the result of other models for the NIRR-1 and other MNSRs found in literature as observed in Table 4.5.

Table 4.5: Comparison of CCCER as Calculated by KENO-VI Model and Other Models for MNSR (HEU-UAl_4)

Model Name	**CCCER (mk)**	**Reactor type (Reference)**
MCNP	4.519	GHARR-1 (Anim-Sampong *et al*, 2007)
CITATION	4.32	PARR-1 (Mahmood *et al*, 2008)
MCNP	4.74	NIRR-1 (Jonah, *et al*, 2009)
CITATION	4.32	PARR-1 (Amjad *et al*, 2012)
VENTURE	5.50	NIRR-1 (Salawu, 2013)
MCNP	4.73	NIRR-1 (Ibikunle, 2018)
KENO-VI	4.83	This work

It was also observed in Table 4.6 that the magnitudes of the CCCER, CRW, and SDM of the alternate LEU cores were in good agreement with the reported values in literature.

Table 4.6: Comparison of alternate LEU cores Calculated CCCER and Reported Values in Literature

LEU Fuel	**CCCER (mk)**	**CRW (mk)**	**SDM (mk)**
U_3Si_2-Al			
Sampong *et al* (2006)	4.27	6.66	2.37
Amjad *et al* (2012)	4.03	6.12	2.09
Ibikunle *et al* (2018)	4.76	6.69	1.93
This work	4.86	6.75	1.89
U_3Si-Al			
Sampong *et al* (2006)	4.04	6.59	2.54
Amjad *et al* (2012)	4.04	6.04	2.00
Ibikunle *et al* (2018)	4.70	6.71	2,01
This work	4.81	6.80	1.99
U_9Mo-Al			
This work	4.9	6.65	1.75
Amjad *et al* (2012)	4.05	4.53	0.48
Ibikunle *et al* (2018)	4.8	6.50	1.71

Furthermore, the criticality safety parameters of the as-built UO_2 core are presented in Table 4.7. The CCCER, CRW, SDM, and SRF, were found to be 3.82 mk, 6.41 mk, 2.61 mk and 1.69 respectively. The bias between measurement and calculation in the magnitude of the CCCER was found to be 0.12 mk which was less than 4% of the measured value. Hence, there was a very close agreement between measured and calculated data which implies that the

KENO-VI model is reliable and adequate for criticality safety analysis of the NITRR-1 and similar MNSRs.

Table 4.7: 3-D KENO-VI Calculated Neutronic Parameters for the As-Built NIRR-1 UO_2 LEU core

Parameter	UO_2 **Calculated**	UO_2 **measured**
k_{eff} CR out	1.00383±0.00005	-
k_{eff} CR in	0.99741±0.00005	-
Excess reactivity (mk)	3.82	3.94
CRW (mk)	6.41	6.49
SDM (mk)	2.61	2.03
SRF= CRW/ER	1.69	1.65

4.3 Moderator-to-fuel ratio and Average Neutron flux distribution

4.3.1 moderator-to-fuel ratio

The moderator-to-fuel ratio of a core is the ratio of hydrogen to ^{235}U in the core. It provides a quick idea of the temperature reactivity feedback mechanism and consequently the safety of a reactor. The standard NIRR-1 HEU core was built to operate in an under-moderation mode with a moderator-to-fuel ratio of 197 (CERT, 2011) while that of the as-built UO_2 LEU core is 147 (CERT, 2019). The moderator-to-fuel ratios of the HEU, as-built UO_2 and alternative LEU cores are presented in Table 4.8. For the HEU core, the moderator-to-fuel ratio was found to be 200. However, this value was found to reduce to 148 for the as-built LEU core. Hence, indicating an increase in the negative moderator temperature coefficient of the core, and thereby improving the temperature feedback effect of the as-built LEU core. This implies that the LEU core is more self-regulating. The advantage of this is that is reduced risk of accident and hence an improvement in reactor economy. A very small difference in the moderator-to-fuel ratio between our calculations and design for the HEU and the as-built LEU cores can be observed in Table 4.8. This difference can be attributed to approximations in the atom density calculations for ^{235}U and Hydrogen in the core. Similarly, the alternative LEU cores were found to have lower moderator-to-fuel ratio when compared to the HEU core. In all the cases, the as-built UO_2 core and alternate cores present the lowest moderator-to-fuel ratios. This implies that these LEU cores would reduce the risk of accident related to power excursion or rise in moderator temperature.

Table 4.8: Moderator-to-Fuel Ratio (HEU and LEU Cores)

Fuel type	Moderator-to-fuel ratio	
	This work	**As-built**
UAl_4 (HEU)	200	197
UO_2	148	147
U_3Si_2-Al	163	-
U_3Si-Al 44	159	-
U9Mo-Al	145	-

4.3.2 Average neutron flux distribution in the NIRR-1 MNSR core

RRs are essentially designed to utilize their neutron flux, the NIRR-1 MNSR and similar LPRRs are no exceptions (Sogbadji *et al*, 2011). Since the NIRR-1 MNSR is extensively used for NAA, which is high efficiency and non-destructive analytical technique used for both qualitative and quantitative elemental analyses in varying geological, environmental and biological samples, knowledge of the expected neutron flux of the LEU cores in this work is extremely important. Thermal neutrons are the major neutron energy group of interest for

NAA. The result of the neutron flux distribution in the core of the NIRR-1 MNSR is presented in Table 4.9.

From the Table 4.9, the calculated thermal neutron flux in Inner Irradiation Channel (IIC) of the NIRR-1 MNSR for the HEU core was found to be $1.159 \times 10^{12} \mathrm{n/cm^2.s}$. This value compared well with the measured nominal thermal neutron flux of $1.0 \times 10^{12} \mathrm{n/cm^2.s}$ at full power (31 kW) for the HEU core. It was observed that the thermal neutron flux of $0.677 \times 10^{12} \mathrm{n/cm^2}.s$ in the Outer Irradiation Channel (OIC) for the HEU core account for about half (0.584) of the flux in the IIC. This data is in agreement with Ibikunle *et al* (2018) and Sogbadi (2012) for the NIRR-1 and GHARR-1 MNSR who reported values of 0.524 and 0.570 respectively.

Table 4.9 also depicted that the thermal neutron flux in the as-built LEU-UO_2 core is essentially the same with that of the HEU. However, the thermal neutron flux in the alternative LEU cores is lower than that in the HEU core. This can be attributed to the reduced enrichment in the LEU cores as compared to the HEU core. This implies higher concentration of ^{238}U at the beginning of cycle. Consequently, fewer neutrons make it to the thermal energy region in the slowing down process due to lower resonance escape probability which results in a decrease in the thermal neutron flux in the core.

The magnitude of the average percentage reduction in thermal neutron flux was found to range from 7.2 – 9.5 % in the alternative LEU cores relative to the HEU cores as can be seen in Table 4.10. This compares well with the reduction by 7 – 10 % reported by Ibikunle (2018). Consequently, the thermal power of the U_3Si_2-Al, U_3Si-Al, U_9Mo-Al LEU cores in this study would have to be increased from 31 kW to 33.5, 33.2, and 33.9 kW respectively to match the nominal flux of the HEU core. In terms of reactor economy, this implies that the thermal neutron flux of the LEU cores would be maintained for utilization in NAA.

Table 4.9: Neutron Flux Distribution in the IIC and OIC of the NIRR-1 MNSR Core (HEU vs LEU)

Fuel type	**Thermal (0 - 0.625 eV) $\times 10^{12}$ $n/cm^2.s$**		**Epithermal (0.625eV – 0.825 MeV) $\times 10^{12}$ $n/cm^2.s$**		**Fast (0.825MeV – 20MeV) $\times 10^{12}$ $n/cm^2.s$**	
Location	IIC	OIC	IIC	OIC	IIC	OIC
UAl_4 (HEU)	1.159±0.01	0.677±0.01	1.298±0.01	0.187±0.01	0.271±0.01	0.0365±0.003
UO_2	1.160±0.01	0.680±0.01	1.299±0.01	0.190±0.01	0.270±0.01	0.0368±0.003
U_3Si-Al	1.075±0.01	0.636±0.01	1.287±0.01	0.187±0.01	0.269±0.01	0.0353±0.003
U_3Si_2-Al	1.066±0.01	0.631±0.01	1.286±0.01	0.186±0.01	0.267±0.01	0.0349±0.003
U9Mo-Al	1.049±0.01	0.611±0.01	1.261±0.01	0.179±0.01	0.258±0.01	0.0344±0.003

Table 4.10: Percentage Reduction in Thermal Neutron Flux

Fuel Type	**% Reduction in Thermal flux (0 - 0.625 eV)_**
UAl_4–Al (HEU)	-
U_3Si_2-Al (LEU)	8.0 %
U_3Si-Al (LEU)	7.2 %
U9Mo-Al (LEU)	9.5 s%

4.4 Uranium Core Loading at the BOC and Core Composition Changes with Burnup

4.4.1 Uranium core loading at the BOC

Table 4.11 shows that the total uranium core loading was found to be 1107.971 g for the standard HEU core. However, this value was found to increase to 10385 g, 6212.341 g, 6375.431 g, and 6954.921 g for the as-built UO_2, U_3Si_2-Al, U_3Si-Al, and U-9Mo-Al cores respectively. The uranium loading for the alternate fuels obtained in the present study compared well with the total uranium core loading of 5515 g, 6319.3 g, and 7548.7 g reported for the PARR-1 system fueled with the U_3Si_2-Al, U_3Si-Al, and U-9Mo-Al cores respectively (Amjad *et al*, 2012). Compared with the HEU core, the ^{235}U core loading required for the as-built UO_2, U_3Si_2-Al, U_3Si-Al, and U-9Mo-Al cores in the present study was found to be 1350.05 g, 1226.992 g, 1259.263 g and 1373.426 respectively. The ^{235}U core loading in the UO_2 core obtained in the present calculations compared very well with the 1350.40 g core loading of the NIRR-1 (CERT, 2019) while U_3Si_2-Al, U_3Si-Al, and U-9Mo-Al ^{235}U core loading compares well with the 1228 g, 1257g and 1361g respectively reported by Ibikunle (2018) and 1230.4 g, 1251.8g and 1833.6 g reported by Amjad *et al* (2012). The high uranium core loading of the LEU cores at the BOC provide enough ^{235}U to sustain the fission chain reaction. It is evident that the ^{238}U in the LEU cores are much greater than that in the HEU core. This is due to reduction in the enrichment from 90.2 % in the HEU core to less than 20 % in the LEU core.

Table 4.11: Uranium Core Loading Requirement (HEU and LEU)

Fuel	**^{235}U**		**^{238}U**		**Total Uranium (g)**	
	Per pin	**core**	**Per pin**	**core**	**Per pin**	**Core**
HEU	2.880	999.360	0.313	108.611	3.193	1107.971
UO_2	4.030	1350.05	26.970	9034.95	31.000	10385.000
U_3Si_2	3.536	1226.992	14.367	4985.349	17.903	6212.341
U_3Si	3.629	1259.263	14.744	5116.168	18.373	6375.431
U9Mo	3.958	1373.426	16.085	5581.495	20.043	6954.921

4.4.2 Core composition changes with burnup

The depletion of the core in the present study was carried out assuming the NIRR-1 MNSR operation regime of 3 hours a day, 3 days a week and 48 weeks a year at full power of 31 kW, equivalent to total exposure cycle length of 216 Effective Full Power Days (EFPD) (Yahaya *et al* 2016) in order to ensure a streamlined comparison between the present work and literature and investigate the behavior and changes in the core concentration at the EOC for the LEU cores. The analysis is presented in the next sub-sections.

4.4.2.1 Changes in ^{235}U concentration

The mass of ^{235}U as a function of burnup (in cycle length) for the HEU core, as-built UO_2,U_3Si_2-Al, U_3Si-Al, and U_9Mo-Al cores are depicted in Figure 4.2. It was observed from the figure that the mass of ^{235}U decreases linearly as a function of cycle length/burnup for all the cores. This is because the ^{235}U is consumed (burnt) as a result of the fission between ^{235}U and thermal neutrons in all the cores. The mass consumed at the EOC for the HEU core was found to be 8.2600 g equivalent to a burnup of 0.83 % which compared well with the mass of 7.999 g equivalent to a burnup of 0.7999 % reported by Yahya *et al* (2016) and 7.8000 g equivalent to a burnup of 0.78 % reported by Salawu (2013). The mass of ^{235}U consumed at the EOC for the as-built UO_2 core and alternative LEU cores was found to be 8.01 g, 8.12 g, 8.15 g, and 8.10 g equivalent to a burnup of 0.59 %, 0.66 %, 0.65 %, 0.59 %, for the UO_2, U_3Si_2-Al, U_3Si-Al and U_9Mo-Al LEU cores respectively. Although the results show that both the HEU and the LEU cores have a burnup of less than 1 % at the EOC, however, the burnup of the uranium-silicide fuels are higher than that of the UO_2 fuel. The difference in burnup of the HEU core and the LEU core can be attributed to the difference in their enrichments (90.2% for HEU, 13% for the as-built UO_2 and 19.75 % for the alternate LEU cores) and the higher core loading in the LEU cores as discussed in section 4.4.1.

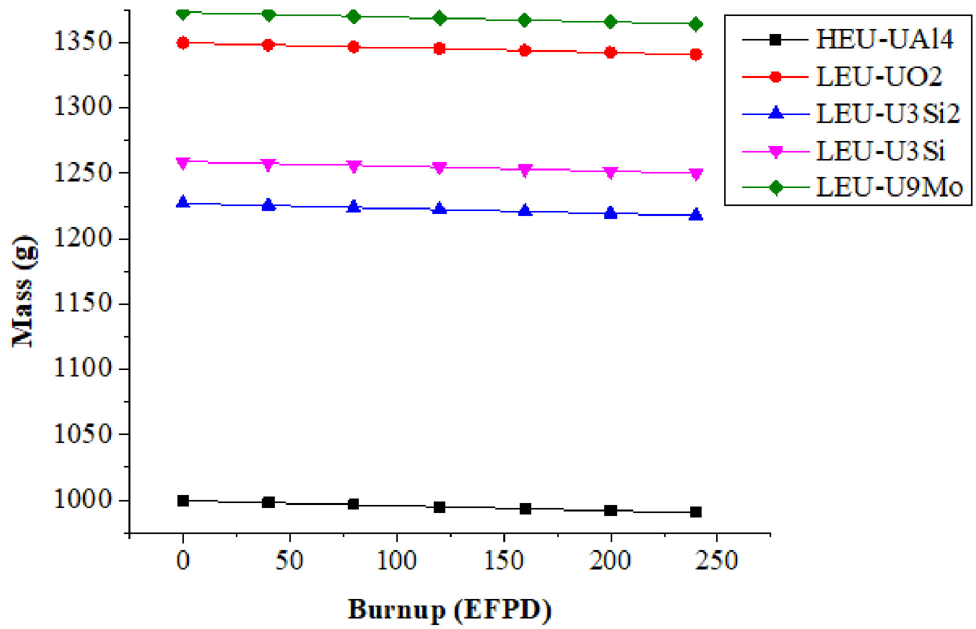

Figure 4.2: ^{235}U Mass as a Function of Cycle Length /Burnup

4.4.2.2 Changes in ^{238}U concentration

The mass of ^{238}U as a function of cycle length for the HEU core, as-built UO_2, U_3Si_2-Al, U_3Si-Al, and U_9Mo-Al cores are shown in Figure 4.3. Similar to the ^{235}U, the mass of ^{238}U decreases linearly with cycle length for both HEU and LEU cores. However, the decrease in mass of ^{238}U at the EOC is not significant when compared to the decrease in the mass of ^{235}U for all the cores. This is because ^{238}U has a low macroscopic fission cross section at thermal energies. The difference between the mass of ^{238}U at the BOC and at the EOC was found to be 0.04 g for the HEU core. This is comparable to 0.05 g reported by Salawu (2013). As for the as-built UO_2, U_3Si_2-Al, U_3Si-Al, and U_9Mo-Al LEU cores, the mass of ^{238}U consumed at the EOC was found to be 1.009 g, 0.968 g, 0.971 g, and 0.987 g respectively. This implies that the difference between the mass of ^{238}U at the BOC and at the EOC for the as-built UO_2, U3Si2-Al, U_3Si-Al, and U_9Mo-Al LEU cores is 19.7, 24.85, 24.93 and 25.75 times that of the HEU core respectively. This is due to the higher amount of ^{238}U/core loading present in the LEU cores compared to the HEU core at the BOC as observed I section 4.4.1.

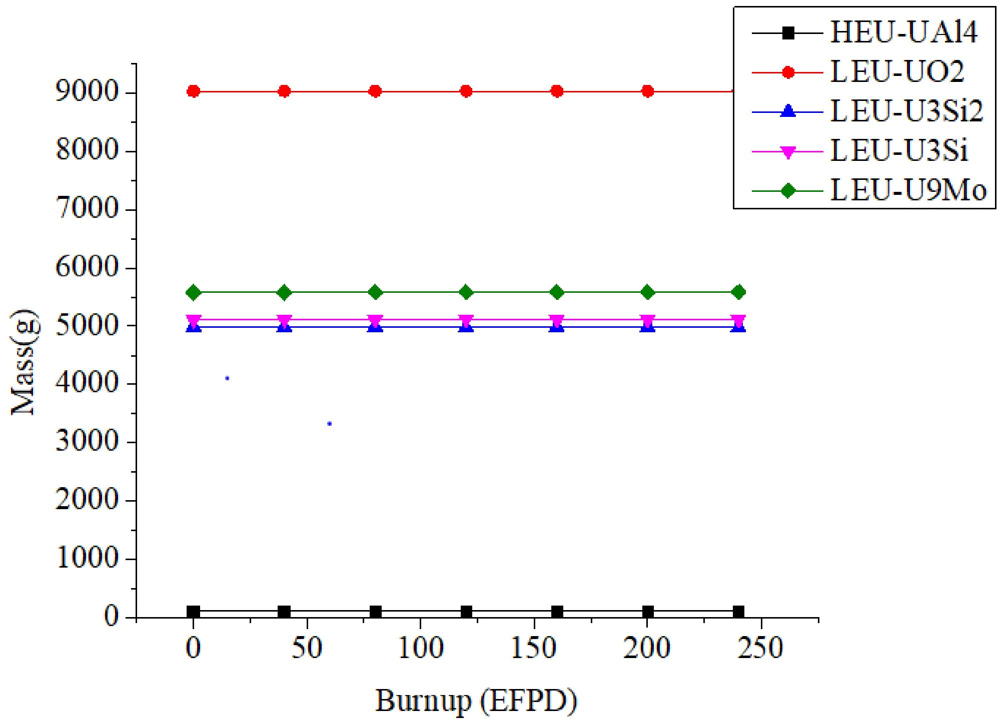

Figure 4.3: ^{238}U Mass as a Function of Cycle Length/Burnup

4.4.2.3 Changes in ^{239}Pu concentration

Figure 4.4 show the changes in mass of ^{239}U during NIRR-1 operation for the HEU, as-built UO_2, U_3Si_2-Al, U_3Si-Al. core with cycle length/burnup. Unlike the decreasing mass of ^{235}U and ^{238}U with burnup, it was observed that the mass of ^{239}U increases linearly with burnup for the HEU core and LEU cores. The buildup of ^{239}Pu at the EOC was found to be 0.036 g for the HEU core. This compared well with values of 0.035 g reported by Yahaya *et al* (2017) and 0.042 g by Salawu (2013). However, the buildup of ^{239}Pu at the EOC was found to be 0.929 g, 0.776 g, 0.781 g and 0.795 g for the UO_2, U_3Si_2-Al, U_3Si-Al and U_9Mo-Al LEU cores respectively. This is about 20 times more ^{239}Pu compared to the HEU core. Consequently, the build-up of ^{239}Pu in the LEU cores is much greater when compared to that of the HEU core. This is due to the increase in the ^{238}U capture reaction in the core. Hence, the contribution of ^{239}Pu to the total radiotoxicity to the spent LEU cores would be greater than that of the HEU core. Because of the higher amount of ^{239}Pu buildup in the LEU cores as compared to the HEU core, the LEU cores would have a higher conversion ratio when compared to the HEU core. However, the conversion ratio at any point in time for the LEU cores would be less than one (< 1). This is because the amount of fissile nuclide (^{235}U) burnt in the fuel at any point in time is greater than the amount of fissile isotope (^{239}Pu) produced.

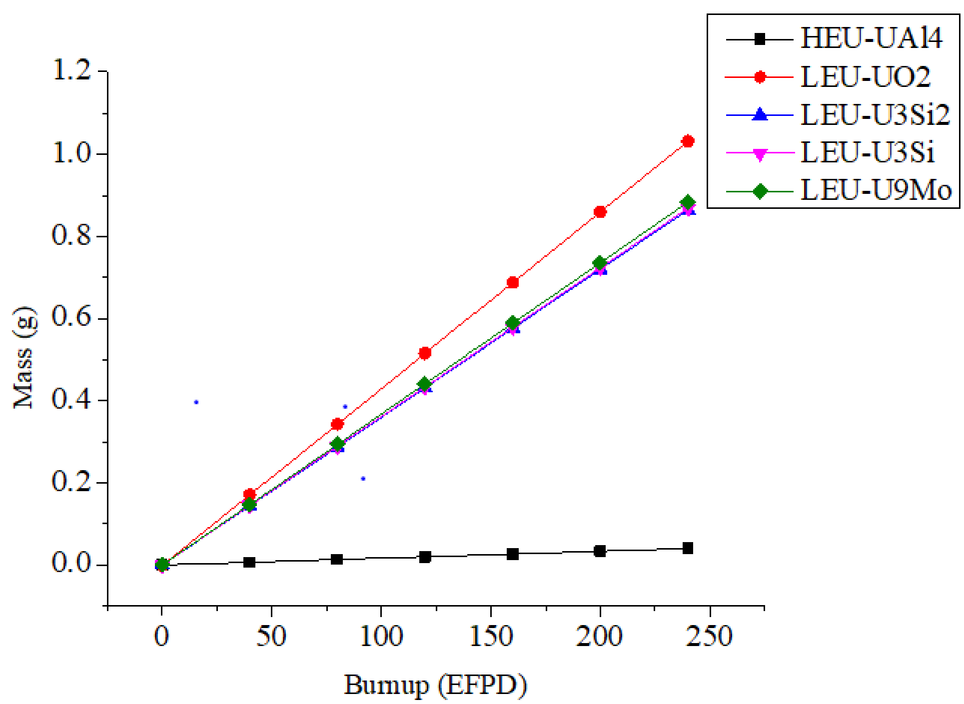

Figure 4.4: ^{239}Pu Mass as a Function of Cycle Length/Burnup

4.4.2.4. Buildup of xenon and samarium fission product poison

Various fission products are produced through the decay of fission fragments generated at the time of fission. The major concern about these fission products in reactors is that they become parasitic neutron absorbers and result in long term sources of heat. Even though the absorption cross section of numerous fission products is significant ^{135}Xe and ^{149}Sm have the most considerable impact on reactor design and operation. Since ^{135}Xe and ^{149}Sm remove neutrons from the reactor, they affect the thermal utilization factor and consequently the reactivity of a core. The changes in the concentration of ^{135}Xe and ^{149}Sm during continuous operation of the NIRR-1 have been presented in Figures 4.5 and 4.6 respectively. Both ^{135}Xe and ^{149}Sm are observed to sharply increase until they reach equilibrium concentration. The equilibrium ^{135}Xe concentration was observed to be in about 3 days of continuous reactor operation. The equilibrium ^{135}Xe concentration is also much higher in the LEU cores as compared to the HEU core. However, ^{149}Sm was found to reach equilibrium concentration in about 1000 and 1600 days of continuous reactor operation for the HEU core and LEU cores respectively. Similarly, the equilibrium ^{149}Sm concentration was higher in the LEU cores compared to the HEU core.

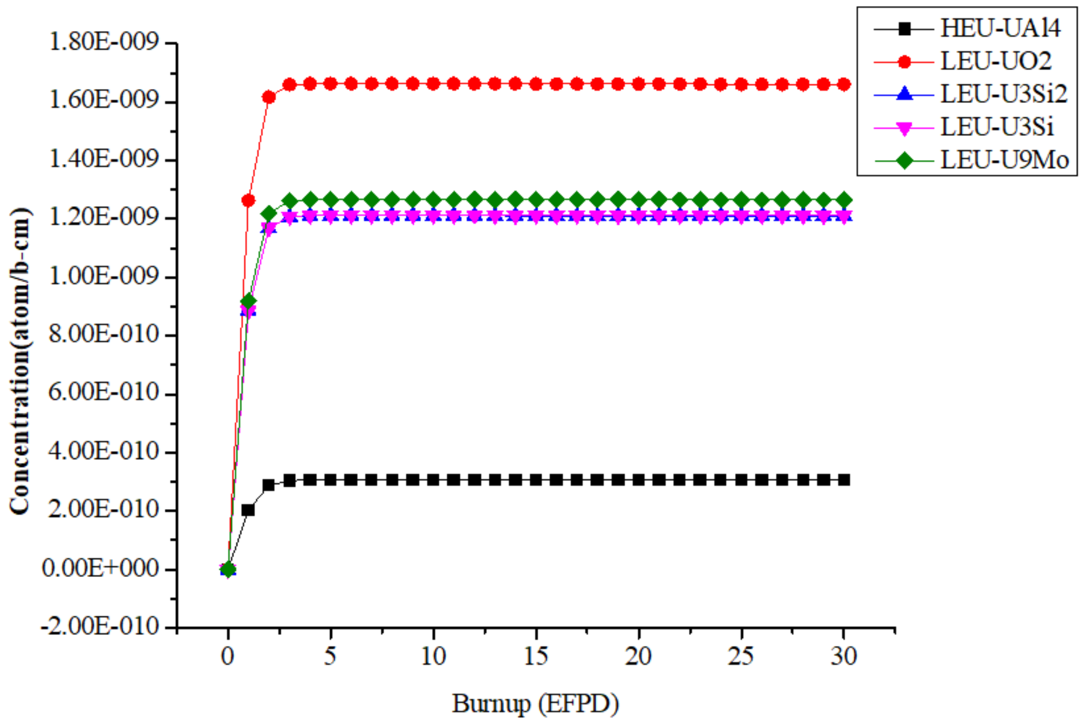

Figure 4.5. Change in ^{135}Xe Concentration with cycle Length/Burnup

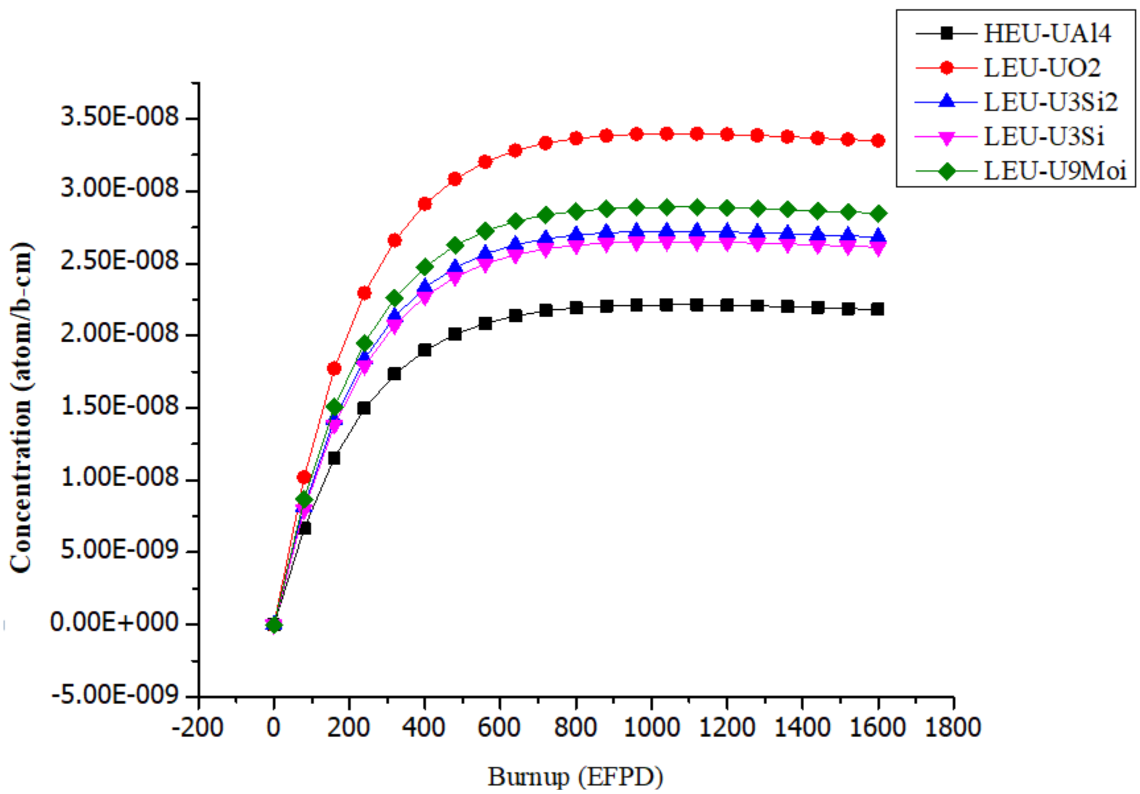

Figure 4.6. Change in ^{149}Sm Concentration with Cycle Length/Burnup

4.5. Effect of NIRR-1 Burnup on Reactivity and Fuel depletion Rate

4.5.1 Effect of NIRR-1 burnup on reactivity

In order to understand the behavior of the NIRR-1 reactivity as the fuel depletes and estimate important fuel cycle parameters such as equilibrium xenon worth, fuel depletion rate, and operational fuel cycle length reactivity rundown calculation was performed and a graph of reactivity against cycle length was plotted. The reactivity rundown calculation was performed assuming the maximum allowed excess reactivity of 4.0 mk for a freshly loaded MNSR core. The results are presented in Figure 4.7 for all the cores. It was observed from Figure 4.7 that the ER followed similar trends for all the fuel types. However, there was large drop in reactivity very early in the reactor core life, from 0 until approximately 3 days of continuous reactor operation when the reactor reached equilibrium xenon. This was due to the buildup of fission products that were absent in the fresh fuel. Most of these fission products have large absorption cross section for thermal neutrons; hence they significantly reduced the reactivity of the core.

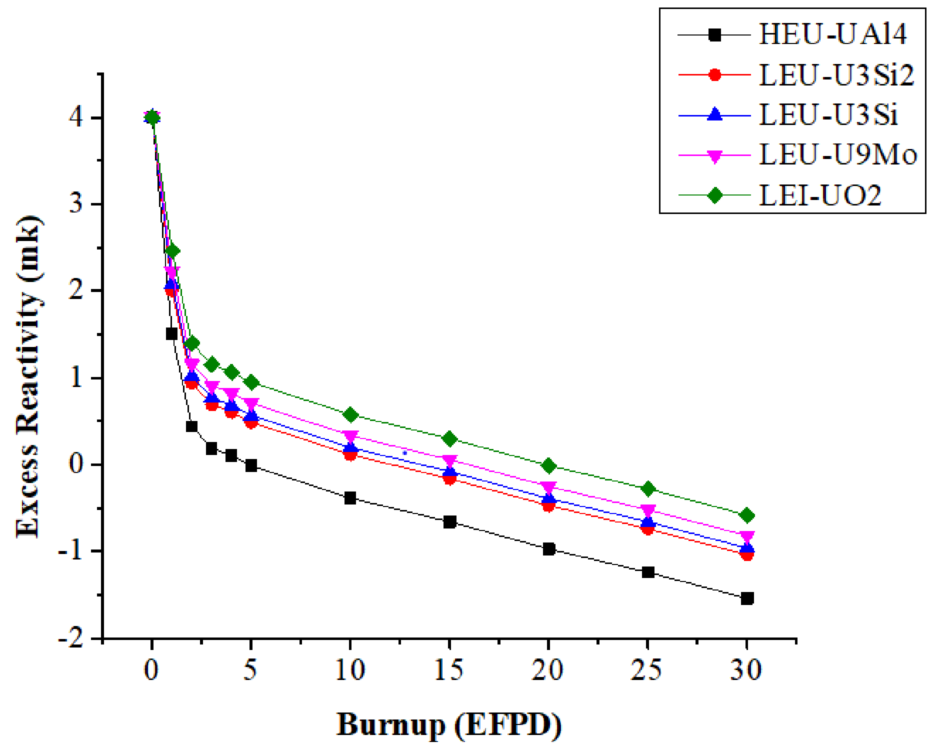

Figure 4.7. Reactivity Behavior with Burnup

4.5.2 Estimated fuel depletion rate and equilibrium xenon worth

The equilibrium xenon worth, including the depletion rate is presented in Table 4.12 for all the cores. The equilibrium xenon worth for the HEU, UO_2, U_3Si_2, U_3Si and U-9Mo cores was found to be 3.81 mk, 2.85, 2.31 mk, 3.23 mk, and 3.09 mk respectively. The depletion rate of the HEU was found to be – 0.00158 mk. This compared well with – 0.00177 mk/h, 0.002036 mk/h and 0.002038 mk/h reported by Amjaad *et al* (2012), Liaw and Matos (2007) and IAEATECDOC1844 (2012) for the PARR-1, NIRR-1 and GHARR-1 respectively**.** However, the depletion rate was found to be – 0.00120 mk/h, - 0.00124 mk/h, - 0.00123 mk/h and – 0.00105 mk/h for the as-built UO_2, U_3Si_2, U_3Si and U-9Mo cores. Hence, all the LEU cores depleted at a slower rate than the HEU core. This is because the rate of conversion of ^{238}U to ^{239}Pu is higher in the LEU cores than the HEU core as explained in the result of the ^{239}Pu

buildup in section 4.4.2.3. Consequently, all the LEU cores displayed are improvement in the fuel economy compared to the HEU core.

Table 4.12: Depletion Parameters (HEU and LEU Cores)

Fuel type	Equilibrium xenon worth (mk)	Fuel Depletion rate (mk/day)	Fuel Depletion rate (mk/hour)
HEU	3.81	- 0.0379	- 0.00158
UO_2	2.85	- 0.0288	- 0.00120
U_3Si_2	3.31	- 0.0297	- 0.00124
U_3Si	3.23	- 0.0295	- 0.00123
U-9Mo	3.09	-0.0251	- 0.00105

4.6 Top Beryllium Shim Worth and Core Lifetime

4.6.1 Top beryllium shim worth

In order to estimate the core lifetime of the reactor, the top Be shim worth was calculated. This was done by gradual addition of the top Be shim plates up to the maximum height of 10.95 cm. The reactivity worth of the top Be shim for the HEU and LEU cores is shown in Figure 4.8. The top Be shim worth of the HEU core is 19.93 mk. This compares well with the measured and MCNP calculated values of 18.5 mk, 20 mk, (CERT, 2011, IAEATECDOC1844, 2012) respectively. However, the top Be shim worth of the as-built UO_2, U_3Si_2, U_3Si and U-9Mo LEU cores was found to be 18.87 mk, 19.31 mk, 19.17 mk and 18.95 mk respectively. It is clear, therefore, that the top Be shim worth in the LEU cores is lower than the HEU core. This is associated with the high inventory of ^{238}U at the BOC which reduces the resonance escape probability of neutrons during thermalization. Consequently, there is a reduction in the thermal neutron flux reaching the Be reflector.

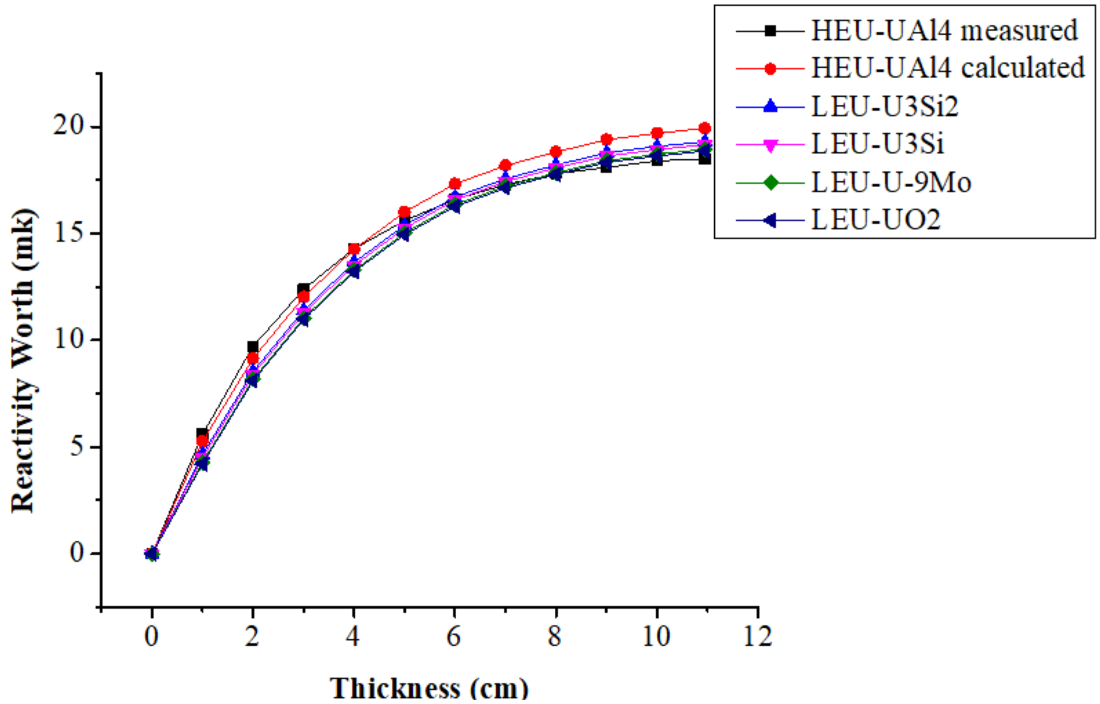

Figure 4.8: Top Beryllium Shim Worth (HEU vs LEU)

4.6.2 Core Lifetime Estimate

Two estimates of core lifetime were made in this work: the core lifetime of the NIRR-1 under continuous reactor operation before addition of top Be shim and the core lifetime after addition of top Be shim.

4.6.2.1 Before addition of top Be shim

The core lifetime estimates before addition of top Be shim is presented in Table 4.13. This was done considering the upper and lower limit of excess reactivity of 4.0 mk and 2.3 mk respectively for MNSRs. This implies that the window of excess reactivity available for depletion for the NIRR-1 is 1.7 mk. As seen from Table 4.13, the NIRR-1 HEU core can be operated at full power (3 hours per day, 3 days per week, and 48 weeks per year) for 2.20 years. However, for the as-built UO_2, U_3Si_2, U_3Si and U-9Mo LEU cores the reactor can be operated for 3.28, 3.17, 3.20 and 3.75 years respectively. Hence the addition of top Be shim plates per cycle for the LEU cores can be defined on a longer core lifetime basis for the NIRR-1. Hence, the frequency of top Be plates addition in the LEU cores as compared to the HEU core is reduced. This is an improvement in the fuel economy of the LEU cores as compared to the HEU ore. This result suggests that the LEU cores are better than the HEU core in terms of fuel management.

Table 4.13 Core Lifetime Estimate before Addition of Top Be Shim Plates

Fuel type	**HEU**	**UO_2**	**U_3Si_2**	**U_3Si**	**U-9Mo**
Hours to operate	1075.949	1416.667	1370.968	1382.114	1519.048
Weeks to operate	119.550	157.407	152.330	153.568	179.894
Years to operate	2.20	3.28	3.17	3.20	3.75

4.6.2.2 After addition of top Be shim

In order to estimate the core lifetime of the NIRR-1 after addition of top Be shim plates, the maximum allowed excess reactivity was added to top Be shim worth of each core type and then the equilibrium xenon worth was subtracted from the result. This resulted in a net reactivity available in the core. This reactivity was then used for the burnup cycles to estimate the cycle length in Effective Full Power Hour (EFPH) and then converted to years. This result is presented in Table 4.21.

Table 4.14 Core Lifetime Estimate after Addition of Top Be Shim Plates

Fuel type	**HEU**	**UO_2**	**U_3Si_2**	**U_3Si**	**U-9Mo**
Net Reactivity	20.12	20.02	20.00	19.94	19.85
EFPH	12734.177	16683.333	16129.032	16211.382	18904.762
Core lifetime (years)	29.48	38.62	37.34	37.53	43.78

As presented in Table 4.14, the net reactivity of 20.12 mk yields an estimated cycle length of 12734.177 EFPD corresponding to a core lifetime of 29.48 years for the HEU core. This is in good agreement with reported values of 30.3 and 21.21 years for the NIRR-1 and PARR-1 system by Yahya *et al* (2017) and Amjad *et al* (2012) respectively. As for the UO_2, U_3Si_2, U_3Si and U-9Mo LEU the reactor net reactivity of 20.02, 20.00, 19.94, and 19.85 mk yields and estimated cycle length of 16683.333, 16129.032, 16211.382, and 18904.762 EFPD which corresponds to a core lifetime of 38.62, 37.34, 37.53, and 43.78 years respectively. Generally, it can be observed from the Table 4.21 that the core lifetime of the LEU cores is higher than that of the HEU core. This is attributable to the higher core loading of the LEU core, lowr burnup, and higher fissile isotope ^{239}Pu produced in the core. Hence, the LEU cores contributed additional reactivity over burn-up thereby reducing their depletion rate compared to the HEU core and thus extending the core lifetime of the LEU cores over that of the HEU core.

CHAPTER FIVE

5.0 SUMMARY, CONCLUSION AND RECOMMENDATIONS

5.1 Summary

In this work, the SCALE 6.2.3 code system was used to simulate reactor criticality safety and depletion parameters for the "as built" UO_2 core and the alternate U_3Si_2-Al, U_3Si-Al, and U_9Mo-Al LEU cores using a standard MNSR HEU core as a benchmark. Two models were developed: a 1D TRITON-XSDRNPM model and a 3D KENO-VI model. Both models were used to calculate CCCER of the as built UO_2 and the alternate U_3Si_2-Al, U_3Si-Al, and U_9Mo-Al LEU cores and a comparison was made between measurement and calculation for the LEU and standard HEU cores. However, only the 3D model was used for detailed neutronics and further depletion calculations. The 1D TRITON-XSDRNPM was developed assuming only major components of the NIRR-1 whereas the 3-D model involved detailed representation of nearly both major components and their associated units. Both models presented an alternative approach to criticality safety and depletion calculations for MNSRs and can be extended to other LPRRs. For the neutronic parameters, CCCER, SDM, CRW and SRF were calculated. Furthermore, moderator-to-fuel ratio, neutron flux distribution and the core condition at the BOC were also considered. The depletion calculation investigated the core composition of fissionable nuclide burnup and fission product build-up including fission poisons at the EOC of 216 EFPD. Finally, burn-up effects on reactivity was investigated and the result was used with calculated data for top Be shim worth to estimate the core lifetime of the reactor before and after addition of top Be shim plates.

This research highlights the importance of evaluating alternative fuel types for MNSRs to optimize their performance and contribute to the sustainable development of Research Reactors in the nuclear industry.

5.2 Conclusion

Based on the applied methodology and results obtained in this study, the following conclusions are drawn:

The 1-D TRITON-XSDRN model overestimates the CCCER of the NIRR-1. However, the calculated CCCER, CRW and SDM using a 3D KENO-VI model results closely agree with reported values in literature. Consequently, the 3D KENO-VI module of the SCALE code is an additional tool that can be used to perform criticality safety calculations for the NIRR-1, and similar MNSRs.

There is an increase in the ^{235}U and total Uranium initial core loading in the LEU cores when compared to the HEU cores. This mean an increase in the initial core loading cost for operation of the LEU cores.

There is a reduction in the magnitude of the average thermal neutron flux in the LEU cores in the range of 7 – 10 % when compared to that of the HEU core. This proposes that the thermal power of the U_3Si_2-Al, U_3Si-Al, and U_9Mo-Al LEU cores would have to be raised to 33.5, 33.2, and 33.9 kW respectively to match the flux performance of the HEU core.

Both the HEU and LEU cores have a burnup of less than 1 % at the EOC of 216 EFPD. However, the burnup of the uranium-silicide fuels is higher than that of the UO_2 fuel. In addition, the buildup of ^{239}Pu in the LEU cores is about 20 times when compared to the HEU core, which suggests that the LEU cores have a higher conversion ratio. However, similar to the HEU core, the conversion ratio at any point in time for the LEU cores is less than one (< 1). Thus, the LEU cores cannot be used to breed fissile ^{239}Pu isotope, which is of regulatory concern.

The equilibrium ^{135}Xe concentration occurs in about 3 days of continuous reactor operation while that of ^{149}Sm is in approximately 1000 days of continuous reactor operation. Consequently, both the HEU and LEU cores cannot be allowed to operate continuously for up to 3 days in order for the NIRR-1 to have enough excess reactivity to sustain the fission chain reaction in the core, which is necessary for operation.

The depletion rate of the HEU core is higher than that of the LEU cores. This implies that the reactivity loss for the LEU cores occur at a much slower rate compared to the HEU core. Hence there is an improvement in the fuel economy of the LEU cores compared to the HEU core.

The worth of the top Be shim plates for the HEU core is lesser in comparison to the LEU cores. This implies that there is an apparent reduction in the effectiveness of the top Be shim plates in the LEU cores.

The core lifetime of the reactor before addition of top Beryllium Shim plates when operated continuously for 216 EFPD for the HEU core has been found to be 2.20 years while that of the UO_2, U_3Si_2-Al, U_3Si-Al and U_9Mo-Al LEU cores is 3.28, 3.17, 3.20 and 3.75 years respectively. Thus, there is a reduction in the frequency of top Be plates addition in the LEU cores as compared to the HEU core. This is an improvement in the fuel economy of the LEU cores as compared to the HEU ore. Similarly, the core lifetime of the reactor after addition of top Beryllium shim plates has been found to be 29.48 years for the HEU core while that of the

UO_2, U_3Si_2, U_3Si and U-9Mo LEU cores is 38.62, 37.34, 37.53, and 43.78 years respectively. Therefore, the LEU cores can be operated for a longer period compared to the HEU core before and after addition of top Be shim plates. Consequently, the LEU cores demonstrate better performance in terms of fuel management and an advantage of extended utilization period for NAA. However, compared to the UO_2 LEU core, the U_3Si_2, and U_3Si, showed comparable core lifetime while the U9Mo core demonstrated a higher core lifetime.

Nigeria has continued to demonstrate its interest and commitment in the peaceful application of nuclear technology. In this regard, Nigeria plans to obtain a multipurpose research reactor (MPRR) and a power reactor in the near future to meet her industrial needs and improve her economy. However, human capacity building is one of the milestones towards actualizing these plans. In line with Nigeria's policy on human capacity building in the nuclear industry, the code used and model developed in the present study can be adopted or modified for detailed neutronics/criticality safety analysis of Nigeria's planned nuclear reactors.

The RERTR program has continued to support, technically and financially, the conversion of RRs from the use of HEU to LEU cores to mitigate the security risks of nuclear threats. However, following the Fukushima Nuclear accident in Japan on March 11, 2011, the concept of ATF was introduced by the U.S and IAEA. The fundamental idea was to improve safety margins and fuel management. The present work has shown that U_3Si_2, U_3Si and U-9Mo LEU cores fuels exhibit increased uranium loading, higher burnup, lower depletion rates, with an enrichment of 19.75%. Hence, in addition to their higher thermal conductivity, which lead to lower temperatures than those generated by UO_2, in terms of fuel cycle performance, the U_3Si_2, U_3Si and U-9Mo LEU cores can be used as promising alternatives to the UO_2 to improve safety, optimize fuel management, and can support the conversion of other MNSRs to LEU.

The U_3Si_2 is currently used as fuel for several operating RRs around the world. Since Nigeria plans to acquire a MPRR, U_3Si_2 can be considered as an option in order to enhance its operational safety when commissioned.

5.3 Recommendation

1. An investigation of the decay heat and shielding requirements for spent fuel storage of the LEU fuels studied in this work should be conducted to examine the requirements for spent fuel storage for the fuels.

2. An investigation of the behavior of the fuels studied in this work under severe accident conditions for MNSR should be performed to examine the safety margins of the fuels.

3. The thermo-physical behavior of the fuels in this work irradiate with MNSR flux range should be investigated to examine their irradiation performance.

REFERENCES

Ahmed, Y.A., Ewa I.O.B., Umar I.M., Bezboruah T., Johri M. and Akaho E.H.K. (2006), The low power miniature neutron source reactors: Design, safety and applications; *UNESCO/IAEA/ICTP Publication* IC/2006/020, The Abdus Salam International Centre for Theoretical Physics, Trieste.

Albarhoum M. (2011) "Neutronic Calculations of the U_3Si LEU as a Dispersed Fuel for Low-Power Research Reactors" *Annals of Nuclear Energy 38 (2011) 2304–2508.*

Amjad N., Sikander, M. M., Nasir, M. M. and Muhammad, S., (2012) "Analyses of Core life-time and Neutronic Parameters for HEU and Potential LEU/HEU fuels in a Typical MNSR' *Annals of Nuclear Energy 47 (2012) 46–52.*

Anim-Sampong, S., E.H.K. Akaho, B.T. Maakuu, J.K. Gbadago, A. Andam and J.J.R. Liaw, J.E. Matos, (2007). Neutronics Analysis for Conversion of the Ghana Research Reactor-1 Facility using Monte Carlo Methods and UO2 LEU Fuel. IRRFM 2007/IGORR, Session VI - Safety. Operation and Research Reactor Conversion, pp: 44-54.

Balogun, G. I, Jonah, S.A. and Umar I.M. (2005). Measures aimed at enhancing safe operation of the Nigeria Research Reactor-1 (MNSR). In Book of Contributed Papers, International Conference on Operational Safety Performance in Nuclear Installations, 30 November –2 December, 2005, IAEA, Vienna Austria, IAEA-CN-133/19, Pg. 93 – 96.

CERT (2011) *Final Safety Analyses Report (SAR) of Nigeria Research Reactor-1*, CERT Technical Report, CERT/MNSR/FSAR-01.

CERT, (2019). Loading of LEU core and Commissioning Report for NIRR-1 facility with LEU core. Centre for Energy Research and Training (CERT). CERT/NIRR-1/TR-004

CIAE (1993). Safety Analyses Report (SAR) for the Syrian Miniature Neutron Source Reactor, China.

CNSC Canadian nuclear safety commission (CNSC. 2003), Science and reactor fundamentals: Reactor physics technical group.

Dawahra S., Khattab K., Saba G. (2015) Calculation of fuel burnup and radionuclide inventory in the 10 MW MTR type research reactor using the GETERA code *Annals of Nuclear Energy* 78 (2015) 89-92

DOE. (1993). Department of Energy Fundamentals Handbook-Nuclear Physics and Reactor Theory Volume 2 of 2, DOE-HDBK-1019/2-93, pp: 1-33

Eugene Wigner (2003) Training course for reactor physics experiment, Atomic Institute Vienna H, Bock and A. Zeilinger AIAU 89302

Glaser .A. (2005) “Neutronic calculation relevant to the core conversion of research reactoes tolow enriched fuels” Ph.D. Thesis pg 25-50

Glaser, A. (2007). “Performance Gain with Low-Enriched Fuel and Optimized Use of Neutrons” *The 29th International Meeting on Reduced Enrichment for Research and Test Reactors* (RERTR) Program on Science and Global Security, Princeton University Prague, Czech Republic

Global threat Reduction Initiative National Nuclear security administration (GTRI) (2014) GTRI National academy of science washington, DC.

Goluoglu .S., L. M. Petrie, Jr., M. E. Dunn, D. F. Hollenbach, and B. T. Rearden, (2011). “Monte Carlo Criticality Methods and Analyses Capabilities in SCALE,” *Nuclear Technology* 174, 214–335

Neutronics Assessment of Accident-Tolerant Fuel in Advanced Power Reactor 1400 (APR1400). (2020). D. Hartanto, A. Alshamsi, A. Alsuwaidi, A. Bilkhair, H.A. Hukal and M. Zubairet al. / Atom Indonesia Vol. 46 No. 3 (2020) 177 – 186

Ibikunle, K.I., 2018. Neutronics Analyses of Dispersion Fuels for Core Conversion of NIRR-1. PhD Thesis. Department of Physics, Ahmadu Bello University Zaria, Nigeria.

International Atomic Energy Agency (1992) *Research Reactor Core Conversion* GuidebookVolume 4: Fuels (APPENDICES I-K) IAEA, VIENNA,IAEA-TECDOC-643ISSN 1011 4289

International Atomic Energy Agency, IAEA (2002) *safeguard glossary. 2001 Edition.International nuclear verification series*, No. 3. Vienna

International Atomic Energy Agency, IAEA (2006) *A newsletter of the Division of Nuclear Fuel Cycle and Waste Technology Vol. 2, No. 1*

Ibikunle Kola, Ibrahim Y.V., Jonah S.A. (2015) ‘Neutronics Analyses of Dispersion Fuels as Alternate Fuels for the Conversion of MNSR to LEU using MCNP., RERTR 2015 — 36th International Meeting on Reduced Enrichment For Research And Test Reactors, OCTOBER 11-14, the Plaza hotel Seoul, South Korea.

International Atomic Energy Agency, 1844 (2012) Analyses Supporting Conversion of Research Reactors From High Enriched Uranium Fuel To Low Enriched Uranium Fuel, IAEA TECDOC-1844

James .I. Cole, Barry H. Rabin, James A. Smith, Clark L. Scott, Bradley C. Benefiel, Eric D.Larsen, Paul . Lind, David A. Sell (2016) “US Progress on property Characterization to support U-10 Mo Monolithic fuel development” conference proceedings, *European Research Reactor conference, Berlin, Germany* p139-142

Jessee, M.A., Dehart, M.D., (2011).‘‘TRITON: A Multipurpose Transport, Depletion, and Sensitivity and Uncertainty Analyses Module,” Tech. Rep. ORNL/TM-2005/39 Version 6.1 Sect. T1, Oak Ridge National Laboratory.

Jonah S.A. Umar I.M., Oladipo M.O.A, Balogun G.I., Adeyemo D.J (2006), Standardizatioof MNSR Irradiation and Counting Facilities for Instrumental Neutron Activation Analyses. Appld Rad. & Isotopes, 64, 818-822

Jonah, S.A., Ibikunle, K, Li, Y., (2009) A Feasibility Study of Low Enrichment Uranium (LEU) fuels for MNSR conversion using MCNP, *Annals of Nuclear Energy*, (36) 1285–1286.

Jordi, R. (2014) “GTRI Reactor conversion programme” *scope and objectives,* Nuclear Engineering division, Argonne National Laboratory.

Jordi Roglans-Ribas and Christopher Landers (2011) “Research and test reactor conversion to Low Enriched Uranium Fuel: Technical and Programmatic Progress” International Conference on Research Reactors: Safe Management and Effective Utilization

Khattab K. (2005) ‘Calculations of fuel burn-up and radionuclide inventory in the syrian miniature neutron source reactor using the WIMSD4 code’ Annals of Nuclear Energy, 32:1122–1130

Kontogeorgakos D., K. Derstine, A. Wright, T. Bauer, J. Stevens (2013) “Initial Neutronics Analyses for HEU to LEU Fuel Conversion of the Transient Reactor Test Facility (TREAT) at the Idaho National Laboratory”.

Lamarsh J. R and Baratta A. J., (2001), Introduction to Nuclear Engineering, New Jersey 07458: Upper Saddle River, , p. 389.

Leenaers, A., Van Renterghem, W., Van den Berghe, S.. (2016) ‘High burn-up structure of U(Mo) dispersion fuel’ Journal of Nuclear Materials (476) 218-230

Lell R.M. and Matos J.E. (2005) ‘Feasibility study of potential LEU Fuels For A generic MNSRReactor, International meeting on reduced enrichment for Research and Test Reactors’ November 6-10 2005, Boston, Massachusetts.

Liaw, J.R., Matos, J.E., (2007). MNSR flux performance and core lifetime analysis with HEU and LEU fuels. In: Paper Presented at the International Meeting on Reduced Enrichment for Research and Test Reactor Held Prague, Czech Republic, September, pp. 23–27.

Mahmood T., Showket P., Masood I. (2008) Neutronic analysis for core conversion (HEU LEU) of Pakistan research reactor-2 (PARR-2). *Annals of Nuclear Energy* 35(8) Volume 35, Issue 8, August 2008, Pages 1440-1446

Marek .M., Kysela .J., Ernes .J., Flibo .S. R, Broz .V., (2007) “Impact of the HEU/LEU Conversion on Experimental Facilities” *The RERTR-2007 International Meeting On Reduced Enrichment For Research And Test Reactors,* Septembe*r 23-27, 2007* Prague Czech Republic

Meyer .M.K. (2015) “History of LEU Fuel Development and Selection of USHPRR Fuel System”, *Paper presentation,* U.S. Department of energy.

Omar H. and Ghazi N., (2013). ‘Decay heat analysis of MNSR reactor core using ORIGEN-2 code.’ Nuclear Engineering and Design 265 (2013) 978–98

Rabba J.A., Muhammad Y.O., Onimisi S. (2020). Estimation of Fuel Burnup Rate for Core Conversion for the Nigeria Research Reactor-1 (NIRR-1) Fueled With 19.75% Enriched UO2 USING VENTURE PC Code. Physical Science International Journal, Volume 24, Issue 2, Page 42-49

Ronald .J. Ellis, Jess C. Gehin, Germina Ilas, and R. T. Primm (2010) Neutron Physics of an LEUU-Mo Fueling Study for the High Flux Isotope Reactor

Salawu A. (2013): “The study of research reactor design parameter for core conversion of NIRR1 from HEU to LEU”. *PhD thesis*, Department of Physics, Ahmadu Bello UniversityZaria, Nigeria

Simon Younan and David Novog (2018) Assessment of Neutronic Characteristics of Accident-Tolerant Fuel and Claddings for CANDU Reactors Hindawi Science and Technology of Nuclear Installations Volume 2018, Article ID 5327146, 17 pages

Simon, J., Ibrahim, Y.V., Adeyemo, D.J., Garba, N.N., Asuku, A., (2021). Comparative analysis of core life-time for the NIRR-1 HEU and LEU cores. Prog. Nucl. Energy 141 (2021), 103970.

J. Simon, Y.V. Ibrahim, D.J. Adeyemo, N.N. Garba, A. Asuku, S. Bello, I.K. Ibikunle. (2022) Radiological consequence analysis for hypothetical accidental release from Nigerian Research Reactor-1. *Applied Radiation and Isotopes 186 (2022)*110308

Sogbadji R. B. M., Nyarko B. J. B., Akaho E. H. K. and Abrefah R. G. A., (2011) "Determination of Neutron Fluxes and Spectrum Shaping Factors in Irradiation Sites of Ghana’s Miniature Neutron Source Reactor (MNSR) by Activation Method after Compensation of Loss of Excess Reactivty," World Journal of Nuclear Science and Technology, vol. 1, no. doi:10.4236/wjnst.2011.12009 Published Online July 2011, pp. 50-56, 2011.

Sogbadji R. B. M., (2012) " Neutronic Study of the Mono-Recycling of Americium in PWR and of the Core Conversion in MNSR using the MURE Code," World Journal of Nuclear Science and Technology, vol. 1, no. doi:10.4236/wjnst.2011.12009 Published Online July 2011, pp. 50-56, 2011.

Weston M.S (2007) edition *Nuclear Reactor Physics*, Second Edition.: Published Online: 10MAY 2007. Print ISBN: 9783527406791

W. A. Wieselquist, R. A. Lefebvre, and M. A. Jessee, Eds., (2020)SCALE Code System, ORNL/TM-2005/39, Version 6.2.4, Oak Ridge National Laboratory, Oak Ridge, TN.

Wiarda, D., Dunn, M. E., Green, N. M., Williams, M., Celik, L C., Petrie, L. M. (2016) 'Ampx- 6: A Modular Code System For Processing Endf/B Evaluations' Oak Ridge National Laboratory Oak Ridge, Tn 37831-6283

Yahaya, B., Ahmed, Y.A., Balogun, G.I., Agbo, S.A., 2017. Estimating NIRR-1 burn-up and core life time expectancy using the codes WIMS and CITATION. *Results in Physics*. Elsevier Science, pp. 596–603.

Yang, Y.W., (1992) MNSR Reactor Complex Manual, CIAE, Beijing, China

Zafar Yasin (2009) 'Comparative Study of Fuel Burn-Up And Radioactive Inventory For Proliferation And Proliferation Resistant Fuel Lattices' *Annals of Nuclear Energy* (36)1635–1638\

APPENDIX I

I.1 HEU Fuel cell model calculation

The characteristics of the NIRR-1 HEU core are presented in Table I.1. The most important parameter in calculating the dimension of the equivalent fuel cell of the NIRR-1 MNSR is the moderator volume per pin for the fuel cell model development. However, the variation in the radial pitch of the ten concentric circles of the NIRR-1 core, the existence of 4 tie rods and 3 dummy pins in the core initially made it difficult to select a single pin from any circle to calculate the moderator volume per pin for the fuel cell model development. In order to simplify this problem, we adopted the assumption of (Salawu, 2013) by assuming that there are no dummy or tie pins in the core. Consequently, the entire core volume per pin was calculated based on the 347 active fuel pins in the core. This was then used to define a total volume for the fuel cell. Hence, the volume of the water region in this fuel cell is a mixture of moderator, tie rods and dummy pins volume. The volume fraction of the materials in this mixture was then calculated and multiplied by their corresponding atom densities to define the effective atom density of the nuclide in the “moderator, tie rods and dummy pins mix region” in the fuel cell model. Below are the details of our calculations: A half symmetry of the fuel cell is shown in Figure I.1. The volume fraction of various regions in the fuel cell is presented in table I.2

Table I.1: Description of the Active Fuel Region of the NIRR-1 HEU Fuel (CERT, 2011)

Description	Value
Material in the active fuel region	UAl_4 –Al
Density of UAl_4 –Al in fuel	3.456 g/cm^3
Type/ enrichment	HEU/ 90.2% ^{235}U
Mass of ^{235}U in each fuel pin	2.88 g
Height of active fuel material	23.0 cm
Diameter of active fuel region	0.43 cm

Using;

radius of the core (r_C) = 11.55 cm

radius of the guide tube (r_{GT}) = 0.6 cm

1-D cylindrical volume = $\pi {r_{i+1}}^2 - \pi {r_i}^2$ (Petrie, 2011)

$$Total\ volume\ of\ fuel\ regions\ in\ the\ core\ (TVFR)$$

$$= Total\ core\ volume (TCV) - guide\ tube\ volume\ (GT)$$

$$= \pi {r_C}^2 - \pi {r_{GT}}^2 = (\pi \times 11.55\ \times 11.55) - (\pi \times 0.6\ \times 0.6) = 417.9653\ cm^2$$

$$Total\ volume\ of\ fuel\ regions\ in\ the\ core\ per\ fuel\ pin = \frac{417.9653}{347} = 1.2045\ cm^2$$

The total volume of fuel regions in the core per fuel pin is equivalent to the fuel cell volume.

The fuel cell outer radius is now calculated as:

$$Fuel\ cell\ outer\ radius = \left(\frac{Total\ volume\ of\ fuel\ regions\ in\ the\ core\ per\ fuel\ pin}{\pi}\right)^{1/2}$$

$$= 0.6192\ cm$$

Thus, the fuel cell diameter = $2 \times Fuel\ cell\ outer\ radius =$ 2 ×0.6192 = 1.2384 cm

Now,

Since the radius of the dummy pins = radius of tie rods = 0.275 cm

$$\text{T}otal\ vol.of\ 3\ dummy\ pins\ and\ 4\ tie\ riods = 7 \times (\pi \times 0.275 \times 0.275) = 1.6631\ cm^2$$

But,

$$Total\ vol.of\ fuel\ rods = 347 \times (\pi \times 0.275 \times 0.275) = 82.4413\ cm^2$$

Hence,

$$Total\ vol.of\ water\ in\ the\ core$$

$$= Total\ volume\ of\ fuel\ regions\ in\ the\ core - Total\ vol.of\ fuel\ rods$$

$$- \text{Total vol. of 3 dummy pins and 4 tie rods}$$

$$= 417.9653 - 82.4413 - 1.6631 = 333.8609\ cm^2$$

Thus;

$$Total\ vol.of\ water, tie\ rods\ and\ dummy\ rods\ in\ the\ core = 333.8609 + 1.6631$$

$$= 335.524\ cm^2$$

Therefore,

$$Volume\ fraction\ of\ "dummy\ pins\ and\ tie\ rods",$$

$$in\ the\ "water, tie\ rod\ and\ dummy\ pin\ mix"\ region\ of$$

$$the\ fuel\ cell$$

$$= \frac{1.6631}{335.524} = 4.95702\ e^{-3}$$

$$volume\ fraction\ of\ moderator\ (water) in\ the\ "water, tie\ rod\ and\ dummy\ pin\ mix"\ region\ of$$

$$the\ fuel\ cell$$

$$= \frac{333.8609}{335.524} = 9.95043\ e^{-1}$$

Table I.2 Volume fractions in the water region for fuel cell model development

Description	Value
Total volume of fuel regions in the core	417.9653 cm^2
Total volume of the core per fuel pin	1.2045 cm^2
Fuel cell outer radii	0.6192 cm
Fuel cell diameter	1,2384 cm
Total volume of mixture of water + Tie rods +dummy rods	335.524 cm^2
Volume fraction of dummy pins plus tie rods in water and Aluminum mix region of the fuel cell	4.95702 *e*-3
Volume fraction of moderator in water and Aluminum mix region of the fuel cell	9.95043 *e*-1

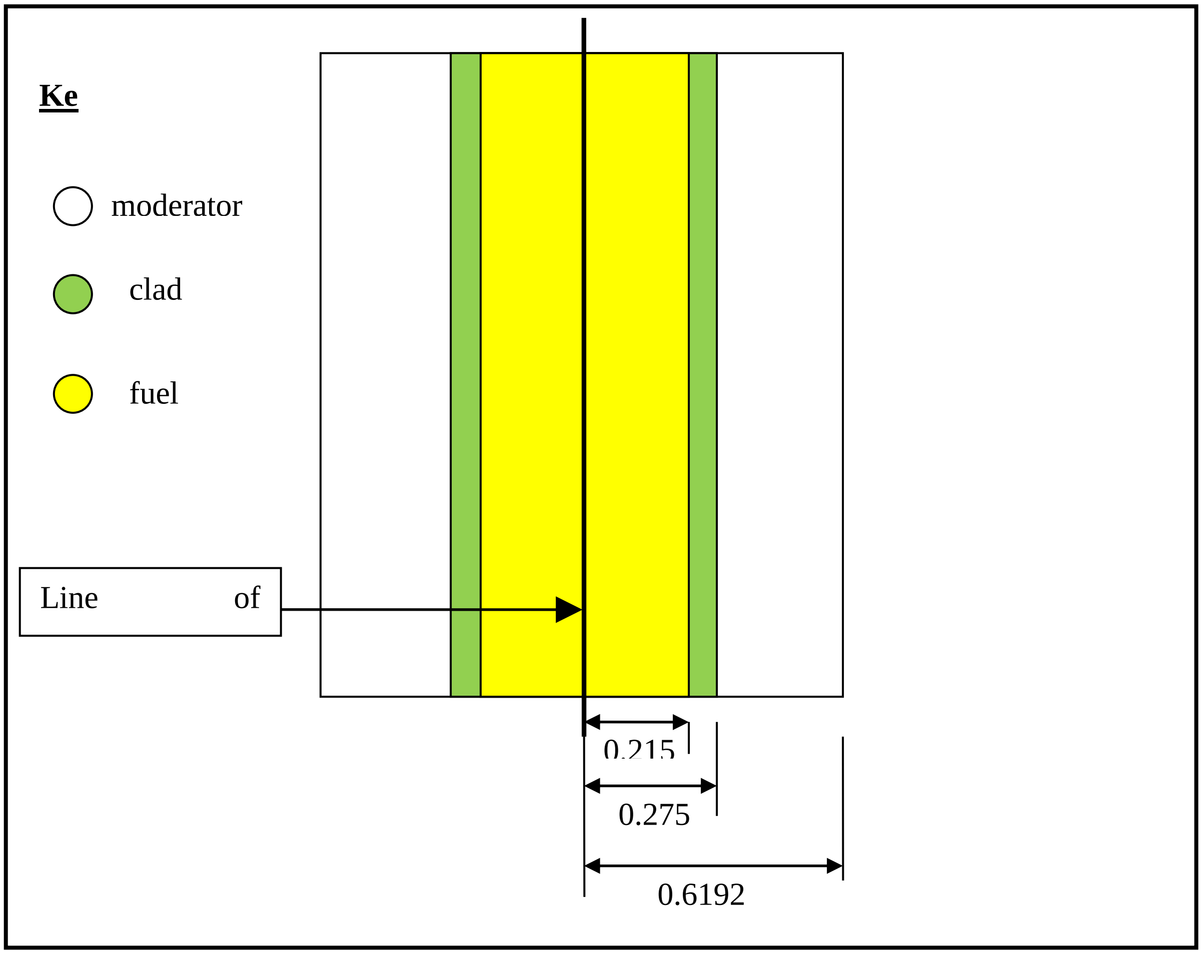

Figure I.1: A half symmetrical representation of a unit fuel cell model for a the NIRR-1

The data in Figure I.1 was used to calculate the total distance in Table I.3

Table I.3 Material geometry and layout of NIRR-1 HEU fuel cell model

Zone Number	Material Number	Description	Width (cm)	Total distance (cm)
1	1	Fuel	0.2150	0.2150
2	2	Clad	0.0600	0.2750
3	3	Moderator	0.3442	0.6192

I.2 Homogenized atom density for NIRR-1 HEU fuel cell model

To obtain the homogenized atom density for the nuclides in the fuel, clad and moderator zones of the fuel cell, the volume of the fuel, clad and moderator in the fuel cell was first calculated using the data from Figure I.1 and Table I.3. Thereafter, sing equation (2.6), the atom densities for nuclides in each of the the region was then calculated. The results of the volume and volume fraction of each zone/region in the fuel cell, their volume is presented in Tables I.4 and I.5 respectively.

$$volume\ of\ fuel\ = \frac{\pi d^2}{4} = \frac{\pi \times 0.43^2}{4} = 0.1452\ cm^2$$

$$volume\ of\ fuel + clad = \frac{\pi d^2}{4} = \frac{\pi \times 0.55^2}{4} = 0.2376\ cm^2$$

$$volume\ of\ clad = (volume\ of\ fuel + clad) - volume\ of\ fuel = 0.0924$$

$$volume\ of\ moderator = volume\ of\ fuel\ cell - (volume\ of\ fuel + clad)$$

$$= (\pi \times 0.6172^2) - 0.2376 = 0.9669\ cm^2$$

Table I.4: 1-D Cylindrical Volume for Different Regions in the Fuel Cell Model

Material name	Fuel cell	Fuel + clad	Fuel	clad	Moderator
Material Volume (cm^2)	1.2045	0.2376	0.1452	0.0924	0.9669

Table I.5: Zones in the HEU Fuel Cell Model and Their Respective Region Volume Fraction

Region	Volume (cm^2)	Total volume (cm^2)	Volume fraction	Sum of volume fraction
Fuel	0.1452		0.12055	
clad	0.0924	1.2045	0..07671	1.0000
moderator	0.9669		0.80274	

Details of all the region atom density calculations for the NIRR-1 HEU fuel cell is shown as follows:

Since the height of each fuel pin is 23 cm:

$$Volume\ of\ fuel\ pin = \frac{\pi d^2}{4} h = \frac{\pi \times 0.43^2}{4} \times 23 = 3.3405\ \text{cm}^3$$

Using the mass of ^{235}U per pin of 2.88 g, we obtain the ^{235}U density in the fuel as

$$\rho_{235_U} = \frac{2.88g\ of\ U235}{fuel\ pin} \times \frac{fuel\ pin}{3.3405\ cm^3} = 0.8621\ gcm^{-3}$$

The region atom density of ^{235}U is calculated using equation (2.6) as follows:

$$N_{235_U} = \frac{\rho_{235_U} \times N_A}{M_{235_U}} = \frac{0.8621\ \ gcm^{-3} \times 0.6022 \dfrac{atoms.cm^2}{gmol.b}}{235.0439 g/gmol} = 2.209\ e^{-3}\ \ atoms/b - cm$$

However, the density of natural Uranium $\rho_U$in the fuel material is calculated as

$$\rho_U = \frac{0.8621\ g\ of\ U235}{cm^3} \times \frac{1g\ of\ Uranium}{0.9020g\ of\ U235} = 0.9558\ gcm^{-3}$$

The molecular weight of natural uranium in the fuel was calculated as follows:

$$\frac{1}{M_U} = \sum_i \frac{w_i}{M_i} = \frac{0.9020}{235.0439} + \frac{0.098}{238.0508} = 235.3352\ g/gmol$$

Thus, we calculated the region atom density of natural uranium in the active fuel material as

$$N_U = \frac{\rho_U \times N_A}{M_U} = \frac{0.9558\ gcm^{-3} \times 0.6022 \dfrac{atoms.cm^2}{gmol.b}}{235.3352 g/gmol} = 2.446\ e^{-3}\ \ atoms/b - cm$$

We therefore calculated the region atom density of ^{238}U in the active fuel material as:

$$N_{U238} = N_U - N_{U235} = 2.3702\ e^{-4}\ \ atoms/b - cm$$

Because the total density of HEU-UAl_4 fuel is 3.456 g cm^{-3} it was possible to obtain the mass density of Al in the fuel by calculating the difference between the total mass density of Uranium and the mass density UAl_4.

Therefore;

$$\rho_{Al} = \rho_{UAl_4} - \ \rho_U = 3.456 - 0.956 = 2.500\ g/cm^3$$

Hence,

the atom density of Al in the fuel was calculated as:

$$N_{Al} = \frac{2.500 \times 0.6022}{26.9815} = 5.580e - 2\ atoms/b - cm$$

To obtain the atom density of Al in the cladding material which is 99.97% Al we used the density of pure Al, which is 2.7 g/cm^3. Thus, we obtained the atom density of pure Al to be

$$N_{pure\ Al} = \frac{2.7 \times 0.6022}{26.9815} = 6.0261\ e^{-2}\ atoms/b - cm$$

For the region atom density of nuclides within the moderator we used the mass density of water provided in IAEA TECDOC 1844 (2012) to be 0.9982 g/cm^3.

$$N_{H_2O} = \frac{\rho_{H_2O} N_A}{M_{H_2O}},$$

where, $M_{H_2O} = 2M_H + M_O = 2 \times 1.0079 + 15.9994 = 18.0152 g/gmole$

$$N_{H_2\mathrm{O}=} \frac{0.9982 \times 0.6022}{18.0152} = 3.337\ e^{-2}\ molecules/b - cm$$

The effective atom density of moderator (water), $N_{H_2O}^{eff}$, in the moderator region of the fuel cell is the product of the atom density of water and the volume fraction of water in the water, tie rod, and dummy pin region of the fuel cell.

$$N_{H_2O}^{eff} = N_{H_2\mathrm{O}} \times \text{volume fraction} = 3.337\ e^{-2} \times 9.95043\ e^{-1}$$

$$= 3.320\ e^{-2}\ molecules/b - cm$$

The effective density of the nuclides in the moderator region of the fuel cell was calculated as follows:

$$N_H = 3.320\ e^{-2}\ atoms/b-cm \times \frac{2\ atoms\ of\ H}{1\ molecule\ of\ H_2O} = 6.6400\ e^{-2} atoms/b-cm$$

$$N_O = 3.320\ e^{-2} molecules/b-cm\ of\ H_2O\ \times \frac{1\ atoms\ of\ O}{1\ molecule\ of\ H_2O}$$

$$= 3.320\ e^{-2}\ atoms/b-cm$$

$$N_{tie\ rod\ and\ dummy\ pins(Al)}^{H_2O\ plus\ \ Al\ mix\ region} = \ 6.0261\ \ e^{-2}\ atoms/b-cm \times 4.957 e^{-2}\ atoms/b-cm$$

$$= 2.987 e^{-4} atoms/b-cm$$

The homogenize atom density of various nuclides was then calculated using equation (2.6). The result is shown in Table I.6

Table I.6 Material composition data for the XDRNPM fuel cell model

Matl name	Matl #	U235	U238	Al27	O16	H1
fuel	1	2.209e-3	2.370e-4	5.580e-2	-	-
clad	2	-	-	6.026e-2	-	-
moderator	3	-	-	2.987e-4	3.320e-2	6.640e-2

Table I.7: Homogenized Atom Density for the NIRR-1 HEU Fuel Cell

Material Name	$\boldsymbol{f_i}$	**Nuclide**	$\boldsymbol{N_{ij}}$	$\boldsymbol{N_{ij} f_i}$	$\boldsymbol{N_{iz}}$ ***(a/b-cm)***
		U235	2.209e-3	2.617e-4	2.663e-4
Fuel	0.12055	U238	2.370e-4	2.857e-5	2.857e-5
		Al27	5.580e-2	6.727e-3	
Clad	0.07671	Al27	6.036e-2	4.623e-3	1.159e-2
		Al27	2.987e-4	2.398e-4	
Moderator	0.80274	H1	6.640e-2	5.331e-2	5.331e-2
		O16	3.320e-2	2.665e-2	2.665e-2

I.2 Control cell calculations:

I.2.1 The NIRR-1 Control Rod and the Control Cell

The NIR-1 control rod is a Stainless steel (SS) cladded rod (CR) made of neutron poisons (cadmium of density 8.64 g/cm^3), which has a large absorption cross section for neutrons. This property of having relatively large absorption cross section for neutrons makes it attractive for use in fission control in the reactor. Although most reactors have more than one CR, each serving specific purpose of shutdown, real-time control, safety or startup, the NIRR-1 CR has just one central control rod serving all control purposes. The CR cadmium poison has a diameter of 0.39 cm. The inner and outer diameter of the CR guide tube is 0.9 cm and 1.2 cm respectively (Yiguo *et al*, 2007). The control cell was constructed with the poison, SS clad, water, guide tube and homogenized fuel. The geometry and material layout of the control cell "in"(CR "in") is presented in Table I.8 The CR "in" is made up of all the aforementioned control cell material while the CR "out" is made up of all the control cell material excluding the poison and the SS clad. Figures I.2, I.3, I.4, and I.5 shows an illustration of the CR "in" cell, a half symmetric view of the CR "in", the CR "out" and a half symmetric view of the CR "out" respectively for the purpose of clarity. The material composition of the cadmium poison having a density of 8.64g/cm^3 is presented in Table I.9 (Petrie *et al*, 2011). The material composition data for the clad material made of SS304s of density 7.94 g/cm^3 is presented Table I.10 and Table I.11.

Table I.8 Geometry and material layout of CR "in" cell for NIRR-1

Zone Number	Description	Width (cm)	Total distance (cm)
1	Cadmium	0.195	0.195
2	Clad	0.050	0.245
3	Water	0.205	0.450
4	Guide tube	0.150	0.600
5	Fuel	10.95	11.55

Poison material

The atom density of poison material, which is natural cadmium, was calculated as follows

$N_{mix} = \frac{\rho N_A}{M_{mix}} = \frac{8.64 \ x\ 0.6022}{112.411} = 4.629e - 2 \ atoms/cm$

where $\rho = 8.64 g/cm^3$ and $N_A = 0.6022 \ g.cm^2/gmol.b$, N_{mix} is the total atom density of all the cadmium isotopes and M_{mix} is the molecular mass of a natural cadmium.

For the SS clad

The equation $N_i = \frac{w_i \rho N_A}{M_i}$ was used to calculate the isotope atom densities in the SS clad where $\rho = 7.94 g/cm^3$, w_i and M_i are as tabulated in Table 3.8.

For the CR "in" cell model

$$Volume\ of\ CR + SS\ clad + watwer + GT = \pi r^2 = \pi \times 0.6^2 = 1.1310\ cm^2$$

$$Volume\ of\ CR = \pi r^2 = \pi \times 0.195^2 = 0{,}1195\ cm^2$$

$$Volume\ of\ SS\ clad = \pi r^2 = (\pi \times 0.245^2) - 0.1195 = 0.1886 - 0.1195 = 0.0691 cm^2$$

$$Volume\ of\ water\ in\ the\ CR\ guide\ tube = \pi r^2 = (\pi \times 0.45^2) - 0.1886 = 0.4476\ cm^2$$

$$volume\ of\ GT = \pi r^2 = (\pi \times 0.6^2) - (\pi \times 0.45^2) = 0.4948\ cm^2$$

$$Volume\ fraction\ of CR = \frac{0.1195}{1.1310} = 0.1057$$

$$Volume\ fraction\ of SS\ clad = \frac{0.0691}{1.1310} = 0.0611$$

$$Volume\ fraction\ of\ of\ water\ \ CR\ guide\ tube = \frac{0.4476}{1.1310} = 0.3957$$

$$Volume\ fraction\ of\ GT = \frac{0.4948}{1.1310} = 0.4375$$

Now for the **CR "out"**

$$Volume\ of\ water\ in\ GT = \pi r^2 = \pi \times 0.45^2 = 0.6362\ cm^2$$

$$Volume\ of\ GT + water\ = \pi r^2 = \pi \times 0.6^2 = 1.1310\ cm^2$$

thus

$$Volume\ of\ water\ in\ GT = 1.1310 - 0.6362 = 0.4948\ cm^2$$

Similarly,

$$Volume\ fraction\ of\ water\ in\ GT = \frac{0.6362}{1.1310} = 0.5625$$

$$Volume\ fraction\ of\ \ GT = \frac{0.4948}{1.1310} = 0.4375$$

Table I.9 Atom Density (Atom/b-cm) of Various Nuclides in the Control Meat Material

S/No	Nuclide ID	M_i (g/gmol)	γ_i (%)	N_i
1	cd-48106	105.91	1.25	5.786e-4
2	cd-48108	107.90	0.89	4.120e-4
3	cd-48110	109.90	12.49	5.782e-3
4	cd-48111	110.90	12.809	5.925e-3
5	cd-48112	111.90	24.13	1.117e-2
6	cd-48113	112.90	12.22	5.657e-3
7	cd-48114	113.90	28.73	1.330e-2
8	cd-48116	115.90	7.48	3.467e-3

Table I.10 Atom Density of Various Nuclides Present in the Clad Material SS304s

S/No.	Material Name	Nuclide ID	M_i (g/gmol)	w_i (w/o)	N_i
1		14000-Si	28.086	1.000	1.702e-3
2		24000-Cr	51.996	19.00	1.747e-2
3	SS304s	25055-Mn	54.938	2.000	1.741e-3
4		26000-Fe	55.849	68.50	5.865e-2
5		28000-Ni	58.693	9.500	7.739e-3

Table I.11 shows the result of the atom density calculation of the individual nuclides present in the SS. The result is the product of the natural abundance of the individual nuclides present in the SS and their corresponding nuclide atom density. The CR guide tube is made up of aluminum and has a characteristic density of 2.7 g/cm^3. The atom density calculation for Aluminum in the guide tube is the same as that of Aluminum in the fuel clad material.

Table I.11 Atom Density of Nuclides in the SS Clad

S/No	Nuclide	Density	Isotope ID	γ_i (%)	Isotope density
1	Silicon	1.702e-3	14028	92.223	1.570e-3
			14029	4.685	7.975e-5
			14030	3.092	5.263e-5
2	Chromium	1.747e-2	24050	4.345	7.591e-4
			24052	83.789	1.464e-2
			24053	9.501	1.660e-3
			24054	2.365	4.132e -4
3	Manganese	1.741e-3	25055	100.0	1.741e-3
4	Iron	5.865e-2	26054	5.845	3.428e-3
			26056	91.754	5.381e-2
			26057	2.119	1.243e-3
			26058	0.282	1.654e-4
q5	Nickel	7.739e-3	28058	68.0769	5.268e-3
			28060	26.2231	2.029e-3
			28061	1.1399	8.822e-5
			28062	3.6345	2.813e-3
			28064	0.9255	7.163e-5

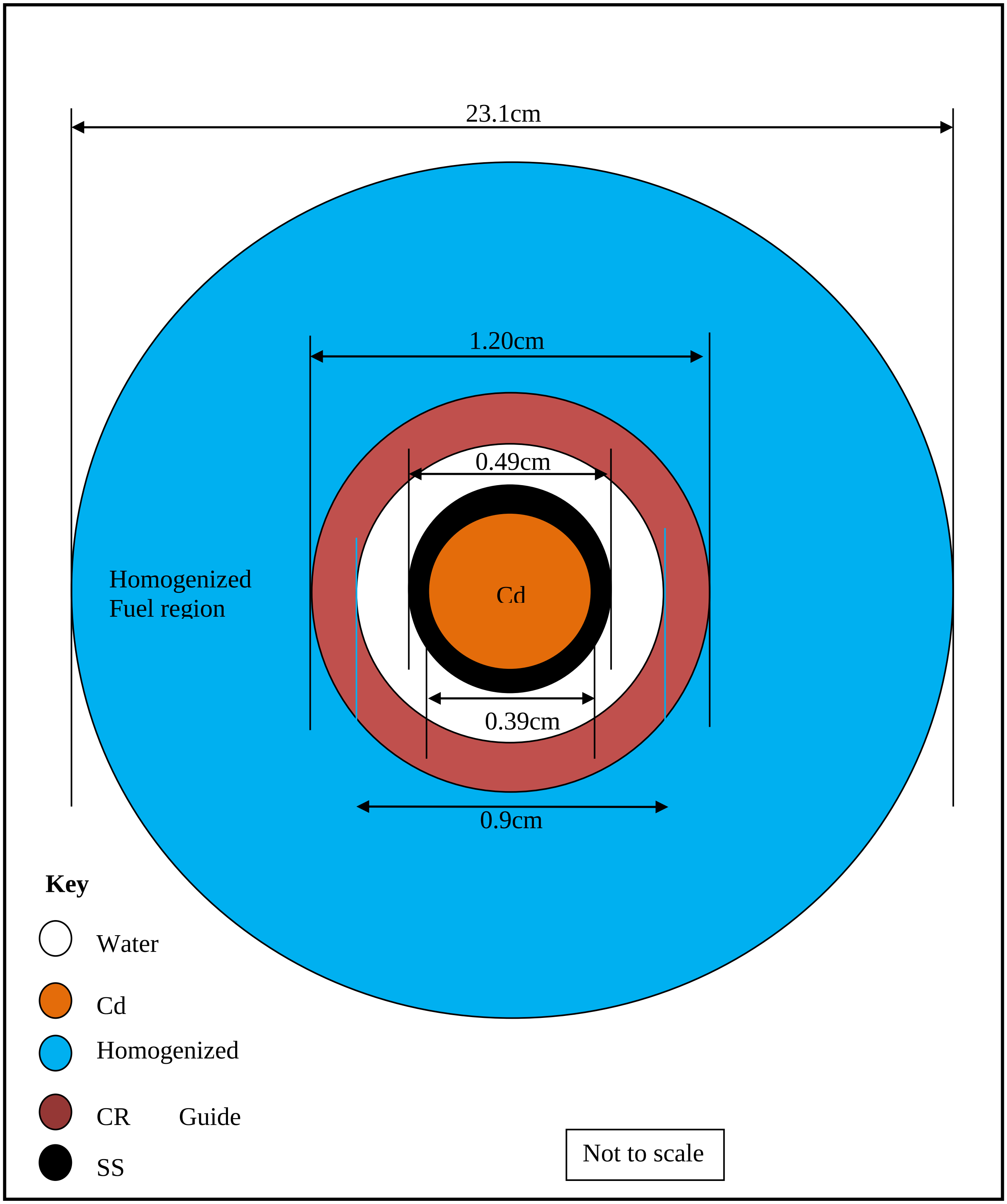

Figure I.2: CR “in” Cell for the NIRR-1

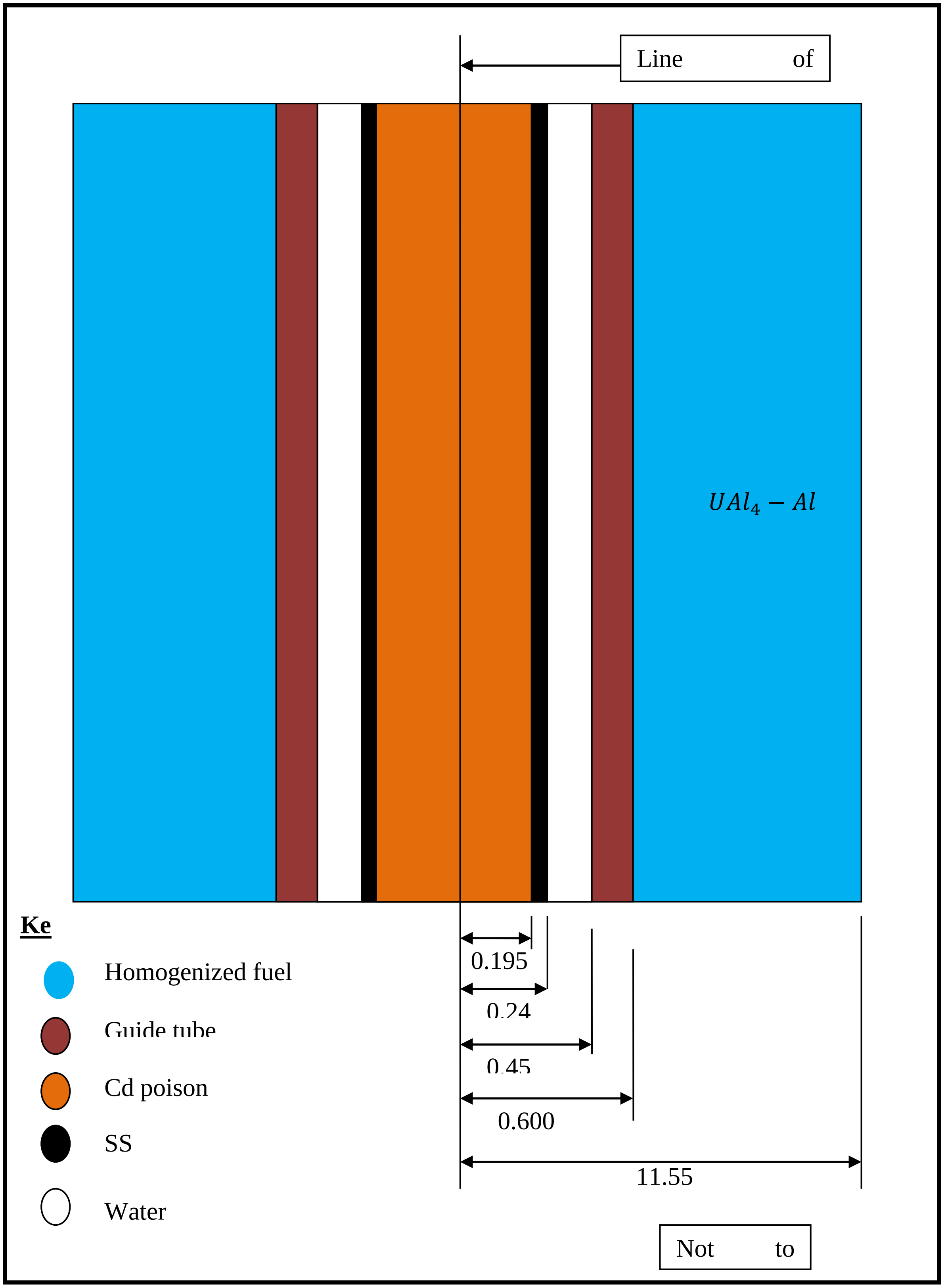

Figure I.3: A Half Symmetric Representation the CR “in” Cell for the NIRR-1

In order to obtain the effective densities of isotopes in the control region for the CR “in” and the CR “out” model, the volume fractions of the different regions in the CR “in” and CR “out” were calculated. The results of the calculation are tabulated in Table I.12, I.13, and I.14. The geometry and material layout of the CR “out” cell model is presented Table I.15.

Table I.12: Geometry and Material Layout for the CR “out” cell

Zone number	description	width (cm)	total distance	material number
1	water	0.45	0.450	1
2	Guide tube	0.15	0.600	2
3	furl	10.95	11.550	3

Table I.13: volume for Different Regions in the CR “in” cell of the NIRR-1

Material Name	CR	SS clad	Water	Guide tube
Material volume (cm^2)	0.1195	0.0691	0.4476	0.4948

Table I.14: Region Volume Fractions for Zones in the CR “in” cell of the NIRR-1

Circle number	Region	Volume (cm^2)	Total volume (cm^2)	Volume fractions	Sum of volume fractions
	CR	0.1195		0.1055	
	SS clad	0.0691		0.0611	
0	Water	0.4476	1.1310	0.3957	1.0000
	Guide tube	0.4948		0.4375	

Table I.15: Region Volume Fractions for the Zones in the Control "out" Cell

circle Number	Region	Volume (cm2)	Total volume (cm^2)	Volume fraction	Sum of volume fractions
	water	0.6362		0.5625	
0	Guide tube	0.4948	1.131	0.4375	1.0000

The final material composition of the CR "in" cell was a combination of the material compositions of poison material, SS clad, guide tube, water and homogenized fuel. This is presented in Table I.16. The final material composition for the CR "out" cell is a combination of the material composition for the water, guide tube and homogenized fuel, is also presented in Table I.17.

Table I.16: Material Composition Data (atom/b-cm) for the CR "in" in Cell

Material #.	Material Name	Nuclide ID#	Region Density
		48106	5.786e-4
1	Poison material	48108	4.120e-4
	(Cadmium)	48110	5.782e-3
		48111	5.925e-3
		48112	1.117e-2
		48113	5.657e-3
		48114	1.330e-2
		48116	3.467e-3
		14028	1.570e-3
		14029	7.974e-5
		14030	5.263e-5
		24050	7.591e-4
		24052	1.464e-2
		24053	1.660e-3
	Clad	24054	4.132e-4
2	(Stainless Steel:	25055	1.741e-3
	SS316)	26054	3.428e-3
		26056	5.381e-2
		26057	1.243e-3
		26058	1.654e-4
		28058	5.268e-3
		28060	2.029e-3
		28061	8.822e-5
		28062	2.813e-4
		28064	7.163e-5
3	water	1001	6.674e-2
		8016	3.337e-2
4	Guide Tube	13027	6.026e-2
5	Fuel	92235	2.663e-4
		92238	2.857e-5
		13027	1.159e-2
		1001	5.330e-2
		8016	2.665e-2

Table I.17: Material Composition Data (atom /b-cm) for the XSDRNPM Control "out" Cell

Material Number	Material Name	Nuclide ID Number	Region density
3	water	1001	6.674e-2
		8016	3.337e-2
4	Guide tube	13027	6.026e-2
5	Fuel	92235	2.663e-4
		92238	2.857e-5
		13027	1.159e-2
		1001	5.330e-2
		8016	2.665e-2

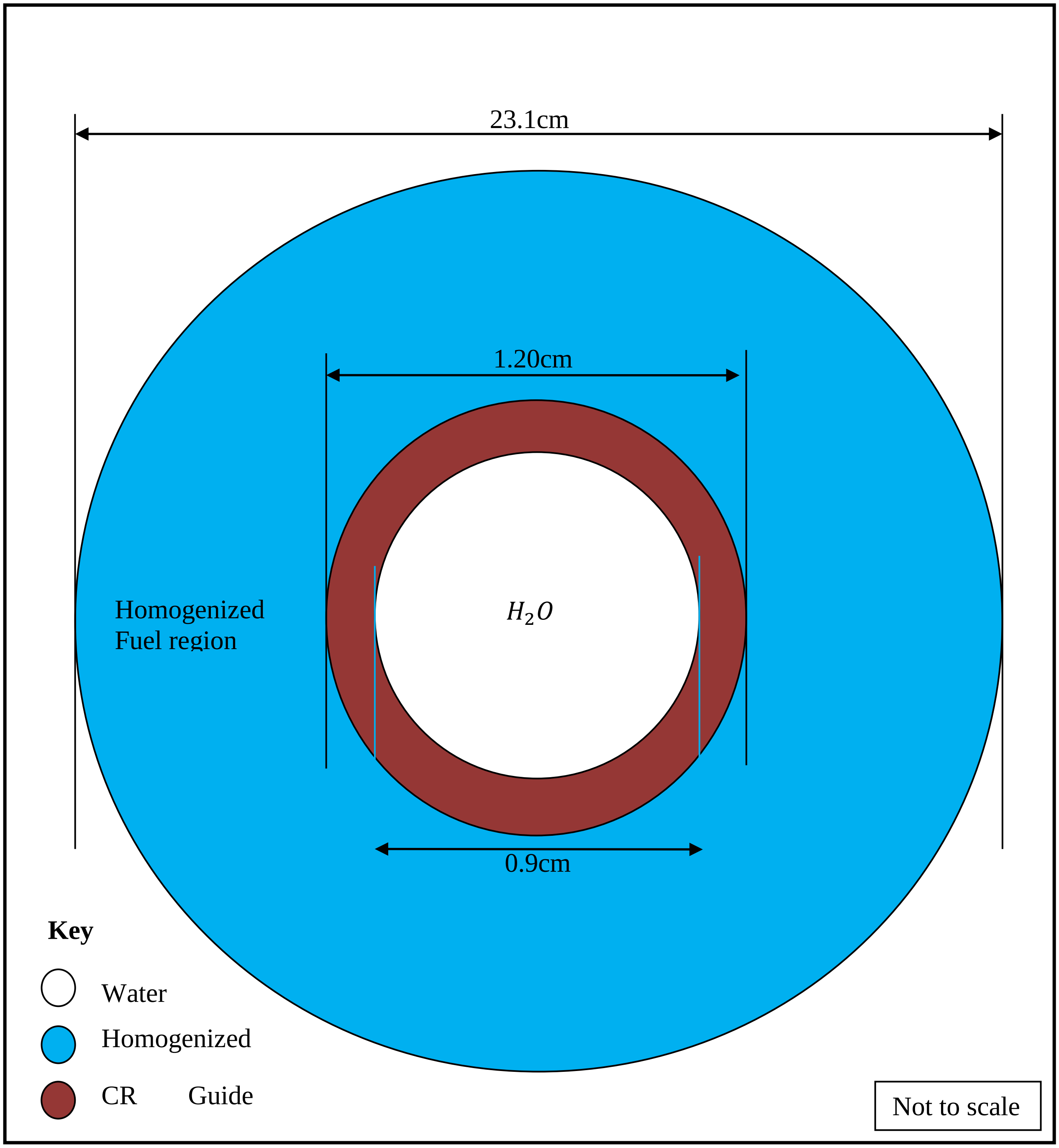

Figure I.4: CR “out” cell for the NIRR-1

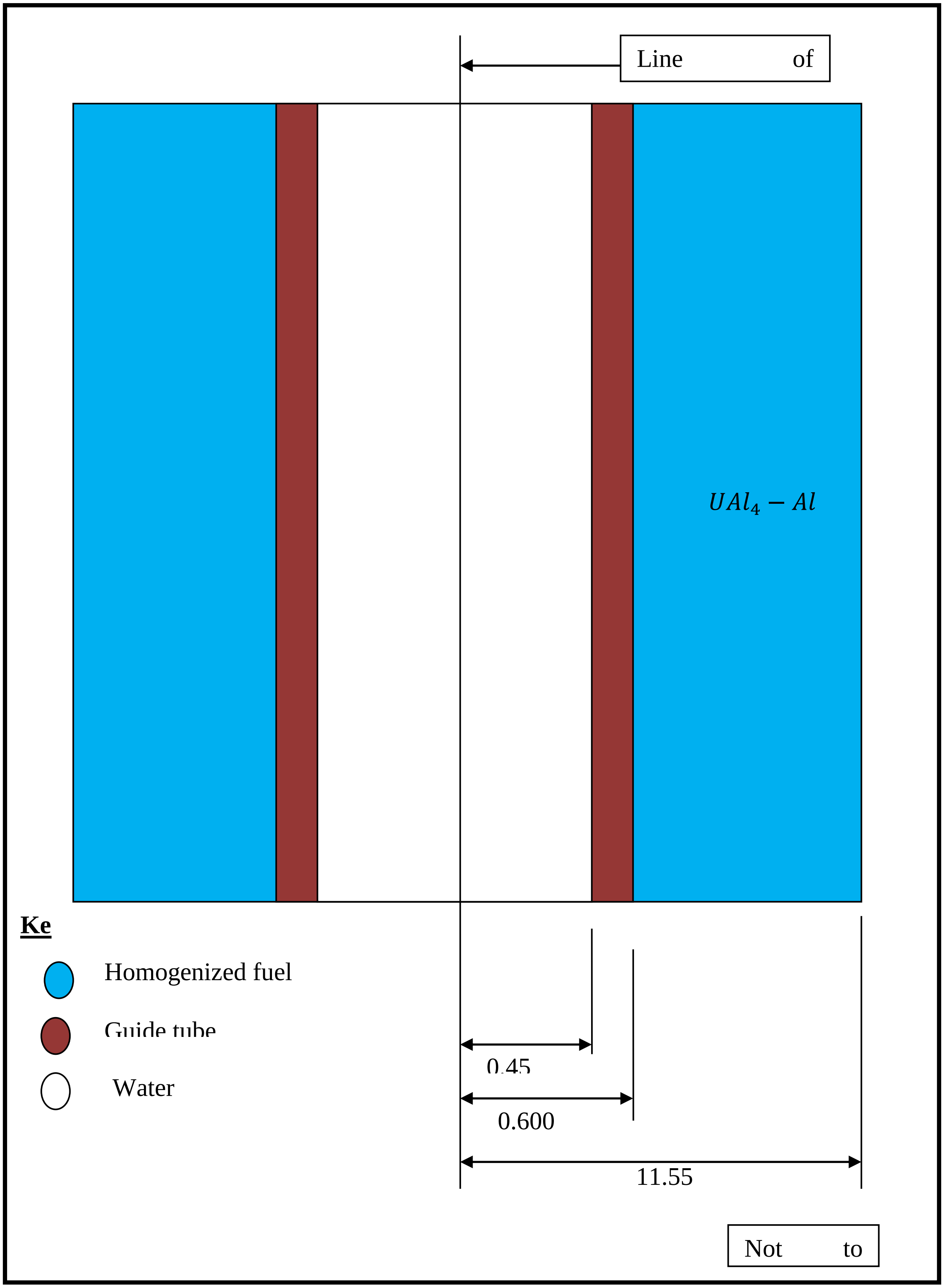

Figure I.5: A Half Symmetric Representation the Unit CR "out" Cell for the NIRR-1

I.2.2 Homogenised Atom Densities for the 1-D Full Core Model with CR “in” and CR “out”.

In order to calculate the homogenised material atom densities for the 1-D full core model, with the CR “in” and CR “out”, each isotope in the material compositions for the CR “in” and CR “out” in Tables I.16 and Table I.17 were multiplied by their region volume fractions in Tables I.14 and I.15 respectively and summed over each isotope. The homogenized atom densities for the CR “in” and CR “out” is presented in the control region of the full core NIRR-1 model as presented in Table I.18 and I.19 respectively. The final homogenized atom desities for all regions is presented in Table I.22 and I.23 for the full core model with CR ‘in’ and CR ‘out’ respectively.

I.3: Calculation for Regions beyond the Control and Fuel Region of the NIRR-1

The detail geometry and dimension of the top view of the NIRR-1 full core has been shown in Figure 3.2a and 3.2b. It can be seen that the regions beyond the control and fuel region include the reflector region, the water outside he reflector region, the reactor vessel, the reactor pool water outside the reactor vessel and the concrete reinforced housing the reactor pool water. The dimensions of all the regions beyond the fuel region were used to calculate the region volume fractions of the various regions and then used to calculate the homogenised atom densities of materials in the regions.

I.3.1 The Annular Beryllium Reflector Region

The annular reflector region made of Beryllium which consisted of the inner irradiation channels, The outer irradiation channels and aluminum tubes. The volume fraction calculations for these regions are as follows:

For the inner irradiation region:

$$Total\ Volume\ of\ 5\ inner\ irradiation\ \ channels = 5 \times \pi \times \frac{d^2}{4} = 5 \times \pi \times \frac{2.5^2}{4}$$

$$= 24.5437\ cm^2$$

$$Total\ Volume\ of\ air\ in\ the\ \ inner\ irradiation\ \ channels = 5 \times \pi \times \frac{d^2}{4} = 2 \times \pi \times \frac{2.2^2}{4}$$

$$= 19.0066\ cm^2$$

$$Total\ Volume\ of\ 5\ Al\ tubes\ in\ the\ \ inner\ irradiation\ \ channels$$

$$= Total\ Volume\ of\ 5\ inner\ irradiation\ \ channel$$

$$- Total\ Volume\ of\ air\ in\ the\ \ inner\ irradiation\ \ channels$$

$$= 24.5437 - 19.0066 = 5.5371\ cm^2$$

$$Total\ Volume\ of\ 2\ fission\ chambers = 2 \times \pi \times \frac{d^2}{4} = 2 \times \pi \times \frac{1.0^2}{4} = 1.5708\ cm^2$$

$$Total\ Volume\ of\ air\ in\ all\ channels\ in\ Be\ reflector$$

$$= Total\ Volume\ of\ air\ in\ the\ \ inner\ irradiation\ \ channels$$

$$+ Total\ Volume\ of\ 2\ fission\ chambers$$

$$= 19.0068 + 1.5708 = 20.5774\ cm^2$$

$$Volume\ of\ \ Be\ reflector +\ holes\ (channels) = (\pi \times 21.75^2) - (\pi \times 11.55^2)$$

$$= 1067.073\ cm^2$$

Where 21.75 cm is the outer radius of the reflector and 11.55 cm is the outer radius of the fuel cage as shown in Figure 3.8.

$$volume\ of\ \ Be\ reflector = 1067.073 - 24.5437 - 1.5708\ \ = 1040.958 cm^2$$

$$Volume\ fraction\ of\ \ Be = \frac{1040.958}{1067.073} = 0.9755$$

$$Volume\ fraction\ of\ \ air\ in\ the\ channels = \frac{20.5774}{1067.073} = 0.0193$$

$$Volume\ fraction\ of\ \ Al\ tubes = \frac{5.5371}{1067.073} = 0.0052$$

$$Density\ of\ beryllium = 1.85 g/cm^3, \qquad M = 9.0122 g/gmol\ and\ \ \gamma_{be}(a/o) = 100$$

$$N_{be} = \frac{\gamma_{be}\rho_{be}N_A}{M_{be}} = \frac{1 \times 1.85 \times 0.6022}{9.0122} = 1.236e - 1\ atom/b - cm$$

Now for the outer irradiation region:

$$Total\ Volume\ of\ \ outer\ irradiation\ region = \pi \times r^2 = (\pi \times 30^2) - (\pi \times 21.75^2)$$

$$= 1.341e^3\ cm^2$$

$$Total\ Volume\ of\ air\ in\ the\ outer\ irradiation\ \ channels$$

$$= \left(2 \times \pi \times \frac{{d_1}^2}{4}\right) + \left(3 \times \pi \times \frac{{d_2}^2}{4}\right) = \left(2 \times \pi \times \frac{3.4^2}{4}\right) + \left(3 \times \pi \times \frac{2.2^2}{4}\right)$$

$$= 29.562\ cm^2$$

$$Total\ Volume\ of\ air + Al\ \ in\ the\ \ outer\ irradiation\ \ channels$$

$$= \left(2 \times \pi \times \frac{{d_1}^2}{4}\right) + \left(3 \times \pi \times \frac{{d_2}^2}{4}\right) = \left(2 \times \pi \times \frac{3.7^2}{4}\right) + \left(3 \times \pi \times \frac{2.5^2}{4}\right)$$

$$= 36.230\ cm^2$$

$$Total\ Volume\ of\ Al\ \ in\ the\ \ outer\ irradiation\ \ channels = 36.230\ cm^2 - 29.562\ cm^2$$

$$= 6.668\ cm^2$$

$$Total\ Volume\ of\ \ air\ in\ outer\ irradiation\ region = 1341.2637 - 36.2304$$

$$= 1305.033\ cm^2$$

$$Volume\ fraction\ of\ Al\ in\ outer\ irradiation\ \ channels\ = \frac{6.668}{1.341e^3} = 0.005$$

$$Volume\ fraction\ of\ \ air\ in\ the\ \ outer\ irradiation\ channels = \frac{29.562}{1.341e^3} = 0.022$$

$$Volume\ fraction\ of\ water\ in\ outer\ irradiation\ channels = \frac{1305.033}{1.341e^3} = 0.9730$$

Table 3.18 presents the volume fractions of regions in the reflector region. The atom density of Be for in the reflector region was calculated to be $1.206\ e^{-1}\ atoms/b-cm$ using its mass density as 1.85 g/cm^3. The atom densities of major nuclides present in dry-air (of density 1.23 g/cm^3) in the irradiation tubes is presented in Table I.19 while the volume fractions of regions in the outer irradiation region is presented in Table I.20.

Table I.18: Volume Fractions for the inner Beryllium Reflector Region

Parameter	Value
Total volume of 5 inner irradiation Channel (cm^2)	24.5437
Total volume of air inner irradiation Channel (cm^2)	19.0066
Volume of 5 Al tubes in the channels	5.5371
Total volume of 2 fission chambers	1.5708
Volume of air in all Channels of Be reflector	20.5774
Volume of beryllium plus holes (channels)	1067.073
Volume of Be reflector	1040.958
Volume fraction of Be	0.9755
volume fraction of Al tubes	0.0052
Volume fraction of air in the channels	0.0193

Table I.19: Atom Density of Various Nuclides Present In Dry-Air In The Irradiation Tubes

Material Name	Nuclide ID	M_i (g/gmol)	w_i (w/o)	N_i a/b-cm)
dry air	7014	14.0031	76.5207	3.949 e-5
	8016	15.9949	23.4793	1.061 e-5

.

Because the volume fractions of Al tubes in the inner reflector region and outer irradiation channels were both 0.005 as can be seen from Table I.18 and I.20, which implied that the total volume of the aluminum tube in the inner and outer irradiation channels is just 0.5% of the total volume of the region, we assumed that the volume of Al tubes in the inner and outer irradiation channels was negligible compared with the total volume of their respective regions. Thus, we ignored the air-filled irradiation channels with aluminum tubes as a separate region for the computational model of the NIRR-1.

Table I.20: The Volume Fractions for The Outer Irradiation Region

Volume of air in outer irradiation Channel (cm^2)	**29.562**
Volume of air + Al in outer irradiation Channel (cm^2)	36.2304
Volume of Al in the outer irradiation channels (cm^2)	6.668
Total volume of outer irradiation region (cm^2)	1.341 e +3
Volume of air in outer irradiation region (cm^2)	1305.033
Volume fractuion of Al in outer irradiation channels	0.0050
Volume fraction of air in outer irradiation channels	0.022
Volume fraction of water in outer irradiation channels	0.9755

The homogenized atom densities of nuclides in the reflector and outer reflector region are presented in Table I.21. Our assumption that the aluminum and air in the air filled inner and outer irradiation regions was negligible compared to the total volume of the region is clearer when the nuclide homogenized atom densities are compared to that of beryllium in the reflector region and water in the outer region as can be observed from Table I.21.

Table I.21: Homogenised Atom Density of Nuclides in the Irradiation Channel Regions

Region name	**Nuclide**	**N_i atom/b-cm**	***fi***	**sum *(NiFi)***
Beryllium plus air filled inner irradiation tubes	Be-4009	1.236e-1	0.9755	1.206e-1
	Al-13027	6.026e-2	0.0052	3.134e-4
	N-7014	3.949e-5	0.0193	7.622e-7
	O-8016	1.061e-5	0.01930	2.048e-7
Water plus air filled outer irradiation tubes	H	6.674e-2	0.9730	6.494e-2
	O	3.337e-2	0.973	3.247e-2
	O-tube	1.061e-5	0.022	2.334e-7
	N-tube	3.949e-5	0.022	8.688e-7
	Al-tube	1.6026e-2	0.005	3.013e-4

Table I.22: Material Composition Data for the 1-D XSDRN HEU Core Model (With CR in)

Actual material Name.	Nuclide ID number	density: (atom/b-cm)	homogenized material name	homogenized material ID
	48106	6.116e-5		
	48108	4.355e-5		
	48110	6.112e-4		
Cadmium	48111	6.263e-4		
	48112	1.181e-3		
	48113	5.979e-4		
	48114	1.406e-3		
	48116	3.665e-4		
	14028	9.593e-5		
	14029	4.872e-6		
	14030	3.216e-6		
	24050	4.638e-5		
	24052	8.945e-4		
	24053	1.014e-4		
	24054	2.525e-5	Control	1
	25055	1.064e-4		
Clad (SS)	26054	2.098e-4		
	26056	3.288e-3		
	26057	7.595e-5		
	26058	1.011e-5		
	28058	3.219e-4		
	28060	1.240e-4		
	28061	5.390e-6		
	28062	1.719e-5		
	28064	4.377e-6		
water	1001	2.639e-2		
	8016	1.314e-2		
Guide tube	13027	2.636e-2		
	92235	2.663e-4		
fuel	92238	2.857e-5		
	13027	1.159e-2	Fuel	2
Water	1001	5.330e-2		
	8016	2.665e-2		
Beryllium	4009	1.236e-1	Reflector	3
Water	1001	6.674e-2	Water	4
	8016	3.337e-2		
Al Vessels	13027	6.026e-2	Vessel	5
water	1001	6.674e-2	Water	6
	8016	3.337e-2		

Table I.23: Material Composition Data for the 1-D XSDRN HEU Core Model (with CR out)

Actual material name .	Nuclide ID number	density: (atom/b-cm)	homogenized material name	homogenized material ID
Water	1001	3.754e-2		
	8016	1.877e-2	Water	1
Guide tube	13027	2.636e-2		
	92235	2.663e-4		
Fuel	92238	2.857e-5		
	13027	1.159e-2	Fuel	2
Water	1001	5.331e-2		
	8016	2.665e-2		
Beryllium	4009	1.236e-1	Reflector	3
Water	1001	6.674e-2	Water	4
	8016	3.337e-2		
Al Vessels	13027	6.026e-2	Vessel	5
Water	1001	6.674e-2	Water	6
	8016	3.337e-2		

APPENDIX II

II.1 Model Calculations for the LEU Cores

The characteristics of the LEU cores are presented in Table II.1, II.2, II.3 and II.4.

Table II.1: Description of the Active Fuel Region of the As-Built NIRR-1 UO_2 LEU Fuel (CERT, 2011)

Description	Value
Material in the active fuel region/clad	**UO_2/** Zircaloy-4
Density of fuel	10.53 g/cm^3
Type/ enrichment	LEU/ 13% ^{235}U
Mass of ^{235}U in each fuel pin	4.03 g
Height of active fuel material	23.0 cm
Diameter of active fuel region	0.43 cm

Table II.2: Fuel Characteristics of the U_3Si_2-Al Dispersed In Aluminum

Description	Value
Density of dispersed phase	12.2 g/cm^2
Uranium density in dispersed phase	11.3 g/cm^3
LEU density in fuel meat	4.41 g/cm^3
Weight % of Uranium in dispersed phase	92.5 %
OD meat	4.74 mm (0.474 cm)
Number of fuel pins	347
Enrichment	19.75 %

Table II.3: Characteristics of the U_3Si-Al LEU Dispersion Fuel

Description	Value
Density of dispersed phase	15.2 g/cm^2
Uranium density in dispersed phase	14.6 g/cm3
LEU density in fuel meat	5.5 g/cm^3
Weight % of Uranium in dispersed phase	96.0 %
OD meat	4.3 mm (0.43 cm)
Number of fuel pins	347
Enrichment	19.75 %

Table II.4: Characteristics of the U-9Mo-Al Dispersion Fuel

Description	Value
Density of dispersed phase	17.3 g/cm^2
Uranium density in dispersed phase	15.7 g/cm3
LEU density in fuel meat	6.0 g/cm^3
Weight % of Uranium in dispersed phase	91.0 %
OD meat	4.3 mm (0.43 cm)
Number of fuel pins	347
Enrichment	19.75 %

II.1.1 The Atom Density Calculation for the As-Built UO_2 LEU Fuel Cell For NIRR-1

The as-built the LEU fuel material of the NIRR-1 core is UO_2 fuel of density 10.6g/cm^3 with Zircaloy-4 (Zirc4) as cladding material. The geometry and dimensions of the LEU fuel material is exactly the same as for the standard HEU fuel. The UO_2 LEU core consist of 350 pins: 335 active fuel pins, 15 dummy pins and 4 tie rods. The dummy pins, and tie rods are also made up of Zirc4.Table II.1 presents the composition of Zirc4 material used in our model which was obtained from the safety analysis report of the NIRR-1.The density of Zircaloy-4 is

6.5 g/cm^3 with a natural zirconium of 97.93 weight percent (IAEA TECDOC 18844, 2012). The geometry of the active LEU fuel region is exactly the same as that of the HEU fuel material. Details of the calculations of the atom density of materials in the fuel region are as follows:

The mass of ^{235}U in the core loading used in our calculations is 4.03 g (NIRR-1). Since the volume of each fuel pin was calculated to be 3.3405 cm^3 the density of ^{235}U in the core loading is:

$$\rho_{235_U} = \frac{\text{4.03 g of U235}}{\text{fuel pin}} \times \frac{\text{fuel pin}}{\text{3.3405 cm}^3} = 1.206406\ gcm^{-3}$$

Hence the atom density of ^{235}U is

$$N_{235_U} = \frac{\rho_{235_U} \times N_A}{M_{235_U}} = \frac{1.206406\ \ gcm^{-3} \times 0.6022 \frac{atoms.cm^2}{gmol.b}}{235.0439 g/gmol}$$

$$= 3.09090\ e^{-3}\ \ atoms/b - cm$$

The actual density of UO_2 used in the fuel was not reported in the NIRR-1 SAR. However, we can calculate the density since we have calculated the atom density of U^{235} in the fuel.

$$N_{U235} = \frac{x\ g\ of\ UO_2}{cm^3} \times \frac{237.6556\ g\ of\ U}{269.6544\ g\ of\ UO_2} \times \frac{0.13 g\ of\ U235}{g\ of\ U} \times \frac{0.6022 \frac{cm^2}{b}\ at.of\ U235}{235.0439 g\ of\ U235}$$

Or

$$3.09090\ e^{-3} \ \ = \frac{x\ g\ of\ UO_2}{cm^3} \times \frac{237.6556\ g\ of\ U}{269.6544\ g\ of\ UO_2} \times \frac{0.13 g\ of\ U235}{g\ of\ U} \times \frac{0.6022 \frac{cm^2}{b}\ at.of\ U235}{235.0439 g\ of\ U235}$$

Thus the density of UO_2 is 10.53 g/cm^3

$$\frac{1}{M_u} = \sum \frac{w_i}{M_i} = \frac{0.13}{235.0439} + \frac{0.87}{238.0508}$$

$Therefore\ M_u = 237.6556\ g/gmol$

To obtain the molecular weight of UO_2 is

$$M_{UO_2} = M_u + 2M_O = 237.6556 + 2(15.9994) = 269.6544\ g/gmol$$

Using the mass density of UO_2 fuel the atom density of U^{235} in the LEU fuel was calculated as:

Now,

The atom density of U^{238} and O in the LEU fuel is obtained as follows

$$N_{U238} = \frac{10.53 g\ of\ UO_2}{cm^3} \times \frac{237.6556 g\ of\ U}{269.6544 g\ of\ UO_2} \times \frac{0.87 g\ of\ U238}{g\ of\ U} \times \frac{0.6022 \frac{cm^2}{b}\ at.of\ U238}{238.0508 g\ of\ U238}$$

$$= 2.042487e-2\ atoms/b-cm$$

$$N_O = \frac{10.53 g\ of\ UO_2}{cm^3} x \frac{2x15.9994 g\ of\ O}{269.6544 g\ of\ UO_2} x \frac{1 g\ of\ O}{g\ of\ U} x \frac{0.6022 \frac{cm^2}{b}\ at.of\ O}{15.9994 g\ of\ O}$$

$$= 4.7032e-2\ atoms/b-cm$$

Since there is a change in the number of dummy pins and active fuel pins in the as-built LEU and the HEU fuel cell model, the volume fraction of the moderator and tie rods plus dummy pins in a water mixed region of the HEU fuel cell as shown in Appendix I were recalculated, as shown below and tabulated in Table II.5. In table II.6, II.7, and II.8 the geometry and volume and volume fraction of each region of the fuel cell is presented. The calculations were necessary to obtain the effective densities of the nuclides in the water mixed region of the as-built LEU fuel cell presented in table II.9. Unlike the HEU fuel cell, the moderating material for the LEU fuel cell is a mixture of water and Zirc4 tie rods plus dummy pins. The atom densities of various isotopes in ziraloy-4 were obtained using equation II.1 and II.2 and the result is as shown in table II.11. The atom densities of various natural isotopes present in the individual nuclide of Zirc4 were calculated by simply multiplying the nuclide atom density in table II.10 by their corresponding natural abundance. The effective atom density of materials in the moderator region of the fuel cell is presented in table II.12. All materials in the fuel cell were homogenized to produce a homogenized atom density data in table II.13 and II.14.

$Total\ volume\ of\ fuel\ regions\ in\ the\ core =$

$Total\ core\ volume (CV) - guide\ tube\ volume\ (GT)$

$= \pi {r_{CV}}^2 - \pi {r_{GT}}^2 = (\pi \times 11.55\ \times 11.55) - (\pi \times 0.6\ \times 0.6) = 417.9653\ cm^2$

$$Total\ volume\ of\ fuel\ regions\ in\ the\ core\ per\ fuel\ pin = \frac{417.9653}{335} = 1.2477\ cm^2$$

$$Fuel\ cell\ outer\ radii = (Total\ volume\ of\ fuel\ regions\ in\ the\ core\ per\ fuel\ pin)^{1/2}$$

$$= 0.6302\ cm$$

Thus the fuel cell diameter = 2 x 0.6302 = 1.2604 cm

Now, since the radius of the dummy pins and tie rods are the same

$Total\ vol. of\ 15\ dummy\ pins\ and\ 4\ tie\ riods = 19 \times (\pi \times 0.275 \times 0.275) = 4.5141\ cm^2$

$$Total\ vol. of\ fuel\ riods = 335 \times (\pi \times 0.275 \times 0.275) = 79.5903\ cm^2$$

$Total\ vol. of\ water\ in\ the\ core$

$$= Total\ volume\ of\ fuel\ regions\ in\ the\ core - Total\ vol. of\ fuel\ rods$$

$$= 417.9653 - 79.5903 - 4.5141 = 333.8609\ cm^2$$

Thus

$$Total\ vol. of\ mixture\ of\ water, tie\ rods\ and\ dummy\ rods\ in\ the\ core$$

$$= 333.8609 + 4.5141 = 338.375\ cm^2$$

Therefore,

$$Volume\ fraction\ of\ dummy\ pins\ and\ tie\ rods\ in\ the\ water\ and\ Al\ mix\ region\ of\ the\ fuel\ cell$$

$$= \frac{4.5141}{338.375} = 1.33405\ e^{-2}$$

$$volume\ fraction\ of\ moderator\ in\ the\ water\ and\ Al\ mix\ region\ of\ the\ fuel\ cell$$

$$= \frac{333.8609}{338.375} = 9.86659\ e^{-1}$$

Table II.5 Volume Fractions in the Water Mix Region for the As-Built LEU Fuel Cell

Description	Value
Total volume of fuel regions in the core	417.9653 cm^2
Total volume of the core per fuel pin	1.2477cm^2
Fuel cell outer radii	0.6302 cm
Fuel cell diameter	1.2604 cm
Total volume of mixture of water + Tie rods +dummy rods	338.375cm^2
Volume fraction of dummy pins plus tie rods in water and Aluminum mix region of the fuel cell	1.33405 e^{-2}
Volume fraction of moderator in water and Aluminum mix region of the fuel cell	9.86659 e^{-1}

Table II.6 Material Geometry and Layout of NIRR-1 As-Built LEU Fuel Cell

Zone Number	Material Number	Description	Width (cm)	Total distance (cm)
1	1	Fuel	0.2150	0.2150
2	2	Clad	0.0600	0.2750
3	3	Moderator	0.3552	0.6302

$$volume\ of\ fuel\ = \frac{\pi d^2}{4} = \frac{\pi \times 0.43^2}{4} = 0.1452\ cm^2$$

$$volume\ of\ fuel + clad = \frac{\pi d^2}{4} = \frac{\pi \times 0.55^2}{4} = 0.2376\ cm^2$$

$$volume\ of\ clad = (volume\ of\ fuel + clad) - volume\ of\ fuel = 0.0924$$

$$volume\ of\ moderator = volume\ of\ fuel\ cell - volume\ of\ fuel + clad$$

$$= (\pi \times 0.6302^2) - 0.2376 = 0.01011\ cm^2$$

The volume fraction of each region is the volume of each region divided by the total volume.

Table II.7 Volume for Different Regions in the NIRR-1 As-Built LEU Fuel Cell

Material name	Fuel cell	Fuel meat + clad	Fuel meat	Clad	Moderator
Material Volume (cm^2)	1.2477	0.2376	0.1452	0.0924	1.01011

Table II.8 Zones in the NIRR-1 Fuel Cell Their Respective Region Volume Fractions

Region	Volume (cm^2)	Total volume (cm^2)	Volume fraction	Sum of volume fraction
Fuel	0.1452		0.1164	
clad	0.0924	1.2477	0.0740	1.0000
moderator	1.01011		0.8096	

Table II.9 Homogenized Atom Density for the As-Built LEU Fuel Cell

Material Name	f_i	Nuclide	N_{ij}	$N_{ij}\, f_i$
		U235	3.0909E-03	3.5975E-4
Fuel	0.1164	U238	2.0425E-02	2.3773E-3
		016	4.7032E-02	5.4741E-3

Using

$$N_{mix} = \frac{\rho N_A}{M_{mix}} \qquad \text{II. 1}$$

$$N_i = \gamma_i N_{mix} \qquad \text{II. 2}$$

Table II.10 Atom density of Nuclides in the Zirc4 Mixture

matl name	nuclide name	nuclide ID	M_i	$w_i(w/o)$	N_{mix} (atoms/b-cm)
Zircaloy-4	zirconium	40000	91.224	97.93	4.2020E-02
	tin	50000	118.71	1.7	5.6055E-04
	iron	26000	55.845	0.24	1.6822E-04
	chromium	24000	51.996	0.13	9.7865E-05

Table II.11 Atom density of Isotopes in the Zirc4 Mixture

Isotope ID	N_{mix}	$y_{i\ (a/o)}$	N_i
Zr-90		51.45	2.1620E-03
Zr-91		11.22	4.7147E-03
Zr-92	4.2020E-02	17.15	7.2065E-03
Zr-94		17.38	7.3032E-03
Zr-96		2.8	1.1766E-03
Sn-112		0.94	5.2692E-06
Sn-114		0.66	3.6996E-06
Sn-116		14.54	8.1504E-05
Sn-117		7.68	4.3050E-05
Sn-118		24.22	1.3577E-04
Sn-119	5.6055E-04	8.59	4.8151E-05
Sn-120		32.58	1.8263E-04
Sn-122		4.63	2.5954E-05
Sn-124		5.79	3.2456E-05
Fe-54		5.845	9.8325E-06
Fe-56		91.754	1.5435E-04
Fe-57	1.6822E-04	2.119	3.5646E-06
Fe-58		0.282	4.7438E-07
Cr-50		4.345	4.2522E-06
Cr-52		83.789	6.9870E-05
Cr-53	9.7865E-05	9.501	7.9230E-06
Cr-54		2.365	1.9720E-06

Table II.12. Effective Atom Density in the Moderator Region of the Fuel Cell

Material name	Volume fraction	Nuclide ID	N^{eff}
Water	9.86659E-01	1001	6.5850E-02
		8016	3.2925E-02
		40090	2.8842E-04
		40091	6.2896E-05
		40092	9.6138E-05
		40094	9.7428E-05
		40096	1.5696E-05
		50112	7.0294E-08
		50114	4.9355E-08
		50116	1.0873E-06
		50117	5.7431E-07
		50118	1.8112E-06
	1.33405E-02	50119	6.4236E-07
15 dummy pins plus		50120	2.4363E-06
4 tie rods		50122	3.4623E-07
		50124	4.3298E-07
		26054	1.3117E-07

				26056	2.0591E-06
				26057	4.7554E-08
				26058	6.3285E-09
				24050	5.6727E-08
				24052	9.3210E-07
				24053	1.0570E-07
				24054	2.6307E-08

Table II.13: The Homogenized Atom Density (atom/b-cm) for the As-Built LEU Fuel cell

Matl name	f_i	Nuclide ID	N_{ij}	$N_{ij}f_j$	N_{iz}(a/bcm)
fuel		92235	3.0909E-03	3.5975E-04	3.5975E-04
	0.11639	92238	2.0425E-02	2.3773E-03	2.3773E-03
		8016	4.7032E-02	5.4741E-03	3.2129E-02
		40090	2.1620E-02	1.6004E-03	1.8339E-03
		40091	4.7147E-03	3.4902E-04	3.9993E-04
		40092	7.2065E-03	5.3348E-04	6.1131E-04
		40094	7.3032E-03	5.4063E-04	6.1951E-04
		40096	1.1766E-03	8.7098E-05	9.9805E-05
		50112	5.2692E-06	3.9006E-07	4.4697E-07
		50114	3.6996E-06	2.7387E-07	3.1383E-07
		50116	8.1504E-05	6.0335E-06	6.9138E-06
		50117	4.3050E-05	3.1869E-06	3.6518E-06
		50118	1.3577E-04	1.0050E-05	1.1517E-05
		50119	4.8151E-05	3.5645E-06	4.0846E-06
		50120	1.8263E-04	1.3519E-05	1.5492E-05
		50122	2.5954E-05	1.9213E-06	2.2016E-06
		50124	3.2456E-05	2.4026E-06	2.7532E-06
clad	0.07403	26054	9.8325E-06	7.2787E-07	8.3407E-07
		26056	1.5435E-04	1.1426E-05	1.3093E-05
		26057	3.5646E-06	2.6388E-07	3.0238E-07
		26058	4.7438E-07	3.5117E-08	4.0241E-08
		24050	4.2522E-06	3.1478E-07	3.6071E-07
		24052	6.9870E-05	5.1723E-06	5.9269E-06
		24053	7.9230E-06	5.8652E-07	6.7209E-07
		24054	1.9720E-06	1.4598E-07	1.6728E-07
		1001	6.5850E-02	5.3311E-02	5.3311E-02
moderator	0.80958	8016	3.320e-2	2.665e-2	combined with fuel
		Zir4		Table II.14	

Table II.14: The Zirc4 average homogenized atom density in the water mix region

matl name	f_i	nuclide ID	N_{ij}	$N_{ij}f_j$	N_{iz}(a/bcm)
mixture of dummy pins and tie rods in the moderator		40090	2.8842E-04	2.3350E-04	combined with homogenized atom density of similar isotopes in the clad
		40091	6.2896E-05	5.0920E-05	
		40092	9.6138E-05	7.7832E-05	
		40094	9.7428E-05	7.8876E-05	
		40096	1.5696E-05	1.2707E-05	
		50112	7.0294E-08	5.6908E-08	
		50114	4.9355E-08	3.9957E-08	
		50116	1.0873E-06	8.8026E-07	
		50117	5.7431E-07	4.6495E-07	
		50118	1.8112E-06	1.4663E-06	
		50119	6.4236E-07	5.2005E-07	
		50120	2.4363E-06	1.9724E-06	
		50122	3.4623E-07	2.8030E-07	
		50124	4.3298E-07	3.5053E-07	
		26054	1.3117E-07	1.0619E-07	
		26056	2.0591E-06	1.6670E-06	
		26057	4.7554E-08	3.8499E-08	
		26058	6.3285E-09	5.1235E-09	
		24050	5.6727E-08	4.5925E-08	
		24052	9.3210E-07	7.5461E-07	
		24053	1.0570E-07	8.5570E-08	
		24054	2.6307E-08	2.1298E-08	

II.1.2 The NIRR-1 Control Rod and the Control cell Model for the As-Built LEU Core

The only difference in the LEU control model of the NIRR-1 and that of the HEU is the material of the guide tube which is made of Zirc4. The material composition data for the Control in and control out cell model is presented in table II.15 and II.16 respectively.

Table II.15 Homogenized Material Composition Data for the XSDRN "Control in" Cell Model for NIRR-1

material number	material name	Nuclide ID No.	Region density
1	poison material cadmium	48106	6.1155E-05
		48108	4.3542E-05
		48110	6.1106E-04
		48111	6.2667E-04
		48112	1.1805E-03
		48113	5.9785E-04
		48114	1.4056E-03
		48116	3.6595E-04
2	Clad Stainless Steel SS304	14028	9.5929E-05
		14029	4.8733E-06
		14030	3.2163E-06
		24050	4.6385E-05
		24052	8.9449E-04
		24053	1.0143E-04
		24054	2.5247E-05
		25055	1.0636E-04
		26054	2.0944E-04
		26056	3.2878E-03
		26057	7.5929E-05
		26058	1.0105E-05
		28058	3.2191E-04
		28060	1.2400E-04
		28061	5.3902E-06
		28062	1.7186E-05
		28064	4.3764E-06
3	water	1001	2.6057E-02
		8016	1.3028E-02
4	Guide tube (Zirc4)	40090	9.4585E-03
		40091	2.0627E-03
		40092	3.1528E-03
		40094	3.1951E-03
		40096	5.1475E-04
		50112	2.3053E-06
		50114	1.6186E-06
		50116	3.5658E-05
		50117	1.8835E-05
		50118	5.9397E-05

50119	2.1066E-05
50120	7.9900E-05
50122	1.1355E-05
50124	1.4199E-05
26054	4.3017E-06
26056	6.7528E-05
26057	1.5595E-06
26058	2.0754E-07
24050	1.8604E-06
24052	3.0568E-05
24053	3.4663E-06
24054	8.6275E-07

Table II.16: CR "out" Homogenised Material Composition

matl zone	matl name	nuclide ID#	N_i(atoms/b-cm)	f_i	$sum(N_i f_i)$
	water	1001	6.6740E-02	0.5625	3.7541E-02
1		8016	3.3370E-02		1.8771E-02
	guide tube	40090	2.1620E-02	0.4375	9.4585E-03
		40091	4.7147E-03		2.0627E-03
		40092	7.2065E-03		3.1528E-03
		40094	7.3032E-03		3.1951E-03
		40096	1.1766E-03		5.1475E-04
		50112	5.2692E-06		2.3053E-06
		50114	3.6996E-06		1.6186E-06
		50116	8.1504E-05		3.5658E-05
		50117	4.3050E-05		1.8835E-05
		50118	1.3577E-04		5.9397E-05
		50119	4.8151E-05		2.1066E-05
		50120	1.8263E-04		7.9900E-05
		50122	2.5954E-05		1.1355E-05
		50124	3.2456E-05		1.4199E-05
		26054	9.8325E-06		4.3017E-06
		26056	1.5435E-04		6.7528E-05
		26057	3.5646E-06		1.5595E-06
		26058	4.7438E-07		2.0754E-07
		24050	4.2522E-06		1.8604E-06
		24052	6.9870E-05		3.0568E-05
		24053	7.9230E-06		3.4663E-06
		24054	1.9720E-06		8.6275E-07

II.2 U_3Si_2-Al fuel Cell Model:

The density of ^{235}U in the fuel is calculated as follows:

$\rho_{U235} = 4.41\ gcm^{-3} \times 0.1975 = 0.870975\ gcm^{-3}$

Where 4.41 gcm^{-3} is the uranium density in fuel meat.

This implies that the region atom density of ^{235}U in atom/b-cm is

$$N_{U235} = \frac{\rho_{U235} \times N_A}{M_{U235}} = \frac{0.870975\ gcm^{-3} \times 0.6022 \frac{atoms.cm^2}{gmol.b}}{235.0439 g/gmol}$$

$$= 2.23150\ e^{-3}\ \ atoms/b - cm$$

Now, since the density of uranium in the fuel meat is 4.41 g/cm^3 we can obtain the density of ^{238}U by multiplying by the uranium density in fuel meat by the weight fraction of ^{238}U

$$\rho_{U238} = 4.41\ gcm^{-3} \times 0.8025 = 3.539025\ gcm^{-3}$$

Therefore we can now calculate the region atom density of ^{238}U as follows:

$$N_{U238} = \frac{\rho_{U238} \times N_A}{M_{U238}} = \frac{3.539025\ gcm^{-3} \times 0.6022 \frac{atoms.cm^2}{gmol.b}}{238.0508\ g/gmol}$$

$$= 8.9527 e^{-3}\ \ atoms/b - cm$$

The atom densities of silicon isotopes in the fuel are calculated as:

For Si28

$$N_{Si28} = \frac{0.55815\ gcm^{-3} \times 0.6022 \frac{atoms.cm^2}{gmol.b} \times 0.922}{27.9769\ g/gmol} = 1.10770 e^{-2}\ \ atoms/b - cm$$

For Si29

$$N_{Si29} = \frac{0.55815\ gcm^{-3} \times 0.6022 \frac{atoms.cm^2}{gmol.b} \times 0.0469}{28.9765\ g/gmol} = 5.4402 e^{-4}\ \ atoms/b - cm$$

For Si30

$$N_{Si30} = \frac{0.55815\ gcm^{-3} \times 0.6022 \frac{atoms.cm^2}{gmol.b} \times 0.0309}{29.9738\ g/gmol} = 3.46504e^{-4}\ \ atoms/b - cm$$

To obtain the atom density of Al in the cladding material which is 100 % Al we use the density of pure Al which is 2.7 g/cm^3. Thus we obtain the atom density of pure Al to be

$$N_{pure\ Al} = \frac{2.7 \times 0.6022}{26.9815} = 6.0261\ \ e^{-2}\ \ atoms/b - cm$$

For the region atom density of nuclides within the moderator we use the mass density of water to be 0.9982 g/cm^3. Similarly using equation I.1

$$N_{H_2\mathrm{O}=}\frac{0.9982 \times 0.6022}{18.0152} = 3.337\ \ e^{-2}\ \ atoms/b - cm$$

$$N_{H_2O}^{eff} = N_{H_2\mathrm{O}} \times volume\ fraction = 3.337\ \ e^{-2} \times 9.95043\ \ e^{-1}$$

$$= 3.320\ e^{-2} atoms/b - cm$$

$$N_H = 3.320\ e^{-2} atoms/b - cm \times \frac{2\ atoms\ of\ H}{1\ molecule\ of\ H_2O} = 6.6400\ e^{-2} atoms/b - cm$$

$$N_H = 3.320\ e^{-2} atoms/b - cm\ moleculesof\ H_2O\ \times \frac{2\ atoms\ of\ H}{1\ molecule\ of\ H_2O}$$

$$= 6.6400\ e^{-2} atoms/b - cm$$

$$N_O = 3.320\ e^{-2} atoms/b - cm\ moleculesof\ H_2O\ \times \frac{1\ atoms\ of\ O}{1\ molecule\ of\ H_2O}$$

$$= 3.320\ e^{-2} atoms/b - cm$$

$$N_{Al}^{H_2O} = \ 6.0261\ \ e^{-2}\ atoms/b - cm \times 4.957 e^{-2}\ atoms/b - cm$$

$$= 2.9870 e^{-4} atoms/b - cm$$

The following volume calculations were made for the different regions in the MNSR LEU fuel cell model to obtain the volume fractions of regions in the fuel cell used for homogenized density calculations.

$$volume\ of\ active\ fuel\ = \frac{\pi d^2}{4} = \frac{\pi \times 0.474^2}{4} = 0.1765\ cm^2$$

$$volume\ of\ active\ fuel\ + clad = \frac{\pi d^2}{4} = \frac{\pi \times 0.55^2}{4} = 0.2376\ cm^2$$

$$volume\ of\ clad = (volume\ of\ active\ fuel + clad) - volume\ of\ active\ fuel = 0.0611$$

$$volume\ of\ moderator = volume\ of\ fuel\ cell - volume\ of\ fuel + clad$$

$$= (1.2045) - 0.2376 = 0.9669\ cm^2$$

II.1.3 U_3Si-Al Fuel Cell Model:

The density of ^{235}U in the fuel is calculated as follows:

$\rho_{U235} = 5.5\ gcm^{-3} \times 0.1975 = 1.08625\ gcm^{-3}$

Where 5.5 $gcm^{-3}$is the uranium density in fuel meat.

This implies that the region atom density of ^{235}U in atom/b-cm is

$$N_{U235} = \frac{\rho_{U235} \times N_A}{M_{U235}} = \frac{1.08625\ gcm^{-3}\ \times 0.6022\,\frac{atoms.cm^2}{gmol.b}}{235.0439 g/gmol}$$

$$= 2.7831\ e^{-3}\ \ atoms/b - cm$$

Now, since the density of uranium in the fuel meat is 5.5 g/cm^3 we can obtain the density of ^{238}U by multiplying by the uranium density in fuel meat by the weight fraction of ^{238}U

$$\rho_{U238} = 5.5\ gcm^{-3} \times 0.8025 == 4.41375\ gcm^{-3}$$

Therefore, we can now calculate the region atom density of ^{238}U as follows:

$$N_{U238} = \frac{\rho_{U238} \times N_A}{M_{U238}} = \frac{4.41375\ \ gcm^{-3} \times 0.6022\, \frac{atoms.cm^2}{gmol.b}}{238.0508\ g/gmol}$$

$$= 11.1655e^{-3}\ \ atoms/b - cm$$

The atom densities of silicon isotopes in the fuel were calculated as:

For Si28

$$N_{Si28} = \frac{0.37874\ gcm^{-3} \times 0.6022 \frac{atoms.cm^2}{gmol.b} \times 0.922}{27.9769\ g/gmol} = 7.5165e^{-3}\ \ atoms/b - cm$$

For Si29

$$N_{Si29} = \frac{0.37874\ gcm^{-3} \times 0.6022 \frac{atoms.cm^2}{gmol.b} \times 0.0469}{28.9765\ g/gmol} = 3.6916e^{-4}\ \ atoms/b - cm$$

For Si30

$$N_{Si30} = \frac{0.37874\ gcm^{-3} \times 0.6022 \frac{atoms.cm^2}{gmol.b} \times 0.0309}{29.9738\ g/gmol} = 2.3512e^{-4}\ \ atoms/b - cm$$

The atom density of nuclides in the clad and moderator material is the same as that in the clad and moderator material of the U_3Si_2-Al LEU fuel.

II.1.4 U_9Mo-Al Fuel Model:

The density of ^{235}U in the fuel is calculated as follows:

$\rho_{U235} = 6.0\ gcm^{-3} \times 0.1975 = 1.185\ gcm^{-3}$

Where 6.0 $gcm^{-3}$is the uranium density in the fuel meat.

This implies that the region atom density of ^{235}U in atom/b-cm is

$$N_{U235} = \frac{\rho_{U235} \times N_A}{M_{U235}} = \frac{1.185\ gcm^{-3}\ \times 0.6022\, \frac{atoms.cm^2}{gmol.b}}{235.0439 g/gmol} = 3.0361\ e^{-3}\ \ atoms/b - cm$$

Now, since the density of uranium in the fuel meat is 5.76 g/cm^3 we can obtain the density of ^{238}U by multiplying by the uranium density in fuel meat by the weight fraction of ^{238}U

$$\rho_{U238} = 6.0\ gcm^{-3} \times 0.8025 == 4.815\ gcm^{-3}$$

Therefore we can now calculate the region atom density of ^{238}U as follows:

$$N_{U238} = \frac{\rho_{U238} \times N_A}{M_{U238}} = \frac{4.815\ gcm^{-3} \times 0.6022 \frac{atoms.cm^2}{gmol.b}}{238.0508\ g/gmol} = 12.1806\ e^{-3}\ \ atoms/b - cm$$

The densities of Mo isotopes in the fuel are obtained as follows:

For Mo92

$$N_{Mo92} = \frac{0.962226\ gcm^{-3} \times 0.6022 \frac{atoms.cm^2}{gmol.b} \times 0.148}{91.9068\ g/gmol} = 9.3331e^{-4}\ \ atoms/b - cm$$

For Mo94

$$N_{Mo94} = \frac{0.962226\ gcm^{-3} \times 0.6022 \frac{atoms.cm^2}{gmol.b} \times 0.0923}{93.9051\ g/gmol} = 5.6955e^{-4}\ \ atoms/b - cm$$

For Mo95

$$N_{Mo95} = \frac{0.962226\ gcm^{-3} \times 0.6022 \frac{atoms.cm^2}{gmol.b} \times 0.159}{94.9058\ g/gmol} = 9.7078e^{-4}\ \ atoms/b - cm$$

For Mo96

$$N_{Mo96} = \frac{0.962226\ gcm^{-3} \times 0.6022 \frac{atoms.cm^2}{gmol.b} \times 0.167}{95.9047\ g/gmol} = 1.0090e^{-3}\ \ atoms/b - cm$$

For Mo97

$$N_{Mo97} = \frac{0.962226\ gcm^{-3} \times 0.6022 \frac{atoms.cm^2}{gmol.b} \times 0.0956}{96.9060\ g/gmol} = 5.7164e^{-4}\ \ atoms/b - cm$$

For Mo98

$$N_{Mo98} = \frac{0.962226\ gcm^{-3} \times 0.6022 \frac{atoms.cm^2}{gmol.b} \times 0.242}{97.9054\ g/gmol} = 1.4323e^{-3}\ \ atoms/b - cm$$

For Mo100

$$N_{Mo100} = \frac{0.962226\ gcm^{-3} \times 0.6022 \frac{atoms.cm^2}{gmol.b} \times 0.0967}{99.9075\ g/gmol} = 5.6085e^{-4}\ \ atoms/b - cm$$

The atom density of nuclides in the clad and moderator material is the same as that in the clad and moderator material of the U_3Si_2-Al and U_3Si-Al LEU fuel. The homogenized atom density data for the alternative LEU cores is presented in Tables II.17, II.18 and II.18.

Table II.17. Homogenized Atom Density for the U_3Si_2-Al LEU Fuel Cell

Material Name	***f_i***	**Nuclide**	***N_{ij}***	***N_{ij} f_i***	***N_{iz} (a/b-cm)***
		92235	2.2315e-3	3.2698e-4	3.2698e-4
Fuel	0.14653	92238	8.9527e-3	1.3118e-3	1.3118e-3
		14028	1.1077e-2	1.6231e-3	1.6231e-3
		14029	5.4402e-4	7.9716e-5	7.9716e-5
		14030	3.4650e-4	5.0773e-5	5.0773e-5
Clad	0.05073	130l27	6.0260e-2	3.0570e-3	
		13027	2.9870e-4	2.3980e-4	3.2960e-3
Moderator	0.80274	1001	6.6400e-2	5.3310e-2	5.3310e-2
		8016	3.3200e-2	2.6650e-2	2.6650e-2

Table II.18. Homogenized Atom Density for the U_3Si-Al LEU Fuel Cell

Material Name	***f_i***	**Nuclides**	***N_{ij}***	***N_{ij} f_i***	***N_{iz} (a/b-cm)***
		92235	2.7831e-3	3.3550e-4	3.3550e-4
Fuel	0.12055	92238	11.1655e-3	1.3460e-3	1.3460e-3
		14028	7.5165e-3	9.0611e-4	9.0611e-4
		14029	3.6916e-4	4.4502e-5	4.4502e-5
		14030	2.3512e-4	2.8344e-5	2.8344e-5
Clad	0.07671	13027	6.026e-2	4.6230e-3	
		13027	2.987e-4	2.3980e-4	4.8628e-3
		1001	6.640e-2	5.3310e-2	5.3310e-2
Moderator	0.80274	8016	3.320e-2	2.6650e-2	2.6650e-2

Table II.19 Homogenized Atom Density for the U-9Mo-Al LEU Fuel Cell

Material Name	***f_i***	**Nuclide**	***N_{ij}***	***$N_{ij} f_i$***	***N_{iz} (a/b-cm)***
		92235	3.0361 e -3	3.660e-4	3.660 e -4
		92238	12.1806e-3	1.4684e-3	1.4684e-3
		42092	9.3310e-4	1.1249e-4	1.1249e-4
		42094	5.6955e -4	6.8659e -5	6.8659e -5
Fuel	0.12055	42095	9.7078e -4	1.1703e -4	1.1703e -4
		42096	1.0090*e* -3	1.2164e-4	1.2164e-4
		42097	5.7164e-4	6.8912e-5	6.8912e-5
		42098	1.4323e-3	1.7266e-4	1.7266e-4
		42100	5.6085e-4	6.7610e-5	6.7610e-5
Clad	0.07671	13027	6.0260e -2	4.6230e-3	
		13027	2.9870e-4	2.3980e-4	4.8628e-3
Moderator	0.80274	8016	3.3200e-2	2.6650e-2	2.665e -2
		1001	6.6400e-2	5.3310e-2	5.3310e-2

APPENDIX III

III.1 SCALE 6.2.3 Graphical User Interphase (GUI) for Input Prepration

The SCALE 6.2.3 GUI for input preparation in the present work is shown in the figures below:

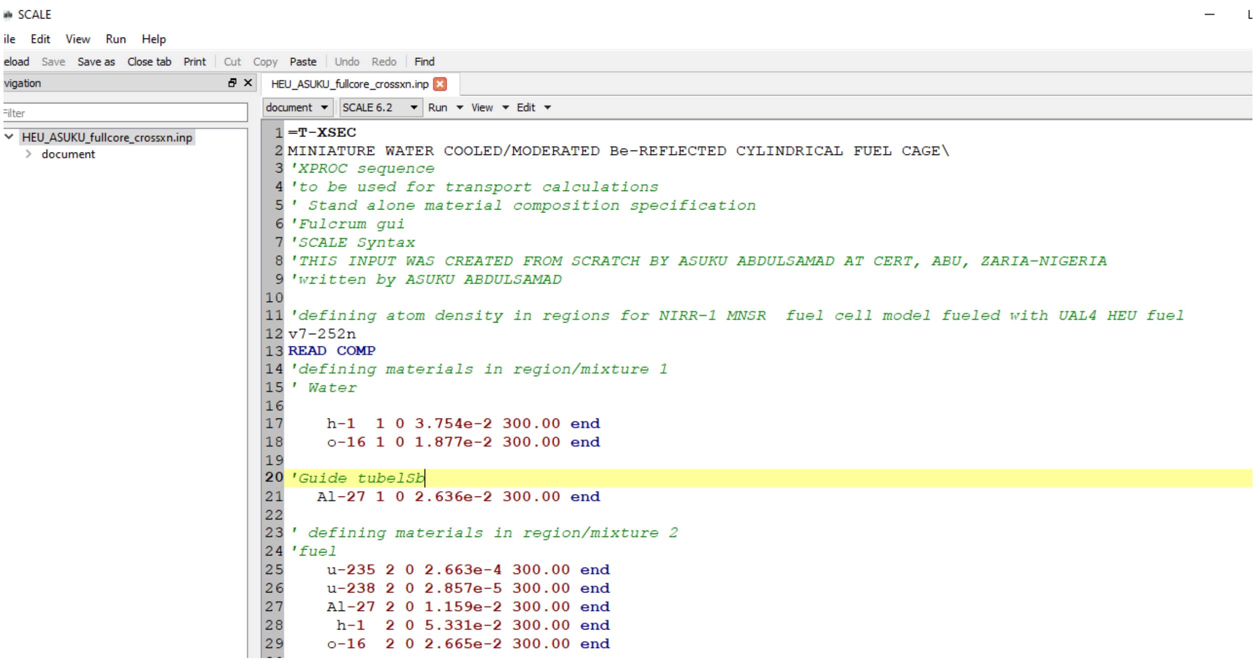

Figure III.1: A Typical XSProc Module Input Showing the "TITLE" and "READ COMPOSITION" Blocks

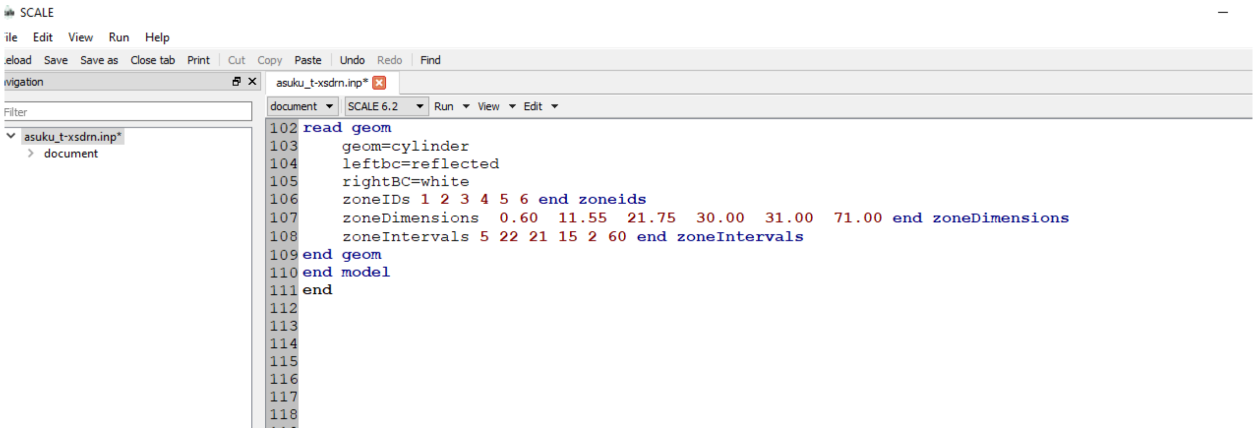

Figure III.2: A Typical T-XSDRN Sequence Showing the "MODEL" Block

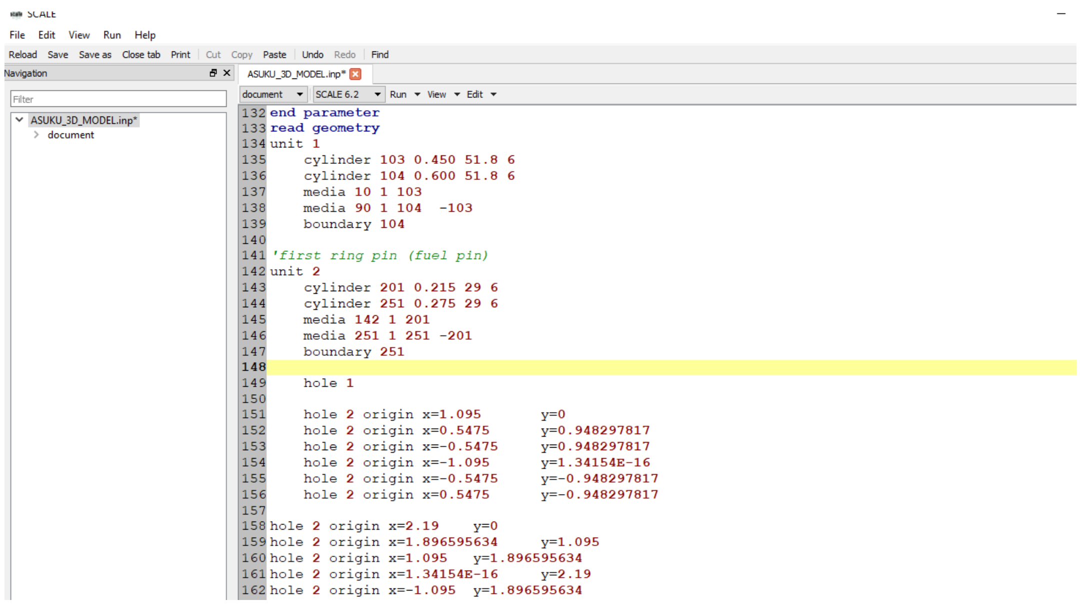

Figure III.3: A Typical 3-D KENO-VI "MODEL" Block